REPORT DOCUMENTATION PAGE

Form Approved
OMB No. 0704-0188

1. REPORT DATE *(DD-MM-YYYY)*	2. REPORT TYPE	3. DATES COVERED *(From - To)*
30-05-2010	Final Technical	1 Dec. 2006 to 30 Nov. 2009

4. TITLE AND SUBTITLE

(U) Supercritical Fuel Pyrolysis

5a. CONTRACT NUMBER

5b. GRANT NUMBER
FA9550-07-1-0033

5c. PROGRAM ELEMENT NUMBER
61102F

6. AUTHOR(S)

M. J. Wornat

5d. PROJECT NUMBER
2308

5e. TASK NUMBER
BX

5f. WORK UNIT NUMBER

7. PERFORMING ORGANIZATION NAME(S) AND ADDRESS(ES)

Louisiana State University
Department of Chemical
Engineering
South Stadium Drive
Baton Rouge LA 70803

8. PERFORMING ORGANIZATION REPORT NUMBER

9. SPONSORING / MONITORING AGENCY NAME(S) AND ADDRESS(ES)

Air Force Office of
Scientific Research
875 North Randolph Street
Suite 325, Room 3112
Arlington VA 22203-1768

10. SPONSOR/MONITOR'S ACRONYM(S)

11. SPONSOR/MONITOR'S REPORT NUMBER(S)
AFRL-OSR-VA-TR-2012-0437

12. DISTRIBUTION / AVAILABILITY STATEMENT

Approved for public release. Distribution is unlimited.

13. SUPPLEMENTARY NOTES

14. ABSTRACT

Supercritical pyrolysis experiments were conducted with the two-ring model fuel 1-methylnaphthalene at 585 °C and pressures of 50 to 110 atm and at 80 atm and temperatures of 550 to 600 °C. Quantification of the product polycyclic aromatic hydrocarbons (PAH) by high-pressure liquid chromatography (HPLC) showed linear increases in PAH yields with increasing pressure; with increasing temperature, rates of PAH yield increases rose steadily. Higher-temperature supercritical pyrolysis experiments with toluene showed that 700 °C, the highest temperature of the reactor, was not hot enough to break aromatic C-C bonds in the supercritical fuel pyrolysis environment. Supercritical pyrolysis experiments were conducted with the model alkane fuel *n*-decane at 570 °C and pressures of 40 to 100 atm and at 100 atm and temperatures of 530 to 570 °C. Application of a newly developed normal-phase HPLC fractionation / reversed-phase HPLC analysis technique led to the identification of 276 individual product PAH of up to 9 aromatic rings—many of which were first-time identifications as products of *n*-decane. Quantification of the PAH products showed exponential increases in PAH yields with increasing pressure or increasing temperature. Yields increased the most sharply for the highest-ring-number PAH, immediate precursors to carbonaceous solids.

15. SUBJECT TERMS

supercritical fuel pyrolysis, polycyclic aromatic hydrocarbons, carbonaceous solid deposits, hypersonic aircraft, PAH formation chemistry, high-pressure liquid chromatography, 1-methylnaphthalene, toluene, *n*-decane, synthetic jet fuel

16. SECURITY CLASSIFICATION OF:			17. LIMITATION OF ABSTRACT	18. NUMBER OF PAGES	19a. NAME OF RESPONSIBLE PERSON
					Julian Tishkoff
a. REPORT	b. ABSTRACT	c. THIS PAGE			19b. TELEPHONE NUMBER *(include area code)*
Unclassified	Unclassified	Unclassified	UL	88	703-696-8478

Grant FA9550-07-1-0033: Supercritical Fuel Pyrolysis

Table of Contents

Cover Page	i
Table of Contents	ii
Background and Introduction	1
Experimental Equipment and Techniques	4
Reactor System	4
Product Analysis	5
Results and Discussion	10
Model Fuel Experiments with 1-Methylnaphthalene	11
Model Fuel Experiments with Toluene	14
Model Fuel Experiments with *n*-Decane	16
Analysis of Stressed Fischer-Tropsch Synthetic Jet Fuel S-8 from AFRL	25
Executive Summary	26
Summary of Results	26
Personnel who Performed the Research	30
Publications and Presentations	30
References	32
Figures	36

Background and Introduction

The fuels used in the next generation of high-speed aircraft will have to operate under very high pressures and will have to sustain very high heat loads (*e.g.*, $\geq$ 30,000 BTU/min) in order to meet aircraft cooling requirements [1-3]. Predictions indicate that within the fuel lines and injection system, where residence times can be several minutes, fuel temperatures and pressures may reach or exceed 540 °C and 150 atm [2]. In a recent review article, Edwards [4] states that "a Mach 8 scramjet engine could require fuel heat-sink levels of 3500 kJ/kg, equivalent to temperatures on the order of 700 °C." These ranges of temperature and pressure substantially exceed the critical temperatures and pressures of most pure hydrocarbons and jet fuels such as JP-7 and JP-8 [1,4], so hydrocarbon fuels under these conditions will necessarily be supercritical fluids. These temperatures and pressures will also cause the fuel to undergo pyrolytic reactions, which have the potential of forming carbonaceous solids that can clog fuel lines, foul fuel nozzles, and lead to undesirable or even disastrous effects for the aircraft.

The difficulty of predicting solids-formation tendencies of fuels under supercritical conditions has been brought to our attention by Dr. Tim Edwards (of the Air Force Research Laboratory, AFRL), who shared with us solid deposition results for various jet fuels and *n*-octane, from scramjet test rigs at United Technologies Research Center (UTRC) [5]. The tests show that the tendency to produce solid deposits increases in the order: JP-7 < RP-1 < JP-8+100 < JP-10 < *n*-octane—an order that would not have been predicted, based solely on the paraffins/naphthenes/aromatics contents in these fuels and the prevalent understanding of how these different component groups behave under pyrolysis conditions. Clearly we need to know more about the pyrolysis reactions of these fuels and fuel components under supercritical conditions. In order to develop reliable fuel systems for high-speed aircraft that will not be subject to solid deposit formation, we need a thorough understanding of the pyrolysis behavior of candidate fuels under the supercritical conditions that they will be operating. Of particular interest are the reactions leading to polycyclic aromatic hydrocarbons (PAH), which can serve as precursors to the carbonaceous solids.

The fact that the fuel pyrolysis environment is a supercritical one introduces several complexities. With regard to physical properties, supercritical fluids have highly variable densities, no surface tension, and transport properties (*i.e.*, mass, energy, and momentum diffusivities) that are comparable to those of gases. Solvent-solute interactions, absent in the gas phase, can exhibit huge effects in supercritical fluids, often affecting chemical reaction pathways by facilitating the formation of certain transition states [6]. Because solvent-solute interactions are very dependent on pressure, chemical reaction rates in supercritical fluids can be highly pressure-dependent [6-9]. The kinetic reaction rate constant k has been shown [7,10] to vary exponentially with pressure, according to the expression $k = A_p \exp[(-\Delta V^{\neq}/RT)p]$, where A_p is the preexponential factor (in sec^{-1}) and $\Delta V^{\neq}$ is the activation volume (in l/mole). As the equation shows, a negative value of $\Delta V^{\neq}$ denotes that the reaction is favored by an increase in pressure. The magnitude of $\Delta V^{\neq}$ is an index of how sensitive the reaction rate is to pressure. For gases, $\Delta V^{\neq}$ is essentially zero; for liquids, $\Delta V^{\neq}$ is on the order of 10^{-2} l/mole; for supercritical fluids, $\Delta V^{\neq}$ is on the order of 1 to 10 l/mole [10].

For the case of fuel pyrolysis reactions, Stewart *et al*. [11,12] have demonstrated that reaction pathways and reaction kinetics indeed differ between the gas phase and the supercritical phase. Their pyrolysis experiments with decalin and methylcyclohexane in an atmospheric-pressure flow reactor and in the supercritical pyrolysis reactor currently in our use show that under supercritical conditions—but not in the gas phase at atmospheric pressure—both decalin and methylcyclohexane are able to produce methylated C_5-ring intermediates that readily convert to structures containing 6-membered aromatic rings. These aromatic rings can then serve as kernels for further cyclic growth to PAH and ultimately carbonaceous solids. For the same two fuels, decalin and methylcyclohexane, Stewart *et al*. [11,12] also report different temperature-dependent global kinetic rate parameters A_T and E_a for their supercritical pyrolysis experiments, compared to their gas-phase experiments. Distinctions between the supercritical phase and gas phase are particularly pronounced for the reactions of PAH formation and growth. Studies in our laboratory [13-15] demonstrate that acetylene-addition mechanisms [16-18]—widely applicable to high-

temperature gas-phase combustion systems—do not hold for the lower temperatures and higher pressures of the supercritical fuel pyrolysis environment, as no acetylene is formed [13-15]. We thus see that reaction pathways and reaction kinetics in the supercritical phase are substantially different from those in the gas or liquid phase. Therefore even for fuels whose gas-phase or liquid-phase pyrolysis behavior is well understood, it is of critical importance to study their pyrolysis in the supercritical phase, if these fuels are to be considered for future high-speed aircraft.

To that end, we have performed supercritical pyrolysis experiments with the three model fuels shown in Figure 1: 1-methylnaphthalene, a two-ring aromatic component of jet fuels [21]; toluene, a one-ring aromatic component of jet fuels [21]; and *n*-decane, an alkane component of both conventional (petroleum-derived) and alternative (non-petroleum-derived) jet fuels such as the Fischer-Tropsch synthetic jet fuel S-8. Because of the critical role that PAH play in the formation of carbonaceous solid deposits [13] and the need to discern PAH reaction pathways with as much specificity as possible, we have analyzed the products of the model fuel experiments by high-pressure liquid chromatography with diode-array ultraviolet-visible absorbance and mass spectrometric detection (HPLC/UV/MS), a technique ideally suited to the isomer-specific analysis of PAH. In the case of the products from the *n*-decane experiments, we also employ a normal-phase HPLC fractionation technique—which we have developed specifically for the complex, highly alkylated PAH product mixtures of alkane fuels—so that the HPLC/UV/MS analyses can be effectively performed. We have also employed normal-phase HPLC fractionation / reversed-phase HPLC analysis in the compositional analyses of samples of the Fischer-Tropsch synthetic jet fuel S-8 stressed in a high-temperature flow reactor at the Air Force Research Laboratory (AFRL) and provided to us by Dr. Matt DeWitt and Dr. Tim Edwards at AFRL.

In the following, we describe the supercritical fuels pyrolysis reactor used in the model fuel experiments and describe our product analysis procedures, including the normal-phase HPLC fractionation / reversed-phase HPLC analysis technique for the analysis of PAH. We then summarize the results we have obtained from the supercritical pyrolysis experiments with the

three model fuels 1-methylnaphthalene, toluene, and *n*-decane—presenting product yields as functions of both pyrolysis temperature and pressure. The results of the normal-phase HPLC fractionation / reversed-phase HPLC analysis of one of the stressed synthetic jet fuel samples from AFRL are then presented, followed by a summary of all of the results presented in this report. Finally, we list the people who performed the research supported by Grant FA9550-07-1-0033 and the publications and conference presentations coming from that research.

Experimental Equipment and Techniques

Since most of the work performed for Grant FA9550-07-1-0033 involves the supercritical pyrolysis experiments with the model fuels, we first describe the reactor used in these experiments. We then describe the instruments and techniques used in the analyses of the products of these experiments as well as in the analyses of stressed fuel samples supplied to us by Dr. Matt DeWitt and Dr. Tim Edwards at AFRL.

Reactor System

The supercritical fuel pyrolysis experiments are conducted in the isothermal, isobaric reactor designed expressly for such purposes by Davis [22] and used by Stewart [11,12] in the AFOSR-sponsored research program supervised by Professor Irvin Glassman at Princeton University. Upon his retirement, Professor Glassman made the reactor available to us, and we have used it for supercritical fuel pyrolysis research over the last several years. The fluidized-alumina bath heater has been replaced, during the period of AFOSR Grant FA9550-1-07-0033, to permit experiments at temperatures higher than could be reached in the original reactor.

The reactor system [13-15] is illustrated in Figure 2. Prior to an experiment, liquid fuel is sparged with nitrogen for three hours [11] to remove any dissolved oxygen that could introduce auto-oxidative effects [23]. The sparged fuel is then loaded into a high-pressure pump, which delivers the fuel to the reactor, as shown in Figure 2. The reactor itself is a silica-lined stainless-steel coil of capillary tubing. (The silica lining prevents wall-catalyzed deposit formation that

occurs with unlined stainless steel [11,22,23].) For the experiments with 1-methylnaphthalene and toluene, the reactor coil tubing has inner diameter, 1 mm, and outer diameter, 1.59 mm. For *n*-decane, which produces solids more readily, a larger-diameter tubing is used (2.16-mm i.d. and 3.17-mm o.d.).

As shown in Figure 2, the reactor coil is immersed in a temperature-controlled fluidized-alumina bath, which ensures isothermality throughout the reactor length. As indicated in Figure 2, the entrance and exit lines of the reactor are passed through a water-cooled (25 °C) heat exchanger to ensure a controlled thermal history and residence time. Exiting the heat exchanger, the quenched reaction products pass through a stainless-steel filter (hole size, 10 μm) and back-pressure regulator before proceeding on to liquid-phase and gas-phase product collection.

Reactor residence time is varied by changing the length of the reactor coil or the flowrate. The reactor system is capable of operating at temperatures up to 700 °C (controlled to within ± 1 °C), pressures up to 110 atm (controlled to within ± 0.2 atm), and residence times up to several minutes. As documented by Davis [22] and Stewart [11], the reactor has been designed to meet Cutler's [24] and Lee's [25] criteria for idealization as plug flow, with regard to species concentration profiles. The resulting radially uniform species concentrations, coupled with the reactor's constant-temperature and constant-pressure operation, render this reactor ideal for supercritical pyrolysis kinetics experiments.

Product Analysis

At the conclusion of a pyrolysis experiment, the gaseous reaction products are removed and injected into a gas chromatograph (GC) with a flame-ionization detector (FID), for analysis of light-hydrocarbon gases. The liquid products are removed from the collection system and transferred to a vial. Most of the liquid product mixture is reserved for analysis by high-pressure liquid chromatography (HPLC), but an aliquot of the liquid product mixture is removed for injection onto an Agilent Model 6890 GC with a FID, in conjunction with an Agilent Model 5973 mass spectrometer (MS). The GC/FID/MS instrument is used to quantify liquid-phase aliphatic

products (if present) and 1- and 2-ring liquid aromatic products—all of which are identified by matching retention times and mass spectra with those of reference standards.

The procedure for HPLC analysis of the liquid-phase products of a supercritical fuel pyrolysis experiment depends on whether the fuel is aromatic, such as the model fuels 1-methylnaphthalene and toluene in Figure 1, or aliphatic, such as the model alkane fuel in Figure 1, *n*-decane. The liquid-phase products from the supercritical pyrolysis of aromatic fuels consist primarily of PAH with a low degree of alkyl substitution ("alkylation"), so the products can be directly analyzed by reversed-phase HPLC/UV/MS, after undergoing a standard sample-preparation procedure. The liquid-phase products from the supercritical pyrolysis of an alkane or alkane-rich fuel, on the other hand, contain large amounts of aliphatic material as well as one-ring aromatics and PAH with a high degree of alkylation. As will be seen in the Results and Discussion section of this report, such highly alkylated product mixtures exhibit poor resolution if analyzed by reversed-phase HPLC directly, so we have developed a normal-phase HPLC fractionation technique to fractionate the liquid-phase products from alkane fuels into 12 fractions, each of which is subsequently analyzed by reversed-phase HPLC/UV/MS. In the following, we first describe the fractionation/analysis scheme for the liquid products of the alkane fuels. We then describe the reversed-phase HPLC analysis method used for the unfractionated liquid-phase products of the aromatic fuels as well as for the normal-phase HPLC fractions of the liquid-phase products of the alkane fuel(s).

Fractionation and Analysis of the Liquid-Phase Products from Alkane Fuels. Figure 3 outlines the different fractionation and analysis steps we have developed for the analysis of the liquid-phase products of the supercritical pyrolysis of an alkane fuel, in particular, *n*-decane. All four of the normal-phase HPLC fractionation steps—each designated as a box labelled as "HPLC/FC normal-phase" in Figure 3—are performed on an Agilent Model 1200 HPLC with diode-array UV absorbance detector, fluorescence detector, and fraction collector (FC)—the HPLC/FC instrument provided to us through a recent DURIP grant (Grant No. FA9550-08-1-0281). For product fractionation, the HPLC/FC instrument is equipped with two normal-phase

Cyano columns in series (each with diameter, 4.6 mm; length, 250 mm; particle size, 5 μm), and 1 ml/min of hexane is used as the mobile phase. The different "fractions" are collected over different ranges of elution time on the normal-phase column—each fraction corresponding to PAH of a common ring number or isomer group, along with alkylated derivatives of those PAH. Table 1 presents the characteristics of the main constituents of the twelve fractions obtained.

Table 1. Contents of the 12 Normal-Phase HPLC Fractions of an *n*-Decane Product Mixture

Fraction Number	Primary Constituents*
1	2-ring, $C_{10}H_8$
2	3-ring, $C_{13}H_{10}$
3	3-ring, $C_{14}H_{10}$
4	4-ring, $C_{16}H_{10}$
5	4-ring, $C_{18}H_{12}$; 5-ring, $C_{18}H_{10}$
6	5-ring, $C_{20}H_{12}$
7	6-ring, $C_{22}H_{12}$; 7-ring, $C_{24}H_{12}$
8	6-ring, $C_{24}H_{14}$
9	7-ring, $C_{26}H_{14}$ and $C_{28}H_{16}$
10	8-ring, $C_{28}H_{14}$
11	7-ring, $C_{28}H_{16}$
12	9-ring, $C_{30}H_{14}$

*The given molecular formula is for the unsubstituted PAH. In most cases, alkylated derivatives of such PAH are also within the fraction.

The analysis scheme of Figure 3 is broken into four sequences, each designated by a circled number, 1 through 4, and tailored to a particular range of product components. Analysis of the aliphatic and one-ring aromatic components in the product mixture is accomplished through sequence 1, which consists of injections (at 2 different dilutions) of the liquid product mixture onto the GC/FID/MS instrument. The two-ring aromatics are analyzed in Sequence 2: First 5 μl of the liquid-phase products are sent through a single normal-phase fractionation step to remove aliphatic material that would potentially co-elute on the GC with the two-ring aromatic products. The two-ring aromatic material is collected from the normal-phase HPLC column as Fraction 1 and then injected onto the GC/FID/MS for analysis.

Analysis of the product PAH requires two sequences: sequence 3 for the 2- to 5-ring PAH; sequence 4 for the PAH of 6 to ≥ 9 rings. Sequence 3 begins with a normal-phase fractionation step on the HPLC/FC, which separates the products into six fractions. To collect enough material in each of the fractions 1-6, the fractionation actually involves 48 separate 1-μl injections of products, each going through a complete 30-min HPLC run before the next injection can be made. (Better resolution is obtained from smaller-diameter columns and smaller injections; hence the need for the numerous injections.) After 48 rounds of the fractionation step, sufficient material is collected for each of the fractions 1-6, which are each then concentrated under nitrogen and subjected to reversed-phase HPLC/UV/MS analysis for compositional analysis of the 2- to 5-ring PAH products.

The 6- to ≥ 9-ring PAH products are produced in yields that are orders of magnitude lower than the smaller-ring-number aromatics, so two fractionation steps are needed in order to obtain sufficient material in fractions 7-12. As indicated in Sequence 4 of Figure 3, the first fractionation step (ten injections and 90-minute HPLC runs) accomplishes the removal of the lighter material and isolates the heavier PAH material. The second fractionation step—accomplished in 50 consecutive 40-min runs, each with 10 μl of material—separates the heavier PAH according to ring number and isomer group, in the 6- to 9-ring PAH fractions 7-12, as indicated in Table 1. Each of the fractions 7-12 is then concentrated down and analyzed by reversed-phase HPLC/UV/MS, as described below, to achieve the compositional analysis of the 6- to 9-ring PAH products of *n*-decane.

PAH Analysis by Reversed-Phase HPLC/UV/MS. In order to determine the identities and quantities of the PAH products of supercritical fuel pyrolysis, each liquid-phase product mixture—or, in the case of *n*-decane, each of the 12 normal-phase HPLC fractions of the liquid-phase product mixture—is concentrated in a Kuderna-Danish apparatus and exchanged, under nitrogen, into 200 μl (40 μl in the case of *n*-decane product fractions) of dimethylsulfoxide, a solvent compatible with the solvents used in the reversed-phase HPLC method employed for PAH analysis. During the concentration and solvent-exchange procedure, portions of the more volatile

aromatics, such as the 1- and 2-ring species, are lost to vaporization; hence these lighter aromatic products are quantified by gas chromatographic analysis, as described above.

For analysis of the large aromatic products ($\geq$ 3 rings) by reversed-phase HPLC, a 20-μl (1- or 5-μl for the *n*-decane product fractions) aliquot of the product/dimethylsulfoxide solution is injected onto an Agilent Model 1100 high-pressure liquid chromatograph, coupled to a diode-array ultraviolet-visible (UV) absorbance detector in series with a mass spectrometer (MS). Employing atmospheric-pressure photo-ionization, the MS monitors mass-to-charge ratios up to 700. The reversed-phase HPLC separation method, optimized for large PAH analysis, utilizes a reversed-phase Restek Pinnacle II PAH octadecylsilica column. (For the aromatic fuels, the column has length, 250 mm; inner diameter, 4.6 mm; and particle size, 5 μm. To accommodate the lower amount of material in the normal-phase HPLC fractions of the alkane fuel products, the column has length, 250 mm; inner diameter, 2.1 mm; and particle size, 4 μm.) A time-programmed sequence of solvents—acetonitrile/water, acetonitrile, and dichloromethane—is pumped through the column, and the PAH product components elute in the order of increasing molecular size. UV absorbance spectra are taken every 0.8 sec—and mass spectra, every 1 sec—of the separated components as they exit the column.

The mass spectrum establishes the C_xH_y formula of the PAH, its molecular mass, and whether there are any substituent groups like methyl attached to the aromatic structure. The UV spectrum establishes the exact aromatic structure of the PAH, so for unsubstituted PAH, the UV spectrum alone is sufficient to establish the exact isomer-specific identity. If a PAH has an alkyl substituent, the UV spectrum looks almost exactly like that of the parent PAH, only shifted a few nm to higher wavelength—the position and length of the substituent dictating the details of the shift [26,27]. Therefore, for PAH, which have a multitude of sites at which substituents can be located, one must have reference standards of all possible positional isomers in order to be certain of the exact position of the alkyl substituent—a condition rarely met for large PAH or for multi-alkylated PAH. Consequently, for many of the alkylated PAH products reported in the Results and Discussion section of this report (especially those from *n*-decane), the exact structure of the

aromatic portion of the PAH is known (from the UV spectrum), but there is uncertainty associated with the number, position(s), and/or chain length(s) of the alkyl substituent(s). In cases where we are sure of the exact alkylated PAH structure—*e.g.*, all of the singly methylated naphthalenes, phenanthrenes, anthracenes, pyrenes, and coronene—we do show the exact position of the methyl substituent.

PAH products from the supercritical fuel pyrolysis experiments are identified by matching HPLC retention times, mass spectra, and UV absorbance spectra with those of our PAH reference standards, which include both commercially available compounds as well as PAH that have been specially synthesized for our identification efforts. In some cases, in which reference standards are not available, product identities are established by matching UV spectra with those published in the literature for those compounds. Quantification of the identified PAH comes from extensive calibration of the HPLC/UV instrument with reference standards, taking into account nonlinearities in the response of diode-array detectors at high analyte concentrations [28].

Since the number of possible PAH structures grows exponentially with ring number [27], the HPLC/UV/MS technique is particularly well suited for analyzing the large PAH molecules that are precursors to fuel-line carbonaceous solids. The HPLC separates each product component; the mass spectrum narrows the field of possible component identities to a particular C_xH_y isomer group; the fingerprint UV spectrum then permits the designation of the exact molecular structure of the product component.

Results and Discussion

Using the reactor of Figure 2, we have conducted supercritical pyrolysis experiments with the three model fuels of Figure 1: 1-methylnaphthalene, a two-ring aromatic component of jet fuel [21]; toluene, a single-ring component of jet fuel [21]; and *n*-decane, an alkane component of both conventional and synthetic jet fuels. The products of the experiments have been analyzed by the methods described in the Experimental Equipment and Techniques section, and the results are

reported below, by fuel, in the order: 1-methylnaphthalene, toluene, *n*-decane. Following the results on the model fuels, results are presented on our compositional analysis of a stressed Fischer-Tropsch synthetic jet fuel sample provided to us by Dr. Matt DeWitt and Dr. Tim Edwards at AFRL.

Model Fuel Experiments with 1-Methylnaphthalene

Supercritical pyrolysis experiments have been conducted, in the reactor of Figure 2, with the model fuel 1-methylnaphthalene (critical temperature, 499 °C; critical pressure, 36 atm) at a fixed residence time of 140 sec, pressures up to 110 atm, and temperatures up to 650 °C. At 140 sec and 110 atm, 585 °C is the highest temperature at which the reactor can be run without solids plugging the reactor. At 140 sec and 80 atm, 600 °C is the highest temperature at which the reactor can be run without solids plugging the reactor. Therefore, for purposes of product quantification, two sets of supercritical pyrolysis experiments have been conducted with 1-methylnaphthalene: one in which temperature is fixed at 585 °C, residence time is fixed at 140 sec, and pressure is varied from 50 to 110 atm; the other in which pressure is fixed at 80 atm, residence time is fixed at 140 sec, and temperature is varied from 550 to 600 °C.

The Final Performance Report [29] for our previous AFOSR grant (FA9550-04-1-0005) and our papers [15,30,31] provide the documentation of our identification of the PAH products of supercritical 1-methylnaphthalene pyrolysis, but for ease of reference, the reversed-phase HPLC chromatogram [15,30] of the aromatic products of 1-methylnaphthalene pyrolysis at 585 °C, 110 atm, and 140 sec is presented in Figure 4. The experimental conditions of Figure 4 correspond to the early stages of carbonaceous solids formation, at approximately 75 % 1-methylnaphthalene conversion. Except for the cluster of > 30 bi-naphthyls and methylated bi-naphthyls (which are better resolved by gas chromatography and thus analyzed by that means), the reversed-phase HPLC chromatogram of Figure 4 shows good component resolution, as is evident in the clearly

defined individual component peaks. (The rise in baseline at 63 min in Figure 4 is not due to unresolved material but to dichloromethane, which absorbs in the UV and is introduced into the HPLC solvent program at this time.) The good chromatographic resolution exemplified by Figure 4 permits most of the product PAH to be quantified.

Figures 5-8 present the yields, as functions of pressure, of the PAH products of supercritical 1-methylnaphthalene pyrolysis at 585 °C and 140 sec: naphthalene, summed di-methylnaphthalenes (with ethylnaphthalene), summed bi-naphthyls and methylated bi-naphthyls, and summed dibenzofluorenes in Figure 5; the four five-ring $C_{22}H_{14}$ PAH in Figure 6; six- and seven-ring product PAH in Figure 7; and eight- and nine-ring product PAH in Figure 8. Figures 5-7 demonstrate that at 585 °C and 140 sec, yields of naphthalene, the dimethylnaphthalenes, the bi-naphthyls, and the 5-, 6-, and 7-ring PAH each increase linearly with pressure. Some curvature is evident, however, in the 8- and 9-ring PAH product yields of Figure 8, indicating that at the higher pressures of our experiments at 585 °C, production of these largest PAH products is very sensitive to pressure. Consistent with this finding is the experimental observation that the highest pressure of Figure 8, 110 atm, corresponds to the onset of carbonaceous solids production from 1-methylnaphthalene.

Figures 9-12 present the yields of the same products as in Figures 5-8 but as functions of temperature from supercritical 1-methylnaphthalene pyrolysis at 80 atm and 140 sec. Figures 9-12 reveal that at 80 atm and 140 sec, the yields of all of the PAH products increase with temperature—the rate of increase rising with temperature for most of the PAH, especially at temperatures > 580 °C. Product-yield sensitivity to temperature is particularly high in Figures 11 and 12, for the highest-ring-number PAH, the immediate precursors to the carbonaceous solids that begin forming at 600 °C, the highest-temperature conditions in Figures 9-12.

The jump in yields of large PAH, just at the point where carbonaceous solids begin to be made, underscores the role of these large PAH as precursors to the solids and underscores the importance of determining the mechanisms of the large PAH formation. The Final Performance Report [29] for our previous AFOSR Grant (FA9550-04-1-0005) and two of our papers [15,31] detail the reaction mechanisms responsible for the formation of the PAH products of supercritical 1-methylnaphthalene pyrolysis in Figures 4-12. Our experiments [15,29] have shown that in the supercritical 1-methylnaphthalene pyrolysis environment, there is no rupture of any of the aromatic C-C bonds (bond-dissociation energy, 122 kcal/mole [20]), so the PAH produced from supercritical 1-methylnaphthalene pyrolysis are constrained to have formed via pathways that preserve the intactness of the 2-ring aromatic naphthalene units involved in the products' construction. Slightly modified from their original forms [15,29], our mechanisms for the formation of naphtho[2,1-*a*]pyrene, the major six-ring PAH product of Figures 4, 7, and 11, and for benzo[*cd*]phenanthro[1,2,3-*lm*]perylene, the identified [31] nine-ring PAH product in Figures 4, 8, and 12, appear in Figures 13 and 14, respectively.

In addition to the fuel molecule 1-methylnaphthalene and the easiest-to-form radical 1-naphthylmethyl, methyl radical also plays a prominent role in the reaction schemes of Figures 13 and 14. We do not measure methyl radical in our experiments, but we do measure the product methane, the only small hydrocarbon produced in significant amounts in our supercritical 1-methylnaphthalene pyrolysis experiments. Figure 15a portrays the pressure-dependent yields of methane from the experiments at 585 °C and 140 sec; Figure 15b, the temperature-dependent yields from the experiments at 80 atm and 140 sec. As Figure 15 reveals, methane yields increase with either increasing pressure or increasing temperature—consistent with the increased availability of methyl radical needed for the production of the large PAH in Figures 13 and 14.

Model Fuel Experiments with Toluene

As the structures of the three model fuels in Figure 1 indicate, the various bond-dissociation energies of the methylated one-ring aromatic fuel toluene are very similar to those of the methylated two-ring aromatic fuel 1-methylnaphthalene. The results [14,29] from our supercritical toluene pyrolysis experiments, reported for our previous AFOSR grant (FA9550-04-1-0005) showed that at temperatures as high as 585 °C (the maximum temperature of our reactor at that time), the mechanisms for PAH formation from supercritical toluene pyrolysis were exactly analogous to those for supercritical 1-methylnaphthalene pyrolysis. In the supercritical toluene pyrolysis environment, PAH were constructed from toluene, benzene, benzyl radical, methyl, and phenyl in a way that preserved the intactness of the one-ring aromatic units involved in the products' formation. The aromatic C-C bonds, whether for toluene or 1-methylnaphthalene, could not be broken at the highest temperature to which our reactor could then go, 585 °C.

During the period of our just-finished AFOSR grant (FA9550-07-1-0033), however, the acquisition of a higher-temperature heater for our reactor has enabled us to perform supercritical pyrolysis experiments at temperatures as high as 700 °C. Toluene does not form carbonaceous solids as readily as 1-methylnaphthalene, so we have been able to conduct experiments with toluene (critical temperature, 319 °C; critical pressure, 41 atm) at 700 °C. Figure 16 presents the HPLC chromatogram of the products of supercritical toluene pyrolysis at 700 °C, 140 sec, and 75 atm, the highest pressure at which we can run toluene experiments at 700 °C without the experiment being aborted by solids clogging the reactor. As the structures of each of the products of Figure 16 reveal, even 700 °C—the highest pre-combustion fuel temperature predicted by Edwards [4] for a Mach 8 scramjet engine—is not hot enough to break the aromatic C-C bonds in the toluene structure: All of the PAH in Figure 16 can be constructed from toluene, benzene,

benzyl radical, methyl, and phenyl in a way that preserves the intactness of the one-ring aromatic units involved in their construction.

Several of the five-ring PAH in Figure 16 have never before been reported as products of toluene pyrolysis or combustion, so the mass and UV spectral data establishing their identities are presented in Figures 17-21: naphtho[2,3-*a*]fluorene and naphtho[2,3-*b*]fluorene, in Figures 17 and 18; naphtho[2,1-*a*]fluorene and naphtho[2,1-*b*]fluorene, in Figures 19 and 20; indeno[1,2-*b*]fluorene in Figure 21. In each of Figures 17-21, part a gives the product component's mass spectrum, which establishes the component's C_xH_y formula; part b gives the product component's UV spectrum along with that of the appropriate PAH reference standard, which establishes the component's structural identity.

As illustrated in Figures 22-24, all of the fused five-ring PAH products of Figures 17-21 are constructed from three one-ring aromatic units (toluene, benzene, benzyl, and/or phenyl). First, two one-ring aromatic units combine to make one of the identified three-ring aromatic products of Figure 16—fluorene, in Figure 22, phenanthrene, in Figure 23, anthracene, in Figure 24. Second, the third one-ring aromatic unit reacts with the respective 3-ring PAH to make the 5-ring PAH product. In Figure 22, benzyl reacting with fluorene in the "3" position yields the 5-ring indeno[1,2-*b*]fluorene. In Figure 23, benzyl reacting with the 3-ring phenanthrene in the "1" position produces naphtho[2,1-*a*]fluorene; in the "3" position, naphtho[1,2-*b*]fluorene. In Figure 24, benzyl reacting with the 3-ring anthracene in the "2" position produces naphtho[2,3-*b*]fluorene; in the "1" position, naphtho[2,3-*a*]fluorene. The five-ring benzo[*a*]fluoranthene in Figure 24 results from phenyl reacting with anthracene in either the "1" or "9" position (position "1" shown in the Figure). The five-ring benzo[*b*]fluoranthene in Figure 23 results from phenyl reacting with phenanthrene in either the "1" or "9" position (position "1" shown in the Figure). The various methylated and unmethylated phenyl-substituted phenanthrenes and anthracenes in

Figure 16 (the dark blue structures) result from one-ring aromatic units reacting with phenanthrene in the "2" or "3" position or with anthracene in the "2" position—positions that do not allow fusion of the newly added ring by the creation of a connecting five-membered ring.

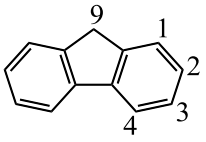

fluorene

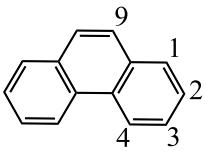

phenanthrene

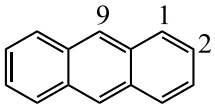

anthracene

At the temperature and residence time of Figure 16, 700 °C and 140 sec, 75 atm is the highest pressure at which we can run the reactor with toluene without solids clogging the reactor and forcing a shutdown. If the temperature is held at 685 °C, however, experiments at a pressure as high as 100 atm can be conducted at a residence time of 140 sec. Therefore two sets of supercritical toluene pyrolysis experiments have been conducted: one at 685 °C, 140 sec, and at four pressures from 50 to 100 atm; the other at 100 atm, 140 sec, and at six temperatures from 550 to 685 °C. The HPLC chromatograms of the products from the four experiments composing the first set appear as Figures 25 and 26; those from the six experiments composing the second set, Figures 27-29. Neither set of experiments' products have yet been quantified, but Figures 25 and 26 show that at 685 °C and 140 sec, the amounts of the higher-ring-number PAH are higher at the higher pressures. Figures 27-29, on the other hand, show that at 100 atm and 140 sec, temperature drastically influences the production of PAH. No PAH of > 3 rings are detected at temperatures $\leq$ 625 °C; relative amounts of the 5-ring PAH, however, steadily increase as temperature is raised from 650 to 685 °C.

Model Fuel Experiments with *n*-Decane

As we have learned from our experiments with 1-methylnaphthalene [15] and toluene [14], the high bond-dissociation energy (122.1 kcal/mole [20]) of the aromatic C-C bonds in these fuels

prevents these bonds from breaking in the supercritical fuel pyrolysis environment (at least up to 700 °C, the highest temperature of our reactor). The product PAH from these fuels are thus constrained to form via radical reactions with unbroken 2-ring (in the case of 1-methylnaphthalene [15,31]) and 1-ring (in the case of toluene [14]) aromatic units. The PAH product distributions are therefore highly selective and the degree of alkylation is small, usually restricted to no more than one methyl group per product PAH structure. Both of these factors lead to reversed-phase HPLC chromatograms with good component resolution, as evident in Figures 4 and 16.

The same is not the case for alkanes, however, and alkane-rich fuels such as the Fischer-Tropsch synthetic jet fuel S-8. As indicated in Figure 1, bond-dissociation energies for the C-C bonds in *n*-alkanes such as *n*-decane are relatively low (86.1 to 87.5 kcal/mole [19]), so these bonds would be expected to be easily broken in the supercritical fuel pyrolysis reaction environment. Confirmation of this expectation is found in Figures 30 and 31, the GC chromatograms of, respectively, the gas-phase products and the liquid-phase products of supercritical *n*-decane pyrolysis at 570 °C, 100 atm, and 140 sec. Figures 30 and 31 show that—in contrast to 1-methylnaphthalene and toluene, whose nonaromatic products consist chiefly of methane [14,15]—supercritical *n*-decane pyrolysis produces a multitude of C_1 to C_9 alkanes and alkenes, which result from the scission of *n*-decane's C-C bonds. (It should be noted that C_5 hydrocarbons, though present in the liquid-phase products, are not evident in Figure 31 since our GC/FID/MS did not have the capability of going to temperatures low enough to separate C_5 products from the solvent peak. The purchase of a cryogenic valve, during the succeeding AFOSR grant, will allow for cooling with liquid N_2 and eliminate this problem.)

The alkane and alkene products of the supercritical pyrolysis of *n*-decane (critical temperature, 345 °C; critical pressure, 20.8 atm) have been quantified for two sets of experiments, and the resulting product yields appear in Figures 32 and 33. Figure 32 portrays alkane and alkene

product yields, versus temperature, at a fixed pressure of 100 atm and residence time of 140 sec; Figure 33, yields of these same products, versus pressure, at a fixed temperature of 570 °C and residence time of 140 sec. The reaction conditions of 140 sec, 100 atm, and 570 °C correspond to the early stages of solids formation. At 100 atm and 580 °C, the reactor clogs instantly; at 100 atm and 575 °C, solids form in sufficient amounts to prevent steady product collection over a sustained period of time.

Figures 32a and 32c show that as temperature increases, yields of the C_1-C_4 alkanes and alkenes increase—a result of the temperature-facilitated decomposition of the *n*-decane fuel into the small hydrocarbons. In contrast, Figures 32b and 32d show that as temperature increases, the yields of the C_6-C_9 alkanes and alkenes decrease with increasing temperature, as they too decompose into smaller hydrocarbons.

Parts a and b of Figure 33 show that as pressure increases, yields of alkanes increase; parts c and d, that yields of alkenes decrease. This contrasting behavior of the alkanes and alkenes is due to the fact that high pressures stabilize alkyl radicals [36], allowing time for the alkyl radicals resulting from *n*-decane C-C bond cleavage to abstract hydrogen from neighboring molecules and form alkanes rather than to decompose by beta scission and form 1-alkenes.

In addition to alkanes and alkenes, Figures 30 and 31 also reveal that supercritical *n*-decane pyrolysis produces a large number of 1-ring aromatics—benzene, toluene, the xylenes, and other aromatics with various numbers and sizes of alkyl substituents. Yields of benzene, toluene, ethyl benzene, and the xylenes appear in Figure 34 for the same two sets of experiments as in Figures 32 and 33. Parts a and b show that yields of each of the one-ring aromatics increase with increasing temperature and pressure, respectively.

The multiplicity of alkyl fragments produced by scission of the alkane C-C bonds in *n*-decane leads not only to a complex variety of alkyl-substituted one-ring aromatics but also to an

extremely complex mixture of alkylated PAH products. For a given parent PAH structure, different numbers of different-length and differently configured alkyl groups can be placed in different positions and combinations of positions around the periphery of the PAH structure—so there can be huge numbers of alkylated versions of that parent PAH, eluting over a range of HPLC elution times. Since reversed-phase HPLC columns are sensitive to alkyl functionalities (in addition to aromatic structure), we would expect reversed-phase HPLC analyses of the supercritical pyrolysis products of alkane fuels to yield chromatograms with much poorer component resolution than those from aromatic fuels.

Evidence that our expectation is correct is found in Figure 35, a reversed-phase HPLC chromatogram of the products of *n*-decane pyrolyzed in our reactor for 140 sec, at 100 atm and 570 °C—conditions corresponding to the early stages of solids formation. Several of the compounds eluting in the first 32 min in Figure 35 are well resolved, but the rising baseline afterward (not due to HPLC solvent here) and merging of component peaks are indicative of poor resolution. Even with the poor resolution, fifty-one of the product components in Figure 35 are well-enough resolved to permit identification by their UV spectra—although there are varying degrees of specificity in these identifications. The 7 red structures in Figure 35 are unsubstituted PAH whose exact identities are certain, and the 8 blue structures with single methyl groups in definite positions are methylated PAH whose exact structures are certain. The 36 other blue structures in Figure 35 are alkylated PAH whose aromatic portion of the structure is known (and shown in blue), but there is uncertainty associated with the number, position(s), and/or length(s) of the alkyl substituent(s).

As we have seen from the 1-methylnaphthalene and toluene results, elucidation of the structures of the PAH products is critical to determining PAH formation mechanisms. Therefore, in order to improve component resolution in the reversed-phase HPLC chromatograms of the

products of *n*-decane and other alkane fuels, we have developed the normal-phase HPLC fractionation / reversed-phase HPLC scheme that is depicted in Figure 3 and described in the Experimental Equipment and Techniques section. Unlike reversed-phase HPLC columns, the normal-phase HPLC column is fairly insensitive to alkyl group functionality and is employed to fractionate the *n*-decane product components into groups by aromatic ring number and parent PAH isomer class, as detailed in Table 1 of the Experimental Equipment and Techniques section.

The supercritical *n*-decane pyrolysis product mixture corresponding to Figure 35 (the reversed-phase HPLC chromatogram of unfractionated *n*-decane products produced at 570 °C, 100 atm, and 140 sec) has been subjected to the normal-phase HPLC fractionation / reversed-phase HPLC analysis method of Figure 3, and the reversed-phase HPLC chromatograms of the twelve normal-phase HPLC fractions appear in Figures 36, 37, and 38. The same color-coding system used in Figure 35 applies to Figures 36-38 as well: Red structures are unsubstituted PAH whose exact identities are certain; blue structures with single methyl groups in definite positions are methylated PAH whose exact structures are certain; and the other blue structures are alkylated PAH whose aromatic portion of the structure is known (and shown in blue), but there is uncertainty associated with the number, position(s), and/or length(s) of the alkyl substituent(s).

The UV spectral matches confirming the identities of one of the seven-ring PAH products in Fraction 9 and of one of the eight-ring PAH products in Fraction 10 are found in Figure 39. The UV spectral matches documenting the identifications of all of the other unsubstituted PAH products of supercritical *n*-decane pyrolysis appear elsewhere [38]. Except for our own work, the two PAH of Figure 39, along with many of the other PAH in Figures 36-38, have never before been reported as products of *n*-decane or other pure alkane fuels.

As Figures 36-38 reveal, the coupling of the normal-phase HPLC fractionation with the reversed-phase HPLC/UV/MS analysis yields a tremendous improvement in the resolution of the

PAH products of supercritical *n*-decane pyrolysis—increasing the number of identifiable PAH to 276 (compared to 45 in the unfractionated product mixture of Figure 35). Table 2 provides a comparison of the number of PAH species identified in the unfractionated and fractionated product mixtures, broken down by PAH ring number and by whether the PAH are unsubstituted or alkylated. As Table 2 reveals, when fractionation is employed, the total number of unsubstituted PAH identified is increased from 7 to 47, and the number of alkylated PAH identified is increased from 38 to 229. (Among these alkylated PAH, the number of methylated PAH in which the exact position of the methyl group is known is increased from 8 to 17.) The increase from 45 to 276 in the total number of identified product PAH represents a six-fold improvement. The effects of the fractionation are even more dramatic for the higher-ring number PAH products as Table 2 reveals. In the unfractionated *n*-decane pyrolysis products, only three PAH of $\geq$ 5 rings (2 unsubstituted; 1 alkylated) are identifiable. In the fractionated products, 117 PAH of 5 to 9 rings (30 unsubstituted; 87 alkylated) are identifiable. This ability to determine the structures of the larger PAH products should be particularly helpful in the elucidation of the reaction pathways responsible for large PAH—and ultimately solids—formation from alkane fuels.

The improved product-component resolution, evident in the fractions' chromatograms of Figures 36-38, not only increases the number of identifiable products but also greatly enhances our ability to quantify the PAH products of supercritical *n*-decane pyrolysis.

Using the normal-phase HPLC fractionation / reversed-phase HPLC analysis method, we have quantified, as functions of temperature and pressure, all of the PAH products whose peaks are sufficiently resolved in the fractions' reversed-phase HPLC chromatograms. The yields of the unsubstituted three- to nine-ring PAH products appear as functions of temperature in Figures 40-45 for the 100-atm, 140-sec set of experiments and as functions of pressure in Figures 46-51 for

the 570-°C, 140-sec set of experiments. Even though the unsubstituted 1- and 2-ring aromatics are quantified by GC, as indicated in Figure 3, their yields are included for comparison in Figures 40 and 46.

Table 2. The Numbers of Identified PAH in the Products of Supercritical *n*-Decane Pyrolysis at 100 atm, 570 °C, and 140 sec: Unfractionated and Fractionated Product Mixtures

	Number of Identified PAH Products	
Type of PAH	in unfractionated products of Figure 12	in fractionated products of Figures 13-15
Two-Ring PAH		
unsubstituted	2[#]	2[#]
alkylated (exact)*	18[¶] (2)	48 (2)
Three-Ring PAH		
unsubstituted	2	5
alkylated (exact)*	6 (3)	48 (11)
Four-Ring PAH		
unsubstituted	1	8
alkylated (exact)*	13 (3)	46 (3)
Five-Ring PAH		
unsubstituted	0	6
alkylated	0	24
Six-Ring PAH		
unsubstituted	2	16
alkylated	1	38
Seven-Ring PAH		
unsubstituted	0	6
alkylated (exact)*	0 (0)	10 (1)
Eight-Ring PAH		
unsubstituted	0	3
alkylated	0	10
Nine-Ring PAH		
unsubstituted	0	1
alkylated	0	5
PAH of All Ring Numbers, Summed		
unsubstituted	7	47[#]
alkylated (exact)*	38 (8)	229 (17)
Total Identified PAH	45	276

*The number in parentheses is the number of mono-methylated PAH whose exact position of the methyl group on the PAH structure is known.

[#]The unsubstituted 2-ring product indene is included even though it is determined by GC/FID/MS of the unfractionated product mixture.

[¶]If alkylated indenes were included, the number would be 24 instead of 18.

Using the normal-phase HPLC fractionation / reversed-phase HPLC analysis method, we have quantified, as functions of temperature and pressure, all of the PAH products whose peaks are sufficiently resolved in the fractions' reversed-phase HPLC chromatograms. The yields of the unsubstituted three- to nine-ring PAH products appear as functions of temperature in Figures 40-45 for the 100-atm, 140-sec set of experiments and as functions of pressure in Figures 46-51 for the 570-°C, 140-sec set of experiments. Even though the unsubstituted 1- and 2-ring aromatics are quantified by GC, as indicated in Figure 3, their yields are included for comparison in Figures 40 and 46.

Figures 40-45 reveal that in the 530-to-550-°C temperature range, the yields of all of the one- to four-ring PAH increase moderately with temperature—the PAH of $\geq$ 5 rings not yet present in significant amounts at these lower temperatures. Above 550 °C, however, the yields of PAH of all ring number rise sharply with temperature—the steepest rises exhibited by the highest-ring-number PAH, as temperature approaches 570 °C, the temperature at which solids production becomes noticeable in the 100-atm, 140-sec *n*-decane experiments. The sharp rise in large PAH product yields, just prior to carbonaceous solids production in the supercritical *n*-decane pyrolysis experiments, provides strong evidence that these large PAH are precursors to the solids.

Similarly Figures 46-51 reveal that yields of most of the one- to four-ring PAH at 570 °C and 140 sec increase moderately with pressure from 40 to 60 atm—the PAH of $\geq$ 5 rings not yet present in significant amounts at these lower pressures. Above 60 atm, however, the yields of PAH of all ring number rise sharply with pressure—the steepest rises exhibited by the highest-ring-number PAH, as pressure approaches 100 atm, the pressure at which solids production becomes noticeable in the 575-°C, 140-sec *n*-decane experiments. Again the sharp rise in large PAH product yields, just prior to carbonaceous solids production, provides strong evidence that these large PAH are indeed precursors to the solids.

As evidenced by the plethora of blue structures in the fractions' chromatograms of Figures 36-38, many of the PAH products of supercritical *n*-decane pyrolysis are alkylated. Several of the singly methylated PAH are well-enough resolved chromatographically to permit their quantification as individual products. The blue curves of Figures 52-56 present, in parts a, yields versus temperature at 100 atm and 140 sec and, in parts b, yields versus pressure at 570 °C and 140 sec, for the singly methylated naphthalenes, fluorenes, phenanthrenes, anthracenes, and pyrenes. Yields of the respective unsubstituted PAH products are included, for comparison, as the red curves of Figures 52-56. The figures show that the yields of the methylated PAH increase with temperature and pressure, similarly to those of their unsubstituted counterparts. Except for a couple of cases at the lowest temperatures, within each "family" of PAH of Figures 52-56, for a given experimental condition, the unsubstituted PAH is higher in yield than each of its singly methylated counterparts. However, the sum of the yields of the singly methylated PAH in each family exceeds the yield of the unsubstituted PAH. This fact—along with the observation that lots of the chromatographic area in the fractions' chromatograms of Figures 36-38 is attributed to alkylated PAH that are not singly methylated (blue structures without methyl groups in particular positions)—reveals that most (both in number and in mass) of the PAH products of supercritical *n*-decane pyrolysis are alkylated structures. Because, as Figure 1 indicates, the bond-dissociation energies of alkyl C-C bonds and arylmethyl C-H bonds are relatively low (~85-88 kcal/mole [19]), it is likely that the alkyl substituents on the supercritical *n*-decane product PAH play key roles in the formation of the larger PAH, just as they have been shown to in supercritical 1-methylnaphthalene pyrolysis (Figures 13 and 14) and in supercritical toluene pyrolysis (Figures 22-24). Experiments to be conducted during the succeeding AFOSR grant period should help to establish whether or not this hypothesis is correct.

Results for a Fischer-Tropsch Synthetic Jet Fuel Stressed in a High-Temperature Flow Reactor at AFRL

The normal-phase HPLC fractionation / reversed-phase HPLC analysis technique of Figure 3 has also been applied to the liquid-phase products of another alkane-rich fuel, the Fischer-Tropsch synthetic jet fuel S-8. In this case, the fuel has been stressed thermally in a high-temperature flow reactor at AFRL, and the products provided to us by Dr. Matthew DeWitt and Dr. Tim Edwards at AFRL. After fractionation by sequence 3 in Figure 3, the fractions each have been analyzed by reversed-phase HPLC/UV/MS, permitting the identification and quantification of 30 (13 unsubstituted and 17 alkylated) PAH products of two to five rings. Figure 57 presents the concentration of each of the unsubstituted PAH measured in the stressed Fischer-Tropsch liquid product mixture—each concentration expressed as μg of PAH per ml of initial stressed product mixture supplied to us. Figures 58 and 59, respectively, present the concentrations of phenanthrene and the singly methylated phenanthrenes and of pyrene and the singly methylated pyrenes in the stressed Fischer-Tropsch fuel product mixture. The results of Figures 57-59 have been shared [39] with AFRL, for use in a study that compares deposition behavior of different fuels under supercritical conditions.

Although the stressing conditions for the Fischer-Tropsch fuel do not appear to have been severe enough to have produced measurable quantities of the larger-ring-number PAH produced by *n*-decane in our reactor of Figure 2, there are still some similarities in the results for the Fischer-Tropsch fuel in Figures 57-59 and *n*-decane in Figures 36-38: (1) generally PAH yields fall by orders of magnitude as the number of aromatic rings increases; (2) for a given number of rings, certain isomer families are produced in higher yield than others (*e.g.*, yields of the four-ring $C_{16}H_{10}$ PAH are an order of magnitude higher than those of the four-ring $C_{18}H_{12}$ PAH); and (3) within a given isomer group, certain PAH are produced in higher yield than others (*e.g.*, among

the $C_{16}H_{10}$ PAH, pyrene is produced in higher yield than is fluoranthene). Therefore it is anticipated that any advances we can make in the understanding of PAH formation from the supercritical pyrolysis of model alkane fuels will also be directly applicable to the supercritical pyrolysis of alkane-rich fuel mixtures such as the Fischer-Tropsch synthetic jet fuel.

Executive Summary

Summary of Results

Using an isothermal, isobaric reactor specially designed for such purposes, we have conducted supercritical pyrolysis experiments with three model fuels: 1-methylnaphthalene, a two-ring aromatic component of jet fuel; toluene, a single-ring component of jet fuel; and *n*-decane, an alkane component of both conventional and synthetic jet fuels. The products of the experiments have been analyzed by gas chromatography and high-pressure liquid chromatography with diode-array ultraviolet-visible absorption detection, a technique ideally suited to the analysis of PAH, precursors to fuel-line deposits in future high-speed aircraft applications.

Two sets of supercritical pyrolysis experiments have been conducted with the model fuel 1-methylnaphthalene (critical temperature, 499 °C; critical pressure, 36 atm): one at 585 °C, 140 sec, and seven pressures from 50 to 110 atm; the other at 80 atm, 140 sec, and six temperatures from 550 to 600 °C. The products from the first set of experiments have been quantified as functions of pressure; those from the second set, as functions of temperature. Results from the first set of experiments show that at 585 °C and 140 sec, yields of 5-, 6-, and 7-ring PAH increase linearly with pressure; yields of the 8- and 9-ring PAH also rise with pressure but at a rate that increases as pressure increases. Results from the second set of experiments show that at 80 atm and 140 sec, yields of all of the PAH products increase with temperature—the rate of increase rising with temperature for most of the PAH, especially at temperatures > 580 °C. Product-yield

sensitivity to temperature is particularly high for the highest-ring-number PAH, the immediate precursors to the carbonaceous solids that begin forming at 600 °C, the highest temperature in the 80-atm set of experiments. The jump in yields of large PAH, just at the point where carbonaceous solids begin to be made, underscores the role of these large PAH as precursors to the solids.

Two sets of supercritical pyrolysis experiments have also been conducted with the model fuel toluene (critical temperature, 319 °C; critical pressure, 41 atm): one at 685 °C, 140 sec, and four pressures from 50 to 100 atm; the other at 100 atm, 140 sec, and six temperatures from 550 to 685 °C. The products of these experiments have not yet been quantified, but a qualitative analysis shows that at 685 °C and 140 sec, increasing pressure effects a moderate increase in PAH production. Temperature, on the other hand, drastically influences PAH production at 100 atm and 140 sec: No PAH of > 3 rings are detected at temperatures $\leq$ 625 °C; as temperature is raised from 650 to 685 °C, however, production of 5-ring PAH steadily increases.

Because toluene does not form solids as readily as the other model fuels, supercritical pyrolysis experiments with toluene have been able to be conducted at 140 sec, 75 atm, and 700 °C, the highest temperature to which our reactor can go, with the higher-temperature heater purchased on this AFOSR grant. At these newly achieved higher-temperature conditions, several five-ring PAH are produced—five of which have never before been identified as products of toluene pyrolysis or combustion: indeno[1,2-*b*]fluorene, naphtho[2,1-*a*]fluorene, naphtho[1,2-*b*]fluorene, naphtho[2,3-*a*]fluorene, and naphtho[2,3-*b*]fluorene.

Our results from the experiments with both 1-methylnaphthalene and toluene show that for aromatic fuels, the aromatic C-C bond cannot be broken even at the highest temperature of our supercritical pyrolysis reactor, 700 °C, and that all of the product PAH can be "built" from sequential additions of the aromatic units plentiful in the respective environments: two-ring aromatic units in the case of the two-ring aromatic fuel 1-methylnapthalene [15,31]; one-ring

aromatic units in the case of the one-ring aromatic fuel toluene [14]. (Alkyl fragments plentiful in the reaction environment (methyl in the case of either 1-methylnaphthalene or toluene) may also participate with the aromatic units in the reaction sequence.) Even though these results have been obtained from supercritical pyrolysis experiments with the 1- and 2-ring aromatic fuels themselves, they apply to the supercritical pyrolysis of all hydrocarbon fuels, including alkanes and cyclic alkanes, since all of these fuels produce one- and two-ring aromatics during supercritical pyrolysis.

In order to analyze the extremely complex mixture of multi-alkylated PAH produced from our third model fuel *n*-decane, we have developed a normal-phase HPLC fractionation / reversed-phase HPLC analysis technique. Compared to reversed-phase HPLC analysis alone, the normal-phase HPLC fractionation / reversed-phase HPLC analysis method brings about a six-fold increase (from 45 to 276) in the number of PAH identified in the products of supercritical *n*-decane pyrolysis. When fractionation is employed, the total number of unsubstituted PAH identified is increased from 7 to 47, and the number of alkylated PAH identified is increased from 38 to 229. The effects of the fractionation are even more dramatic for the higher-ring number PAH products: Without the normal-phase HPLC fractionation, only three PAH of $\geq$ 5 rings are identifiable in the supercritical *n*-decane pyrolysis products; with fractionation, 117 PAH of 5 to 9 rings (30 unsubstituted; 87 alkylated) are identifiable. This ability to determine the structures of the larger PAH products should be particularly helpful in the elucidation of the reaction pathways responsible for large PAH—and ultimately solids—formation from alkane fuels.

Two sets of supercritical pyrolysis experiments have been conducted with *n*-decane (critical temperature, 345 °C; critical pressure, 20.8 atm): one at 100 atm, 140 sec, and six temperatures from 530 to 570 °C; the other at 570 °C, 140 sec, and six pressures from 40 to 100 atm. Products from the first set of experiments have been quantified as functions of temperature; those from the

second set, as functions of pressure. Results from the first set of experiments reveal that at 100 atm and 140 sec, yields of all of the one- to four-ring PAH increase moderately with temperature from 530 to 550 °C—the PAH of $\geq$ 5 rings not yet present in significant amounts at these lower temperatures. Above 550 °C, however, the yields of PAH of all ring number rise sharply with temperature—the steepest rises exhibited by the highest-ring-number PAH, as temperature approaches 570 °C, the temperature at which solids production becomes noticeable in the 100-atm, 140-sec *n*-decane experiments. Results from the second set of experiments reveal that at 570 °C and 140 sec, yields of most of the one- to four-ring PAH increase moderately with pressure from 40 to 60 atm—the PAH of $\geq$ 5 rings not yet present in significant amounts at these lower pressures. Above 60 atm, however, the yields of PAH of all ring number rise sharply with pressure—the steepest rises exhibited by the highest-ring-number PAH, as pressure approaches 100 atm, the pressure at which solids production becomes noticeable in the 575-°C, 140-sec *n*-decane experiments. The sharp rise in large PAH product yields, just prior to carbonaceous solids production in the supercritical *n*-decane pyrolysis experiments, provides strong evidence that these large PAH are indeed precursors to the solids. The mechanisms responsible for large PAH formation in supercritical fuel pyrolysis environments are a major focus of our research in the succeeding AFOSR grant.

We have also applied the newly developed normal-phase HPLC fractionation / reversed-phase HPLC analysis technique to a set of Fischer-Tropsch synthetic jet fuel samples thermally stressed in a high-temperature flow reactor at AFRL and provided to us by Dr. Matthew DeWitt and Dr. Tim Edwards at AFRL. Thirty PAH products (13 unsubstituted and 17 alkylated) of two to five rings have been identified and quantified in the sample subjected to the highest stressing conditions. These results have been shared with AFRL, for use in a study that compares deposition behavior of different fuels under supercritical conditions.

Although the stressing conditions for the Fischer-Tropsch fuel do not appear to have been severe enough to have produced measurable quantities of the larger-ring-number PAH produced by *n*-decane in our supercritical pyrolysis reactor, several similarities exist between these two fuels, with regard to the smaller-ring-number PAH produced. Therefore it is anticipated that any advances we can make in the understanding of PAH formation from the supercritical pyrolysis of model alkane fuels will also be directly applicable to the supercritical pyrolysis of alkane-rich fuel mixtures such as the Fischer-Tropsch synthetic jet fuel.

Personnel who Performed the Research

Principal Investigator: Professor Mary Julia Wornat

Post-Doctoral Research Associates: Dr. Xia Zhang (approximately one month), Davis Maliakal (slightly less than two years), Dr. Jorge Oña (approximately one year).

Graduate Students: Mr. Jorge O. Oña and Mr. Sean Bagley, supported by grant at different times; Ms. Michelle L. Somers and Mr. Khue Nguyen, supported by LSU Department of Chemical Engineering at different times.

Publications and Presentations

Refereed publications reporting results from the research supported by this grant

Walker, M. S., and Wornat, M. J., "First Identification of Benzo[*cd*]phenanthro[1,2,3-*lm*]perylene by High-Pressure Liquid Chromatography with Ultraviolet-Visible Spectroscopy and Mass Spectrometry," *Journal of Chromatography A 1217:* in press (2010).

Oña, J. O., and Wornat, M. J., "The Influence of Solvents on the Ultraviolet-Visible Absorption Spectra of Polycyclic Hydrocarbons: Applications in the Identification of Fuel Products by HPLC/UV/MS," *Polycyclic Aromatic Compounds 28:* 15-38 (2008).

Somers, M. L., and Wornat, M. J., "UV Spectral Identification of Polycyclic Aromatic Hydrocarbon Products of Supercritical 1-Methylnaphthalene Pyrolysis," *Polycyclic Aromatic Compounds 27:* 261-280 (2007).

Oña, J. O., and Wornat, M. J., "Identification of the $C_{30}H_{16}$ Polycyclic Aromatic Hydrocarbon Benzo[*cd*]naphtho[1,2,3-*lm*]perylene as a Product of Supercritical Pyrolysis of a Synthetic Jet Fuel," *Polycyclic Aromatic Compounds 27:* 165-183 (2007).

McClaine, J. W., and Wornat, M. J., "Reaction Mechanisms Governing the Formation of Polycyclic Aromatic Hydrocarbons in the Supercritical Pyrolysis of Toluene: $C_{28}H_{14}$ Isomers,"

Journal of Physical Chemistry C 111: 86-95 (2007).

McClaine, J. W., Oña, J. O., and Wornat, M. J., "Identification of a New $C_{28}H_{14}$ Polycyclic Aromatic Hydrocarbon as a Product of Supercritical Fuel Pyrolysis: Tribenzo[*cd,ghi,lm*]perylene," *Journal of Chromatography A 1138:* 175-183 (2007).

Somers, M. L., McClaine, J. W., and Wornat, M. J., "The Formation of Polycyclic Aromatic Hydrocarbons from the Supercritical Pyrolysis of 1-Methylnaphthalene," *Proceedings of the Combustion Institute 31:* 501-509 (2007).

Doctoral theses produced from research supported by this grant

Walker, M. S., *Supercritical Pyrolysis of 1-Methylnaphthalene*, Ph.D. Thesis, Department of Chemical Engineering, Louisiana State University, 2009.

Oña, J. O., *Identification of Polycyclic Aromatic Hydrocarbons in the Supercritical Pyrolysis Products of Synthetic Jet Fuel S-8 and Methylcyclohexane*, Ph.D. Thesis, Department of Chemical Engineering, Louisiana State University, 2008.

Conference presentations reporting results from the research supported by this grant

Bagley, S. P., and Wornat, M. J., "PAH Formation Mechanisms from Supercritical *n*-Decane Pyrolysis," accepted as a work-in-progress poster at the Thirty-Third International Symposium on Combustion, Beijing, China, August, 2010.

Nguyen, K., and Wornat, M. J., "The Effect of Temperature on the Distribution of Polycyclic Aromatic Hydrocarbons Produced from Supercritical Toluene Pyrolysis," accepted as a work-in-progress poster at the Thirty-Third International Symposium on Combustion, Beijing, China, August, 2010.

Bagley, S.P., and Wornat, M. J., "Formation of Polycyclic Aromatic Hydrocarbons from the Supercritical Pyrolysis of *n*-Decane," Twenty-Second International Symposium on Polycyclic Aromatic Compounds, Charleston, South Carolina, September, 2009.

Oña-Ruales, J. O., Maliakal, D., and Wornat, M. J., "Identification of Polycyclic Aromatic Hydrocarbons from the Supercritical Pyrolysis of Toluene," Twenty-Second International Symposium on Polycyclic Aromatic Compounds, Charleston, South Carolina, September, 2009.

Wornat, M. J., "Supercritical Fuel Pyrolysis," oral presentation at the Multi Agency Coordination Committee for Combustion Research Fuels Summit, Los Angeles, California, September, 2009.

Wornat, M. J., "Supercritical Fuel Pyrolysis," oral presentation at the Multi Agency Coordination Committee for Combustion Research Fuels Summit, Gaithersburg, Maryland, September, 2008.

Bagley, S. P., and Wornat, M. J., "Formation of PAH from the Supercritical Pyrolysis of *n*-Decane," Thirty-Second International Symposium on Combustion, Montreal, Canada, August, 2008.

Somers, M. L., and Wornat, M. J., "The Effects of Pressure on the Yields of Polycyclic Aromatic Hydrocarbons During the Supercritical Pyrolysis of 1-Methylnaphthalene," Thirty-Second International Symposium on Combustion, Montreal, Canada, August, 2008.

Oña, J. O., and Wornat, M. J., "Prediction of the Carcinogenic Activity of Two Large PAH Produced from the Supercritical Pyrolysis of Synthetic Jet Fuel S-8," Two-Hundred Thirty-Fifth National Meeting of the American Chemical Society, New Orleans, April, 2008.

Wornat, M. J., "High-Pressure Liquid Chromatography with Diode-Array Ultraviolet-Visible Absorption Detection for the Analysis of Polycyclic Aromatic Hydrocarbons in Complex Fuel Product Mixtures," invited lecture at the Fifty-Ninth Pittsburgh Conference on Analytical Chemistry and Applied Spectroscopy, New Orleans, March, 2008.

Oña, J. O., and Wornat, M. J., "Identification of Polycyclic Aromatic Hydrocarbons from the Supercritical Pyrolysis of Fischer-Tropsch Synthetic Jet Fuel S-8 by Means of HPLC/UV/MS and Annellation Theory," Two-Hundred Thirty-Fourth National Meeting of the American Chemical Society, Boston, August, 2007.

Oña, J. O., and Wornat, M. J., "The Identification of Polycyclic Aromatic Hydrocarbons from the Supercritical Pyrolysis of Synthetic Jet Fuel S-8," Twenty-First International Symposium on Polycyclic Aromatic Compounds, Trondheim, Norway, August, 2007.

Bagley, S. P., and Wornat, M. J., "Formation of Polycyclic Aromatic Hydrocarbons from the Pyrolysis of *n*-Decane," Twenty-First International Symposium on Polycyclic Aromatic Compounds, Trondheim, Norway, August, 2007.

Somers, M. L., and Wornat, M. J., "Dibenzofluorenes and Benzenoid PAH Formed from Supercritical 1-Methylnaphthalene Pyrolysis," Twenty-First International Symposium on Polycyclic Aromatic Compounds, Trondheim, Norway, August, 2007.

Oña, J. O., and Wornat, M. J., "Identification of Perylene Benzologues in the Products of Supercritical Pyrolysis of a Fischer-Tropsch Synthetic Jet Fuel," Fifty-Eighth Pittsburgh Conference on Analytical Chemistry and Applied Spectroscopy, Chicago, February-March, 2007.

Oña, J. O., and Wornat, M. J., "The Influence of Solvents on the UV Spectra of Polycyclic Aromatic Hydrocarbons: Applications in the Identification of Fuel Products by HPLC/UV/MS," Fifty-Eighth Pittsburgh Conference on Analytical Chemistry and Applied Spectroscopy, Chicago, February-March, 2007.

References

1. T. Edwards, S. Zabarnick, *Industrial and Engineering Chemistry Research* 32 (1993) 3117-3122.

2. S. P. Heneghan, S. Zabarnick, D. R. Ballal, W. E. Harrison III, *Journal of Energy Resources Technology* 118 (1996) 170-179.

3. T. Doungthip, J. S. Ervin, T. F. Williams, J. Bento, *Industrial and Engineering Chemistry Research* 41 (2002) 5856-5866.

4. T. Edwards, *Combustion Science and Technology* 178 (2006) 307-334.

5. T. Edwards, personal communication, AFRL, Wright-Patterson, Ohio, June 12, 2002.

6. C. F. Melius, N. E. Bergan, J. E. Shepherd, *Proceedings of the Combustion Institute* 23 (1990) 217-223.

7. K. P. Johnston, C. Haynes, *AIChE Journal* 33 (1987) 2017-2026.

8. M. E. Paulaitis, G. C. Alexander, *Pure and Applied Chemistry* 59 (1987) 61-68.

9. R. H. Helling, J. W. Tester, *Energy & Fuels* 1 (1987) 417-423.

10. C. A. Eckert, B. E. Knutson, P. G. Debenedetti, *Nature* 383 (1996) 313-318.

11. J. F. Stewart, *Supercritical Pyrolysis of Endothermic Fuels*. Ph.D. Thesis, Department of Mechanical and Aerospace Engineering, Princeton University, 1999.

12. J. F. Stewart, K. Brezinsky, I. Glassman, *Combustion Science and Technology* 136 (1998) 373-390.

13. E. B. Ledesma, M. J. Wornat, P. G. Felton, J. A. Sivo, *Proceedings of the Combustion Institute* 30 (2005) 1371-1379.

14. J. W. McClaine, M. J. Wornat, *Journal of Physical Chemistry C* 111 (2007) 86-95.

15. M. L. Somers, J. W. McClaine, M. J. Wornat, *Proceedings of the Combustion Institute* 31 (2007) 501-509.

16. H. Bockhorn, F. Fetting, H. W. Wenz, *Berichte der Bunsen-Gesellschaft—Physical Chemistry Chemical Physics* 87 (1983) 1067-1073.

17. M. Frenklach, D. W. Clary, W. C. J. Gardiner, S. E. Stein, *Proceedings of the Combustion Institute* 20 (1984) 887-901.

18. H. Wang, M. Frenklach, *Combustion and Flame* 110 (1997) 173-221.

19. Y.-R. Luo, *Handbook of Bond Dissociation Energies in Organic Chemistry.* CRC Press, Boca Raton, FL, 2003, pp. 38, 39, 110.

20. R. T. Sanderson, *Chemical Bonds in Organic Compounds.* Sea and Sand, Scottsdale, AZ, 1976, Chapter 8.

21. M. Bernabei, R. Reda, R. Galiero, G. Bocchinfuso, *Journal of Chromatography A* 985 (2003) 197-203.

22. G. D. Davis, *An Experimental Study of Supercritical Methylcyclohexane Pyrolysis*. M.S.E. Thesis, Department of Mechanical and Aerospace Engineering, Princeton University, 1994.

23. S. Darrah, "Jet Fuel Deoxygenation," AFWAL-TR-88-2081 (1988).

24. A. H. Cutler, M. J. Antal, M. Jones, *Industrial and Engineering Chemistry Research* 27 (1988) 691-697.

25. J. C. Y. Lee, *Simulations of Two-Dimensional Chemically Reactive Flows: Flow Past a Fuel Particle and Inside a Reactor Tube.* Ph.D. Thesis, Department of Mechanical and Aerospace Engineering, Princeton University, 1996.

26. R. N. Jones, *Journal of the American Chemical Society* 67 (1945) 2127-2150.

27. J. C. Fetzer, *Large (C>=24) Polycyclic Aromatic Hydrocarbons: Chemistry and Analysis*. Wiley-Interscience, New York, 2000.

28. E. V. Dose, G. Guiochon, *Analytical Chemistry* 61 (1989) 2571-2579.

29. M. J. Wornat, Final Performance Report for AFOSR Grant No. FA9550-04-1-0005 (2007).

30. M. L. Somers, M. J. Wornat, *Polycyclic Aromatic Compounds* 27 (2007) 261-280.

31. M. S. Walker, M. J. Wornat, *Journal of Chromatography A* 1217 (2010) in press.

32. N. P. Buu-Hoi, C. Marie, and P. Jacquignon, *Bulletin de la Société Chimique de France* 11 (1970) 3958-3962.

33. W. V. Mayneord, E. M. F. Roe, *Proceedings of the Royal Society of London. Series A, Mathematical and Physical Sciences* 152 (1935) 299-324.

34. W. V. Mayneord, E. M. F. Roe, *Proceedings of the Royal Society of London. Series A, Mathematical and Physical Sciences* 158 (1937) 634-650.

35. L. Chardonnens, L. Salamin, *Helvetica Chimica Acta* 51 (1968) 1095-1102.

36. B. M. Fabuss, J. O. Smith, R. I. Lait, A. S. Borsanyi, C. N. Satterfield, *Industrial & Engineering Chemistry Process Design and Development* 1 (1962) 293-299.

37. E. J. Clar, *Polycyclic Hydrocarbons*, volume 2, Academic Press, New York, 1964.

38. S. P. Bagley, *Supercritical Pyrolysis of n-Decane*, Ph.D. Thesis, Department of Chemical Engineering, Louisiana State University, in preparation 2010.

39. M. J. Wornat, e-mail communication to M. J. DeWitt and T. Edwards, September 10, 2009.

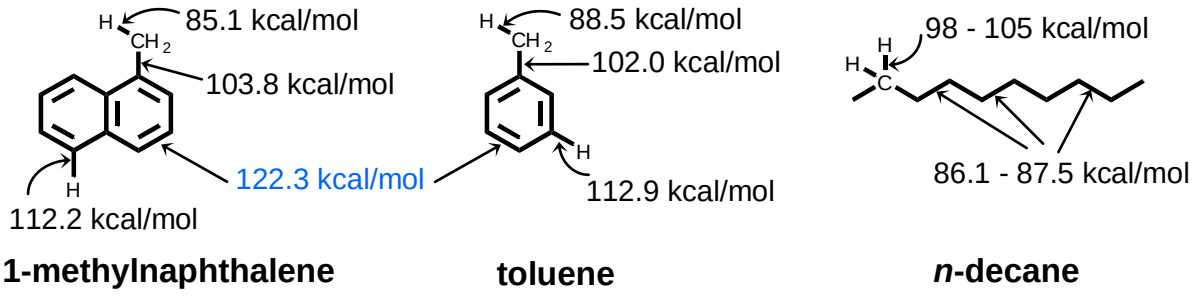

Figure 1. Molecular structures and bond-dissociation energies [19,20] for three model fuels used in the supercritical fuel pyrolysis experiments: 1-methylnaphthalene, toluene, and *n*-decane.

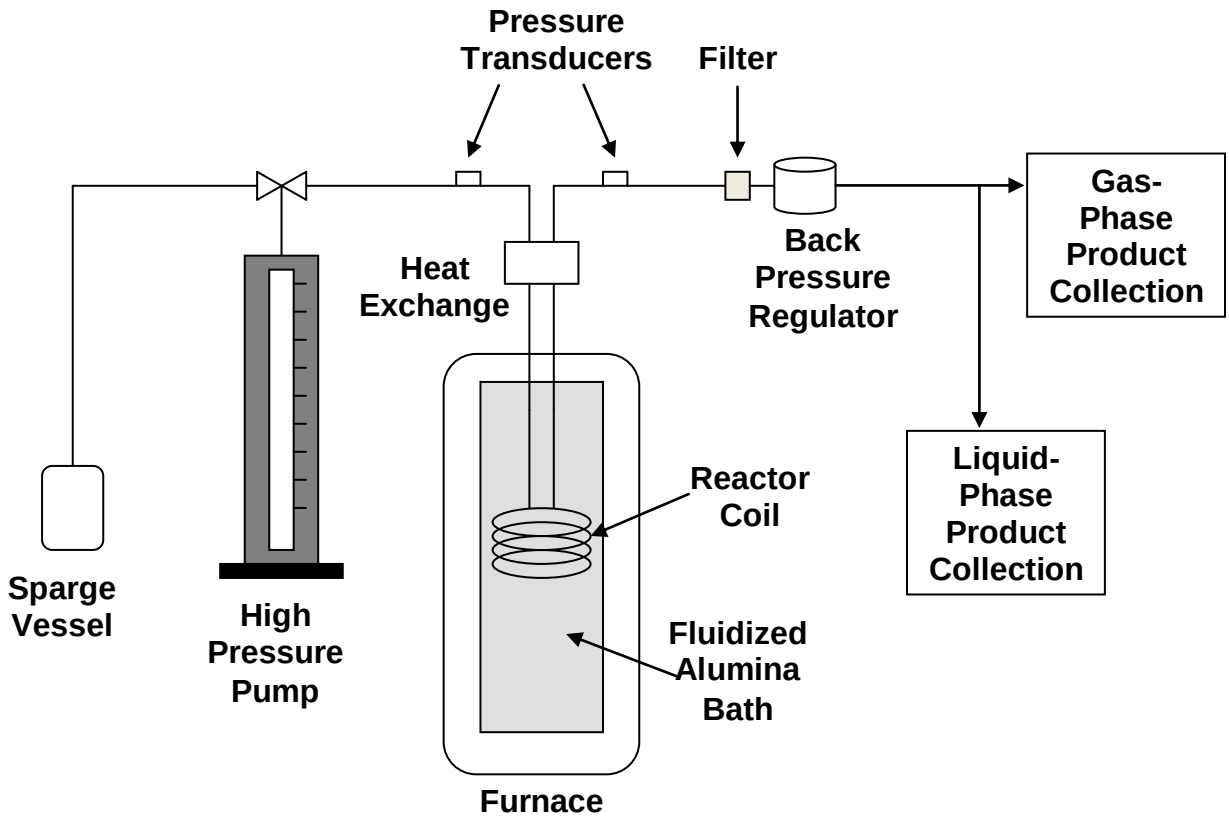

Figure 2. Supercritical fuel pyrolysis reactor system.

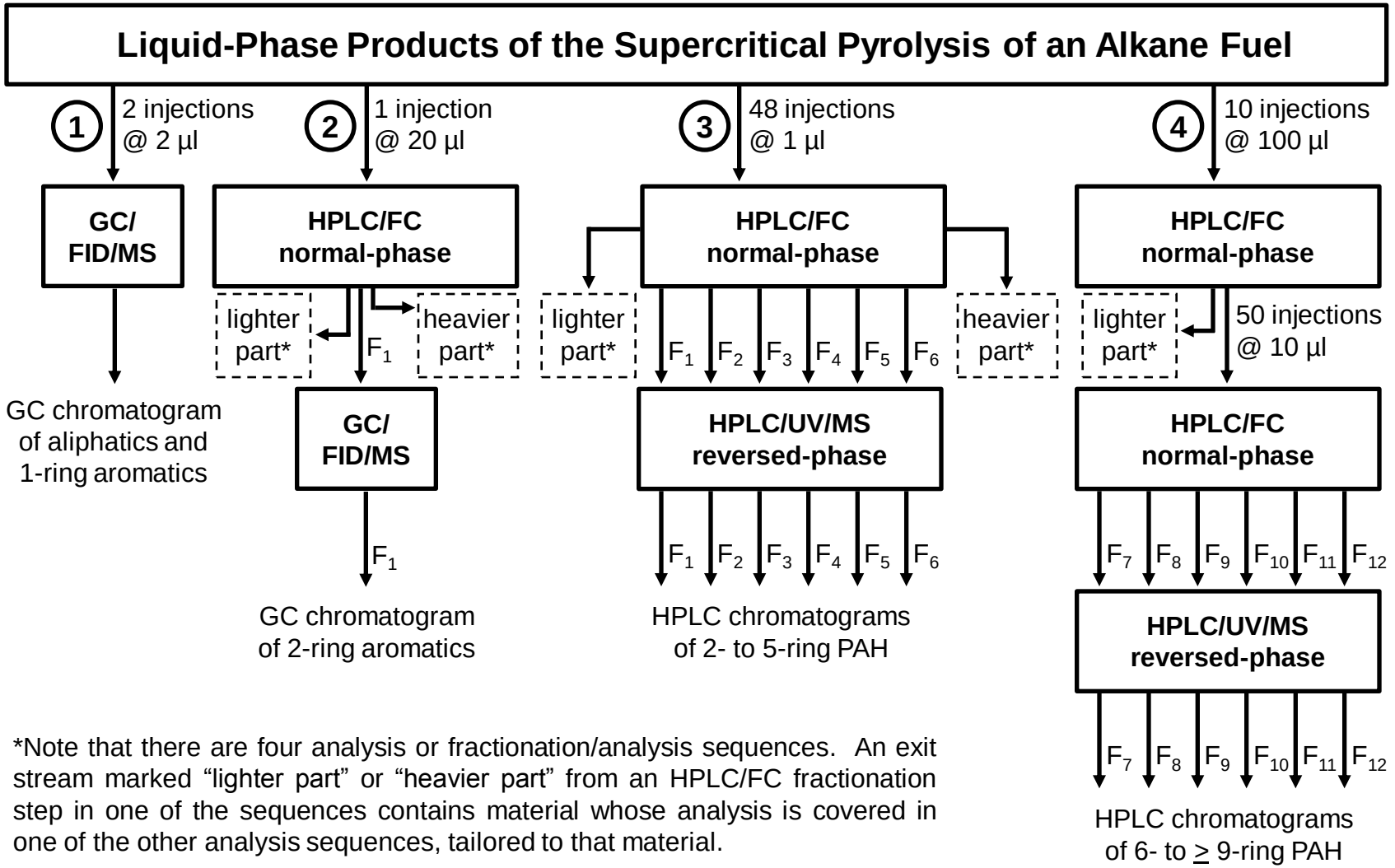

Figure 3. The fractionation and analysis scheme for the liquid-phase products of the supercritical pyrolysis of alkane fuels. Large circled numbers denote sequence number. “F_x” denotes “fraction number x.” For a product mixture from one reactor condition, 81 total hours of HPLC/FC instrument time are needed for all of the fractionation steps to make the twelve fractions, and 36 total hours of HPLC/UV/MS instrument time are needed for the analysis of the twelve fractions.

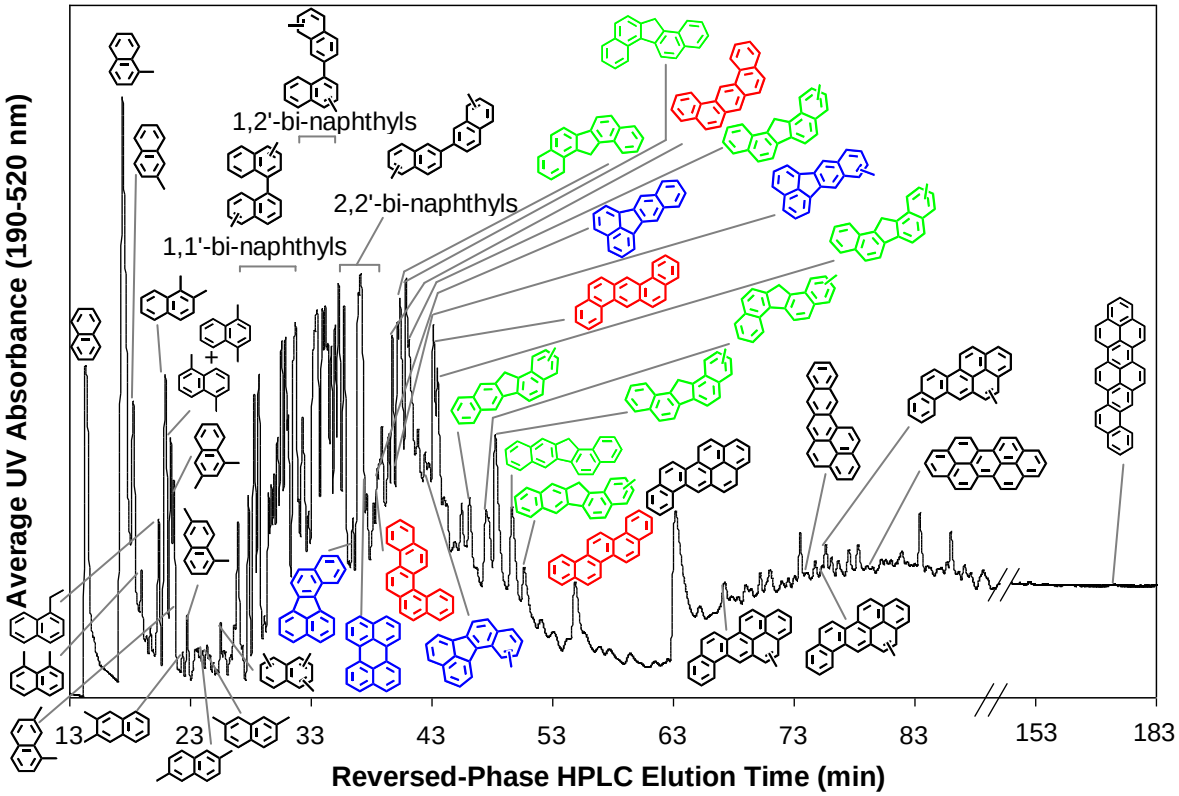

Figure 4. Reversed-phase HPLC chromatogram of products of 1-methylnaphthalene pyrolyzed at 585 °C, 110 atm, and 140 sec. The rise in baseline at 63 minutes corresponds to a change in mobile-phase composition to UV-absorbing dichloromethane. Identified products are listed by class, in order of elution. Classes 1 and 2 (in black): naphthalene; 1-methylnaphthalene; 2-methylnaphthalene; 1,8-dimethylnaphthalene; 1-ethylnaphthalene; 1,2-dimethylnaphthalene; 1,4- and 1,5-dimethylnaphthalene; 1,3- and 1,7-dimethylnaphthalene; 2,3-dimethylnaphthalene; 1,6-dimethylnaphthalene; 2,6-dimethylnaphthalene; 2,7-dimethylnaphthalene; trimethylnaphthalene; 1,1′-bi-naphthyls; 1,2′-bi-naphthyls; 2,2′-bi-naphthyls. Class 3 (blue): benzo[*j*]fluoranthene; perylene; benzo[*k*]fluoranthene; methylbenzo[*k*]fluoranthene; methylbenzo[*j*]fluoranthene. Class 4 (green): dibenzo[*a,i*]fluorene; dibenzo[*a,g*]fluorene; methyldibenzo[*a,i*]fluorene; methyldibenzo[*a,i*]fluorene; methyldibenzo[*a,h*]fluorene; methyldibenzo[*a,g*]fluorene; methyldibenzo[*a,i*]fluorene; dibenzo[*a,h*]fluorene; methyldibenzo[*a,h*]fluorene. Class 5 (red): benzo[*c*]chrysene; dibenz[*a,j*]anthracene; dibenz[*a,h*]anthracene; picene. Class 6 (black): naphtho[2,1-*a*]pyrene; methylnaphtho[2,1-*a*]pyrene; naphtho[2,3-*a*]pyrene; methylnaphtho[2,1-*a*]pyrene; methylnaphtho[2,1-*a*]pyrene; dibenzo[*cd,lm*]perylene; and benzo[*cd*]phenanthro[1,2,3-*lm*]perylene. Results from Somers, *et al* [15,30,31].

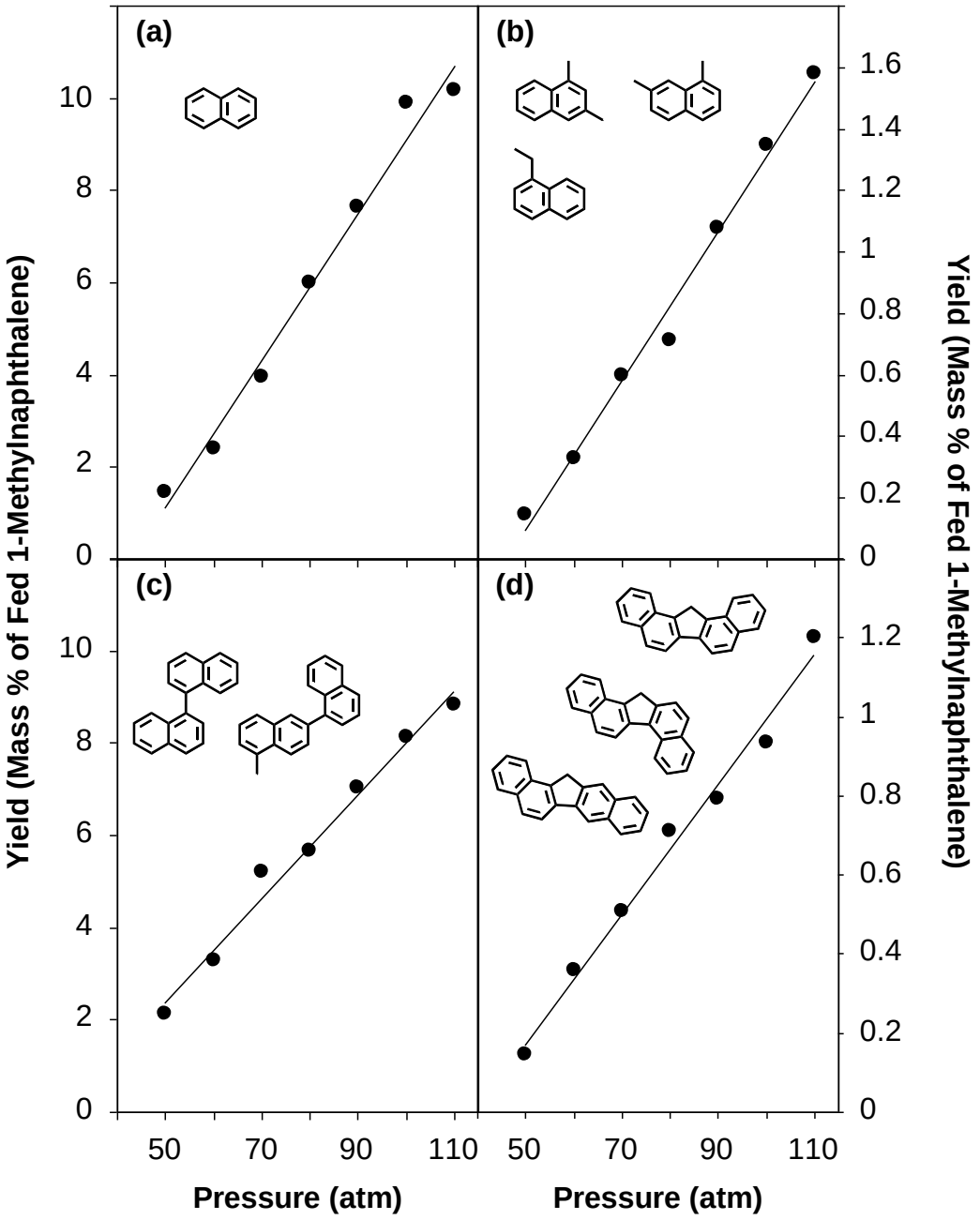

Figure 5. Yields, as functions of pressure, of PAH products of supercritical 1-methylnaphthalene pyrolysis at 585 °C and 140 sec: (a) naphthalene; (b) ethylnaphthalene and dimethyl-naphthalenes summed; (c) bi-naphthyls and methylated bi-naphthyls summed; and (d) dibenzofluorenes summed.

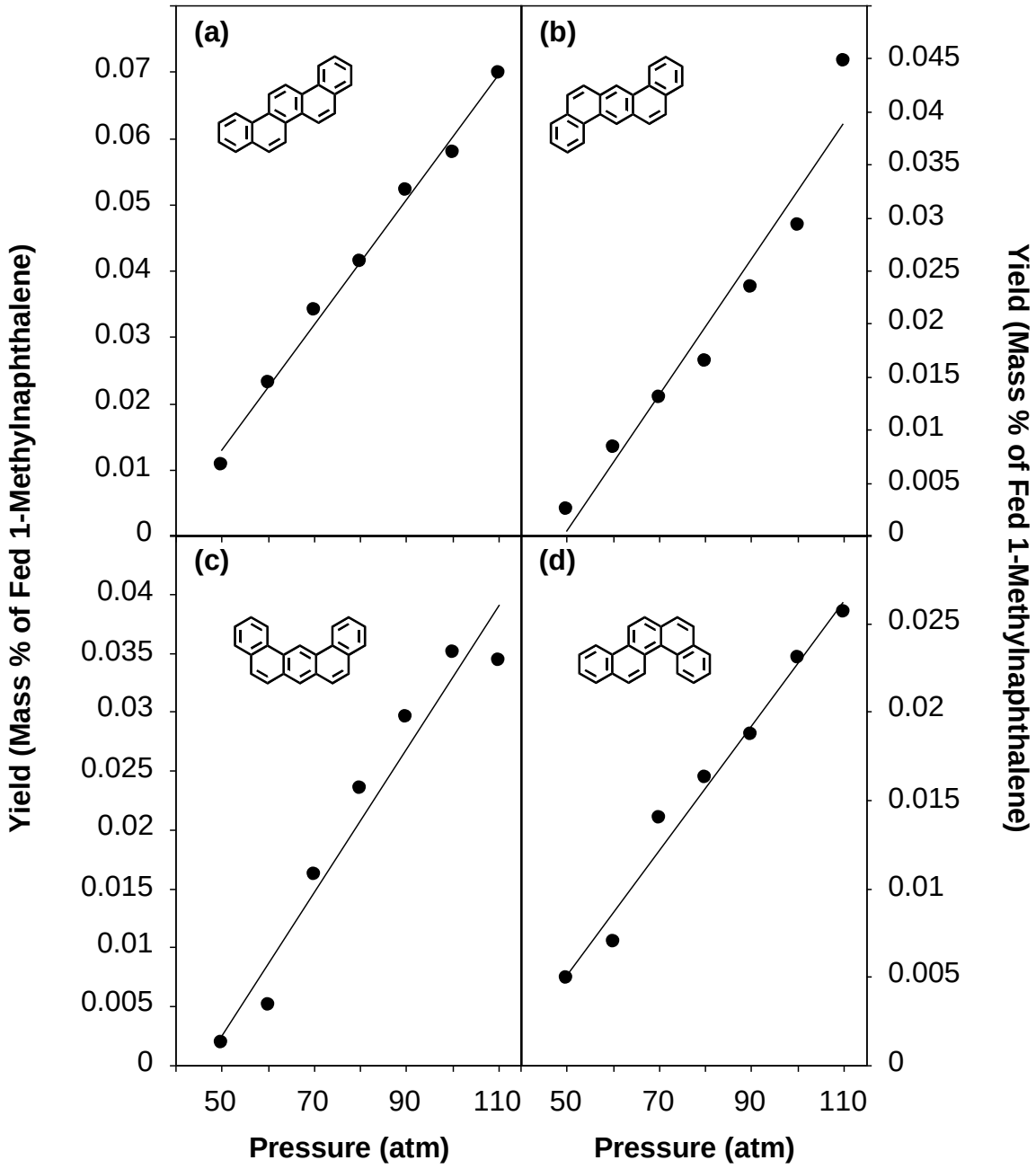

Figure 6. Yields, as functions of pressure of the five-ring $C_{22}H_{14}$ PAH products of supercritical 1-methylnaphthalene pyrolysis at 585 °C and 140 sec: (a) picene; (b) dibenz[*a*,*h*]anthracene; (c) dibenz[*a*,*j*]anthracene; and (d) benzo[*c*]chrysene.

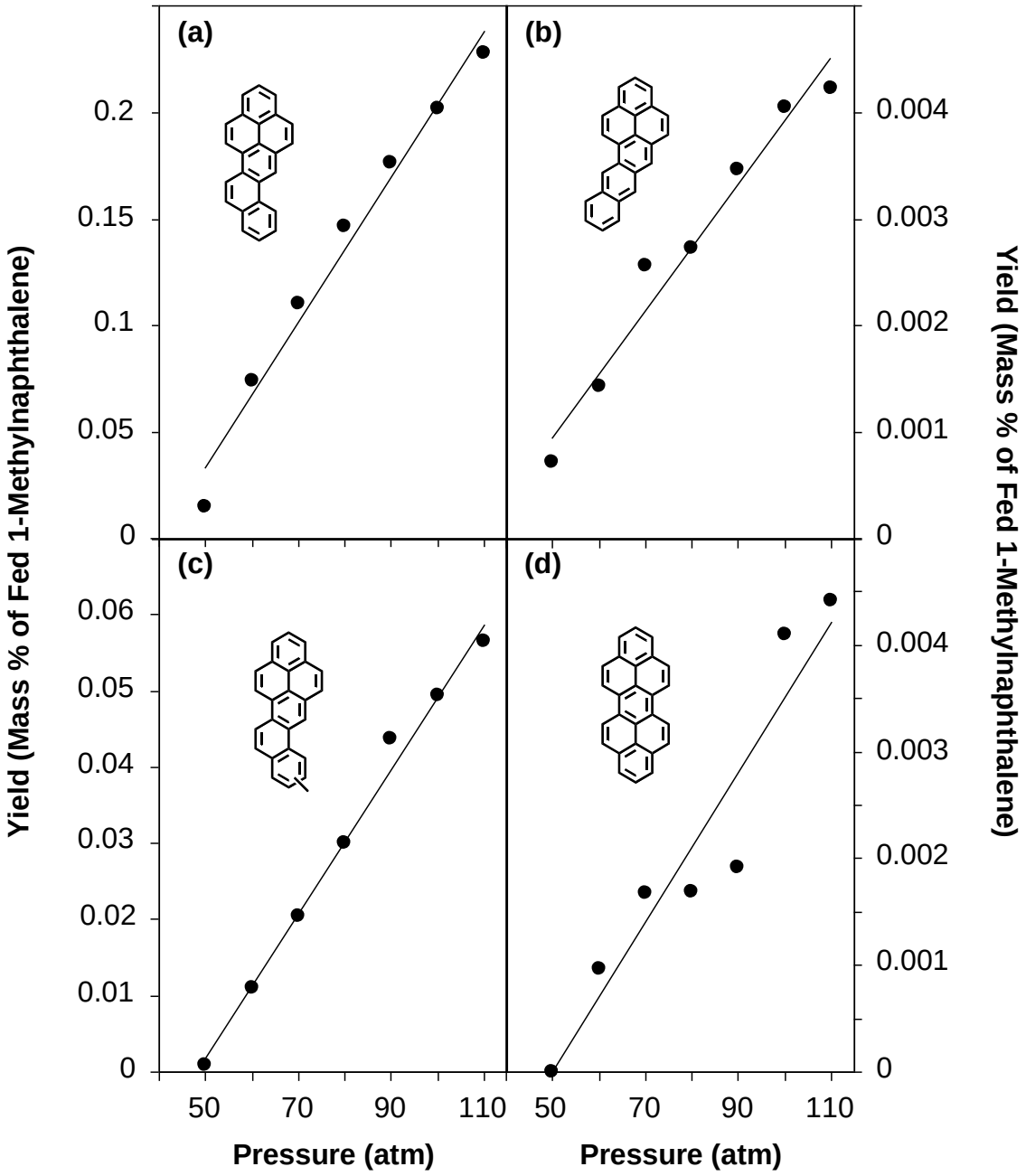

Figure 7. Yields, as functions of pressure, of 6- and 7-ring PAH products of supercritical 1-methylnaphthalene pyrolysis at 585 °C and 140 sec: (a) naphtho[2,1-*a*]pyrene; (b) naphtho[2,3-*a*]pyrene; (c) methylnaphtho[2,1-*a*]pyrenes summed; and (d) dibenzo[*cd*,*lm*]perylene.

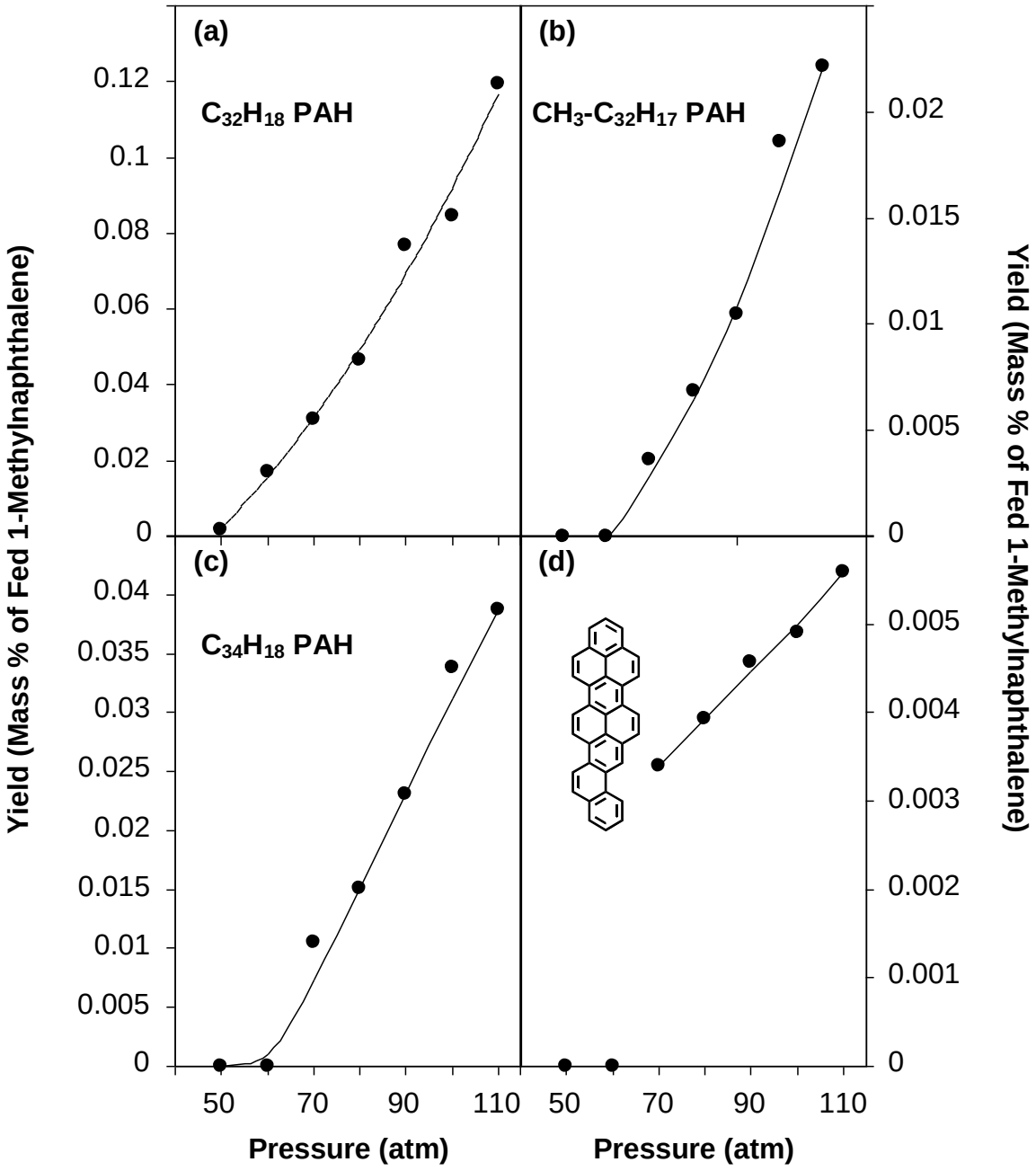

Figure 8. Yields, as functions of pressure, of eight- and nine-ring PAH products of supercritical 1-methylnaphthalene pyrolysis at 585 °C and 140 sec: (a) eight-ring $C_{32}H_{18}$ PAH summed; (b) eight-ring CH_3-$C_{32}H_{17}$ PAH summed; (c) nine-ring $C_{34}H_{18}$ PAH summed; and (d) benzo[*cd*]phenanthro[1,2,3-*lm*]perylene.

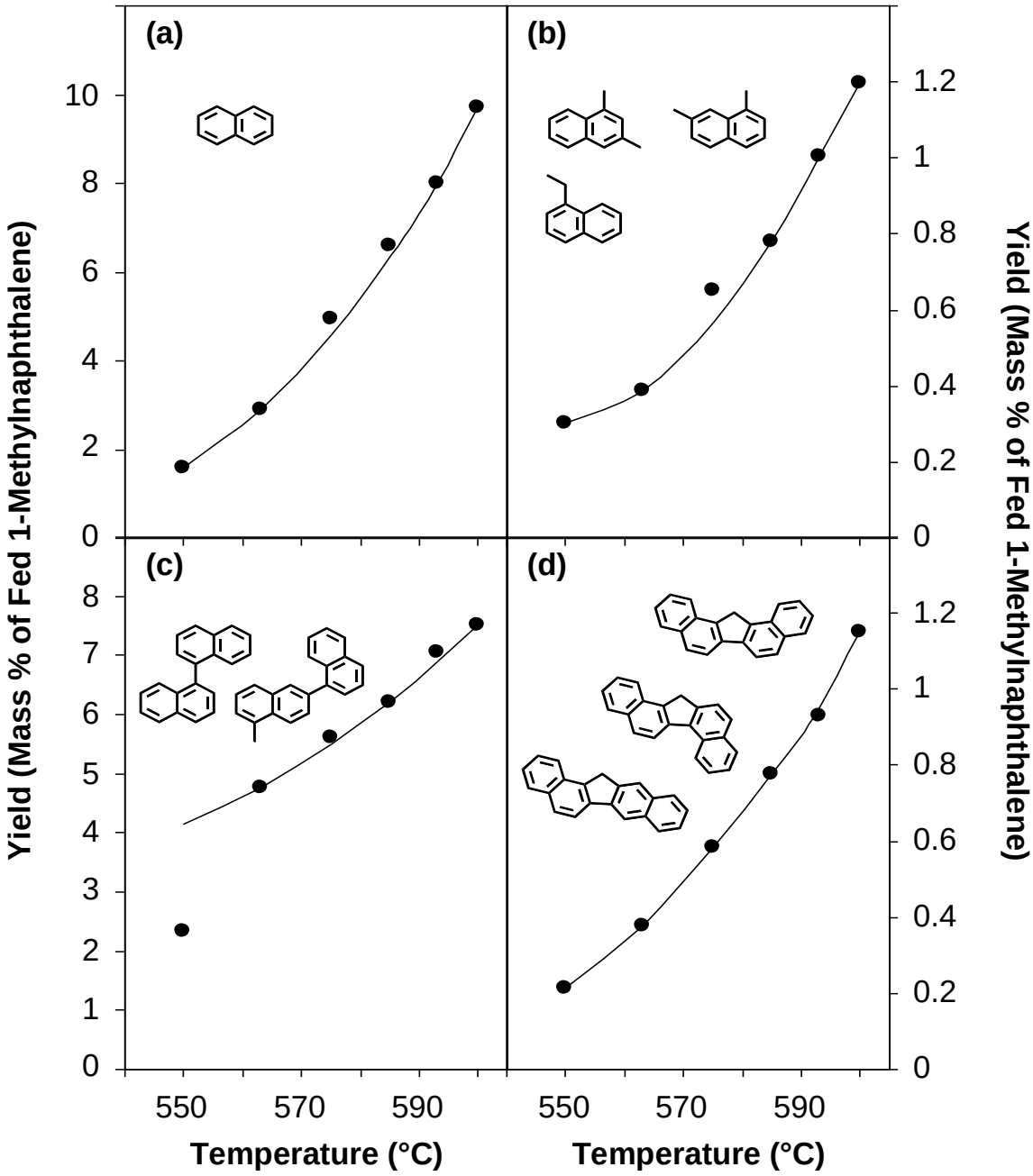

Figure 9. Yields, as functions of temperature, of PAH products of supercritical 1-methylnaphthalene pyrolysis at 80 atm and 140 sec: (a) naphthalene; (b) ethylnaphthalene and dimethyl-naphthalenes summed; (c) bi-naphthyls and methylated bi-naphthyls summed; and (d) dibenzofluorenes summed.

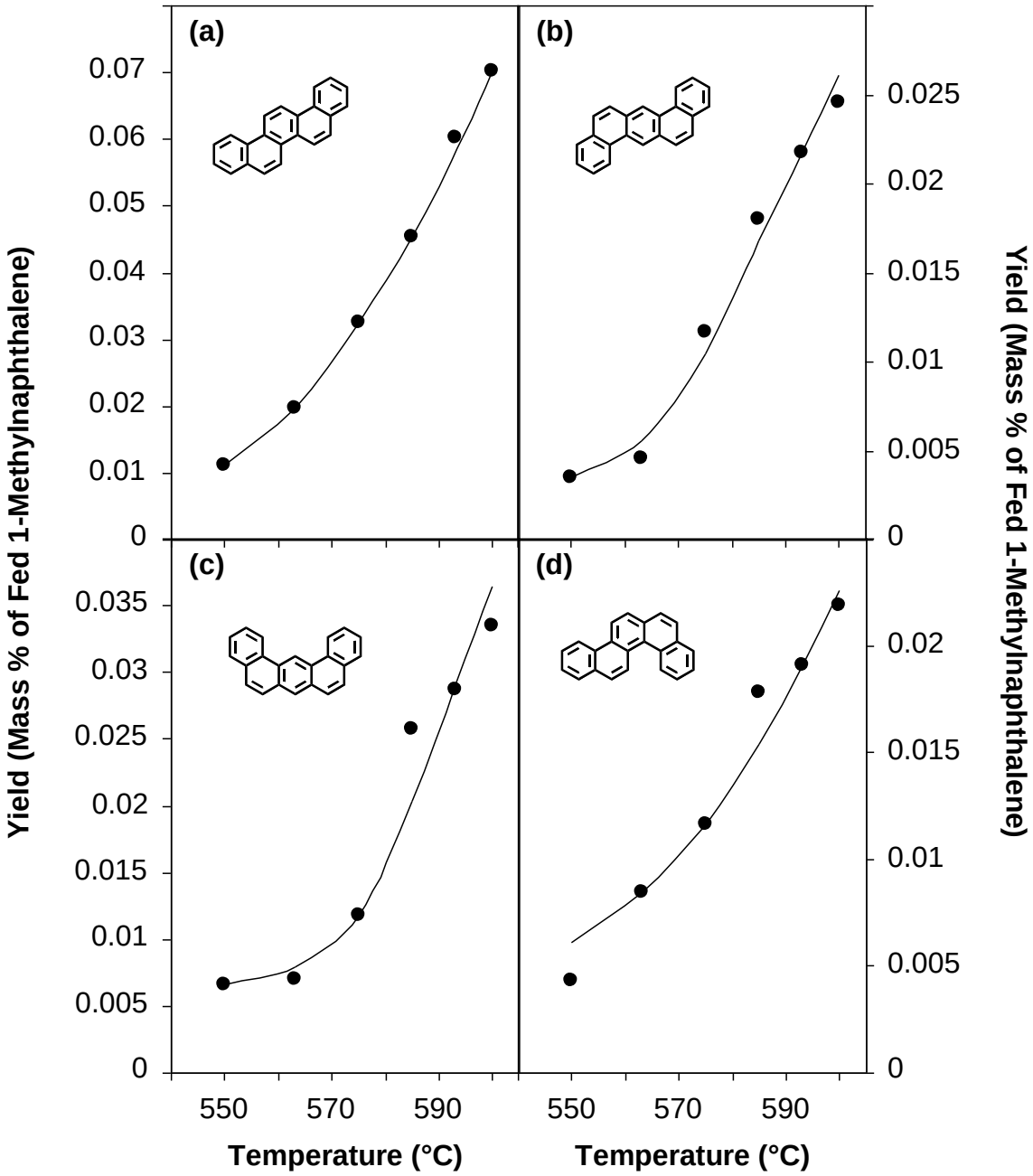

Figure 10. Yields, as functions of temperature, of the five-ring $C_{22}H_{14}$ PAH products of supercritical 1-methylnaphthalene pyrolysis at 80 atm and 140 sec: (a) picene; (b) dibenz[*a*,*h*]anthracene; (c) dibenz[*a*,*j*]anthracene; and (d) benzo[*c*]chrysene.

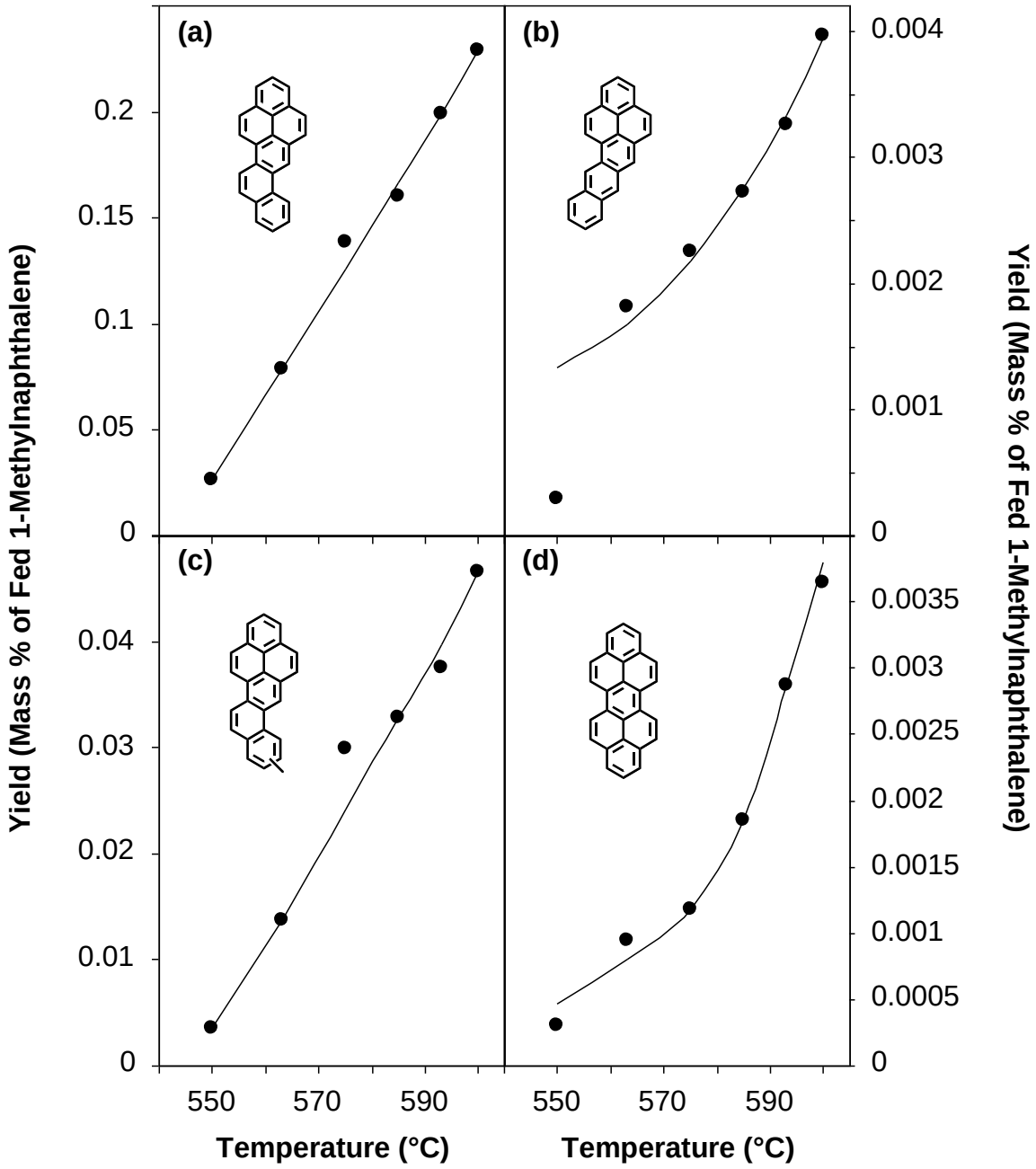

Figure 11. Yields, as funcitons of temperature, of six- and seven-ring PAH products of supercritical 1-methylnaphthalene pyrolysis at 80 atm and 140 sec: (a) naphtho[2,1-*a*]pyrene; (b) naphtho[2,3-*a*]pyrene; (c) methylnaphtho[2,1-*a*]pyrenes summed; and (d) dibenzo[*cd*,*lm*]perylene.

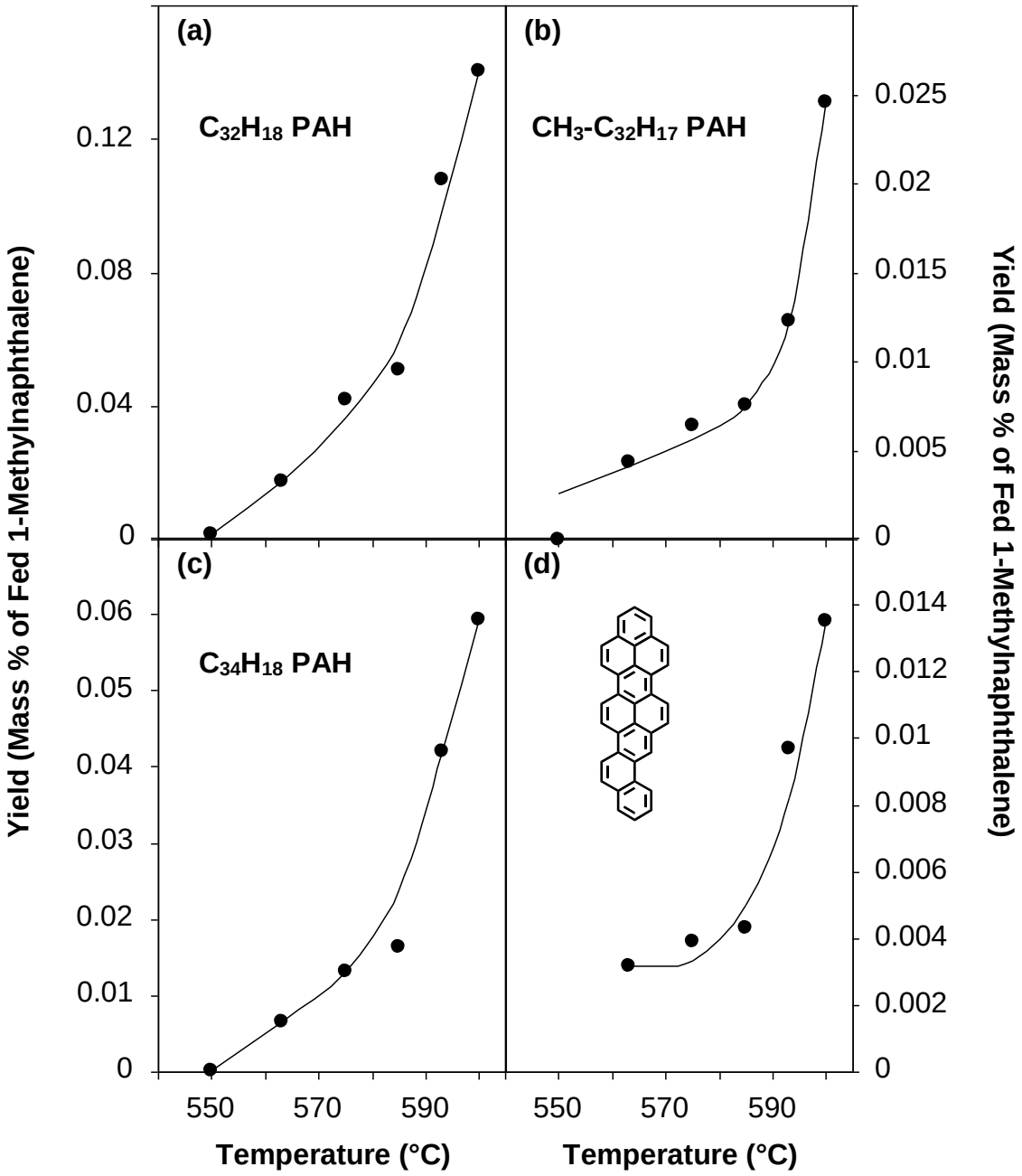

Figure 12. Yields, as functions of temperature, of eight- and nine-ring PAH products of supercritical 1-methylnaphthalene pyrolysis at 80 atm and 140 sec: (a) eight-ring $C_{32}H_{18}$ PAH summed; (b) eight-ring CH_3-$C_{32}H_{17}$ PAH summed; (c) nine-ring $C_{34}H_{18}$ PAH summed; and (d) benzo[*cd*]phenanthro[1,2,3-*lm*]perylene.

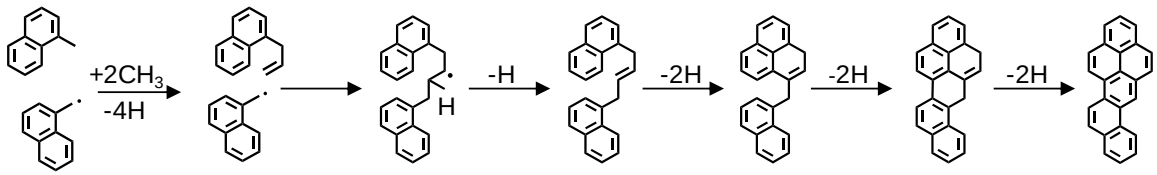

Figure 13. Reaction scheme [31] for the formation of naphtho[2,1-*a*]pyrene during the supercritical pyrolysis of 1-methylnaphthalene.

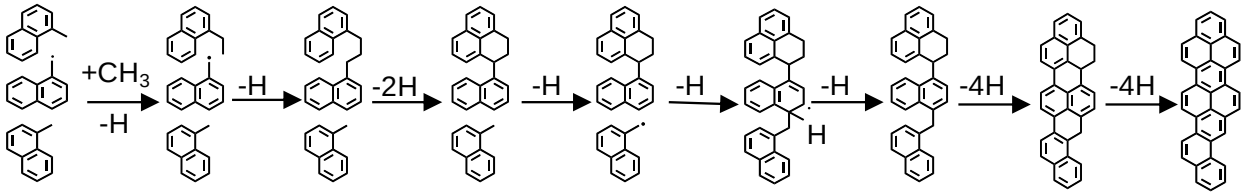

Figure 14. Reaction scheme [31] for the formation of benzo[*cd*]phenanthro[1,2,3-*lm*]perylene during the supercritical pyrolysis of 1-methylnaphthalene.

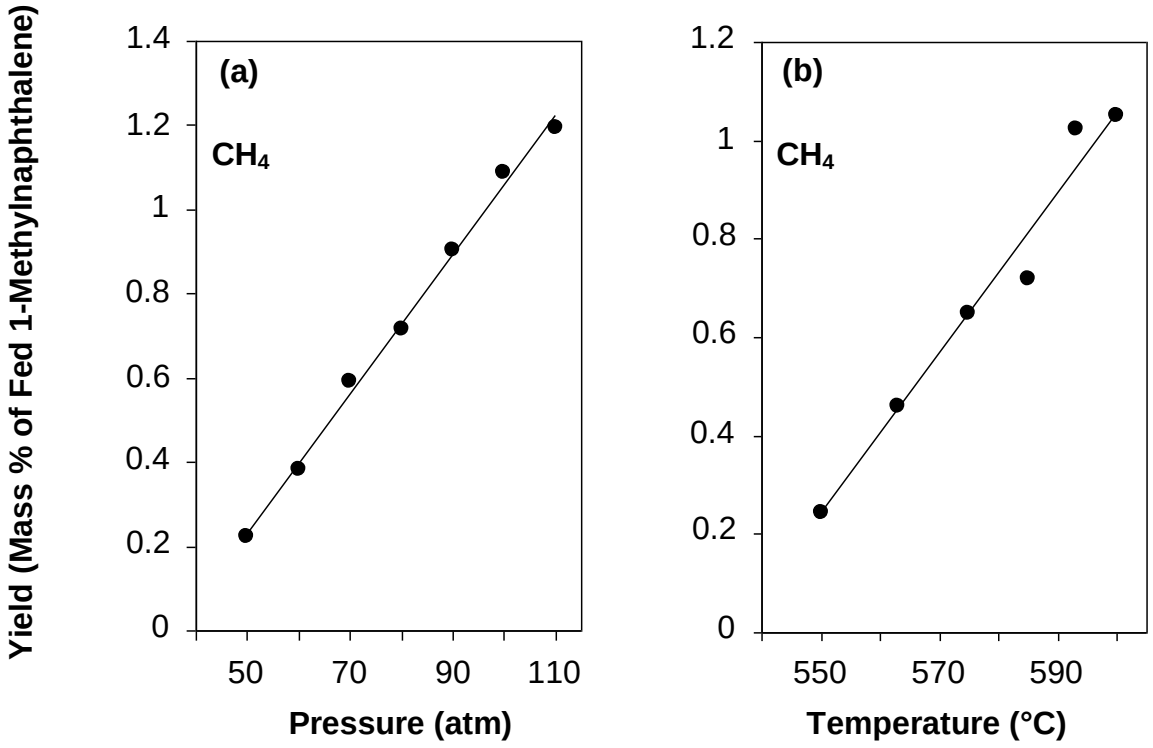

Figure 15. Yields of methane from the supercritical pyrolysis of 1-methylnaphthalene: (a) as a function of pressure at 585 °C and 140 sec; (b) as a function of temperature at 80 atm and 140 sec.

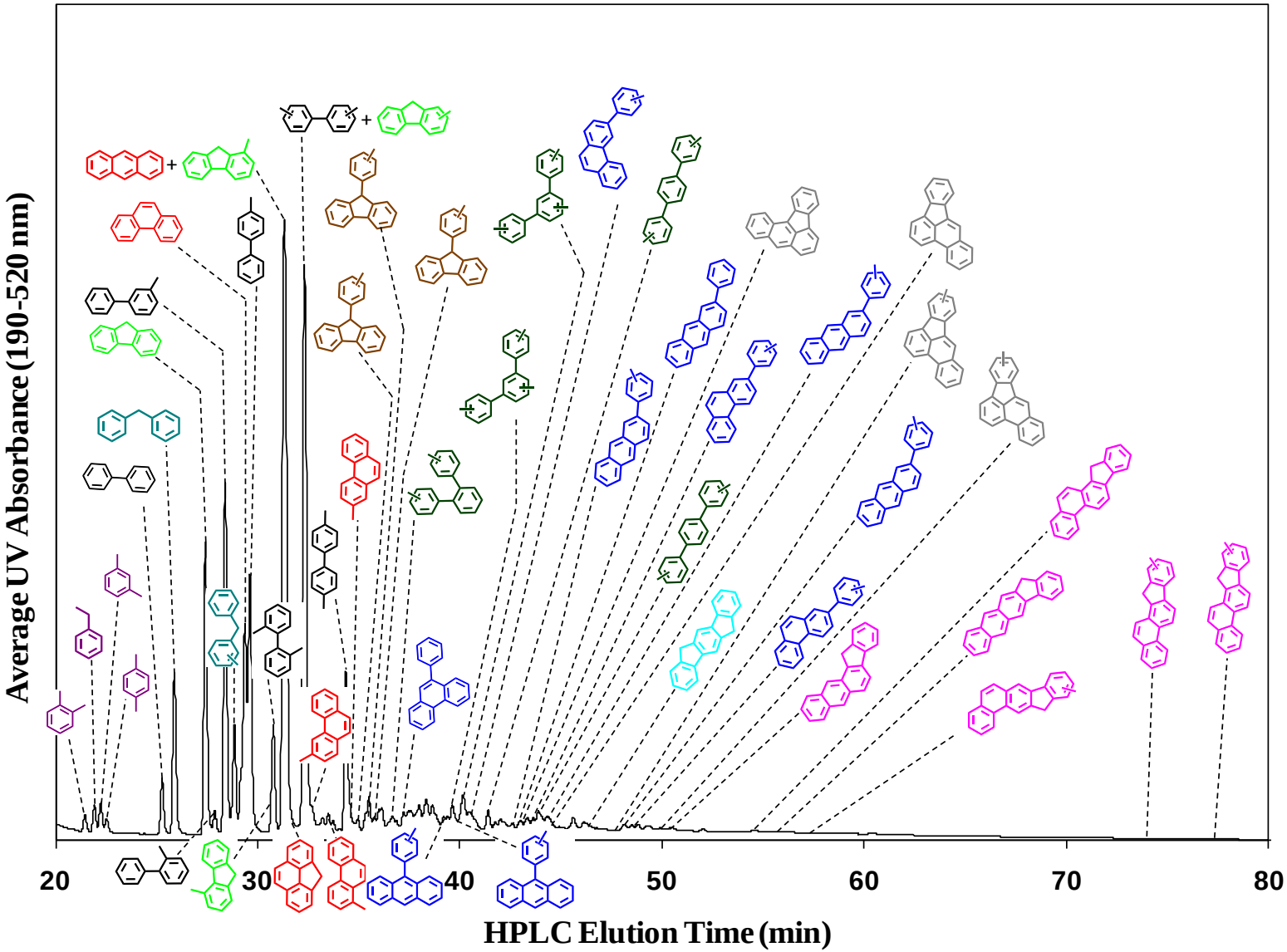

Figure 16. Reversed-phase HPLC chromatogram of the products of supercritical toluene pyrolysis at 700°C, 75 atm, and 140 sec.

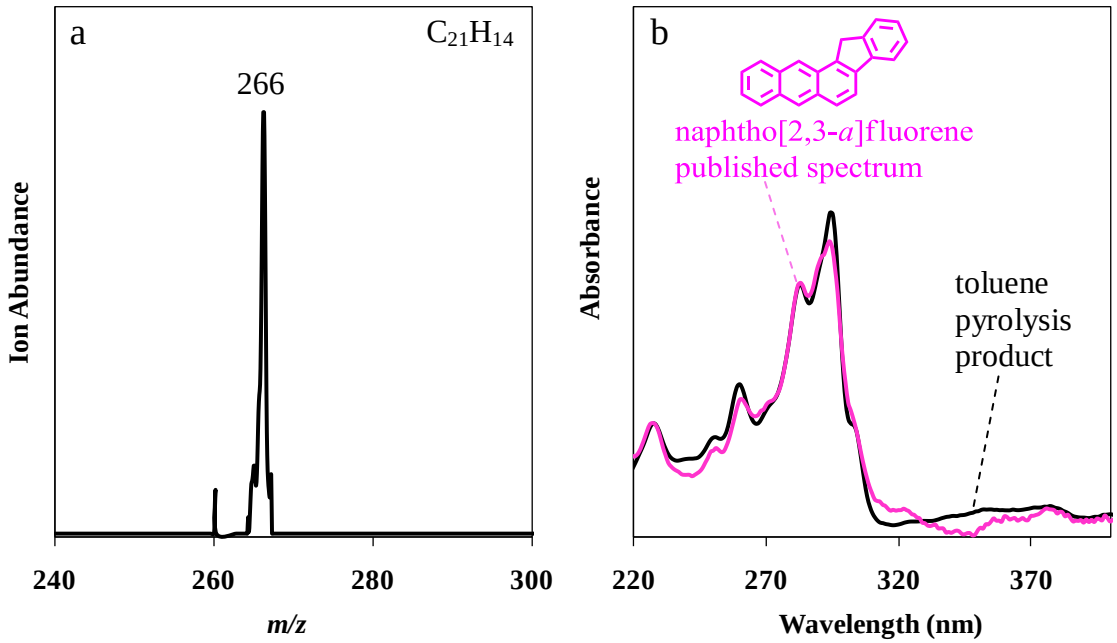

Figure 17. Mass spectrum (a) and UV spectrum (b) of a supercritical toluene pyrolysis product component. The published spectrum [32] of naphtho[2,3-*a*]fluorene is included in (b).

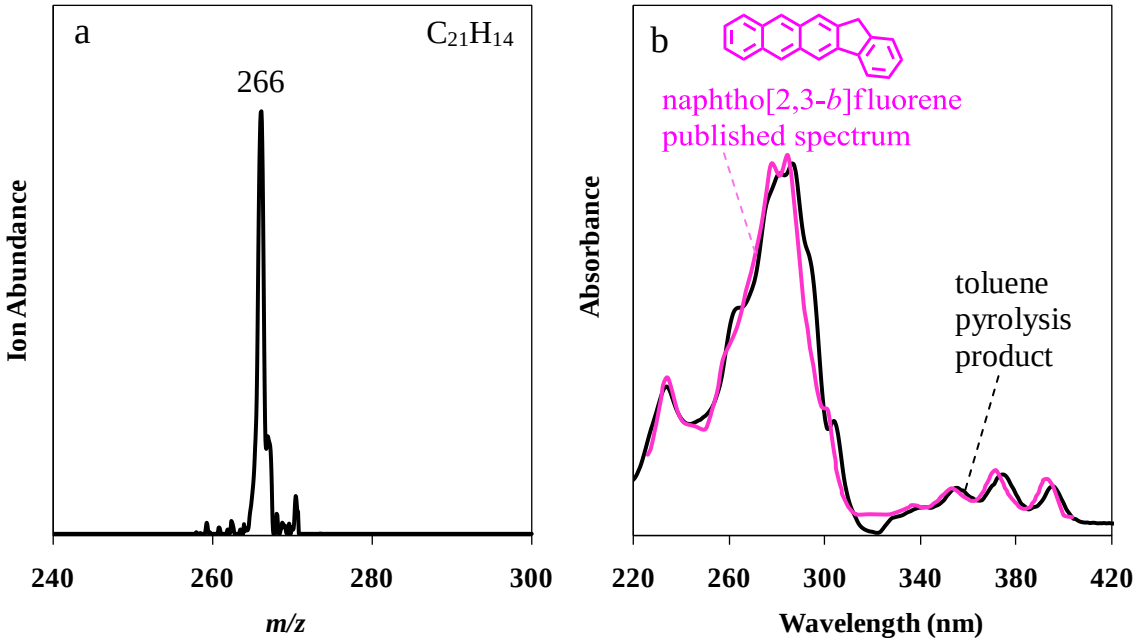

Figure 18. Mass spectrum (a) and UV spectrum (b) of a supercritical toluene pyrolysis product component. The published spectrum [32] of naphtho[2,3-*b*]fluorene is included in (b).

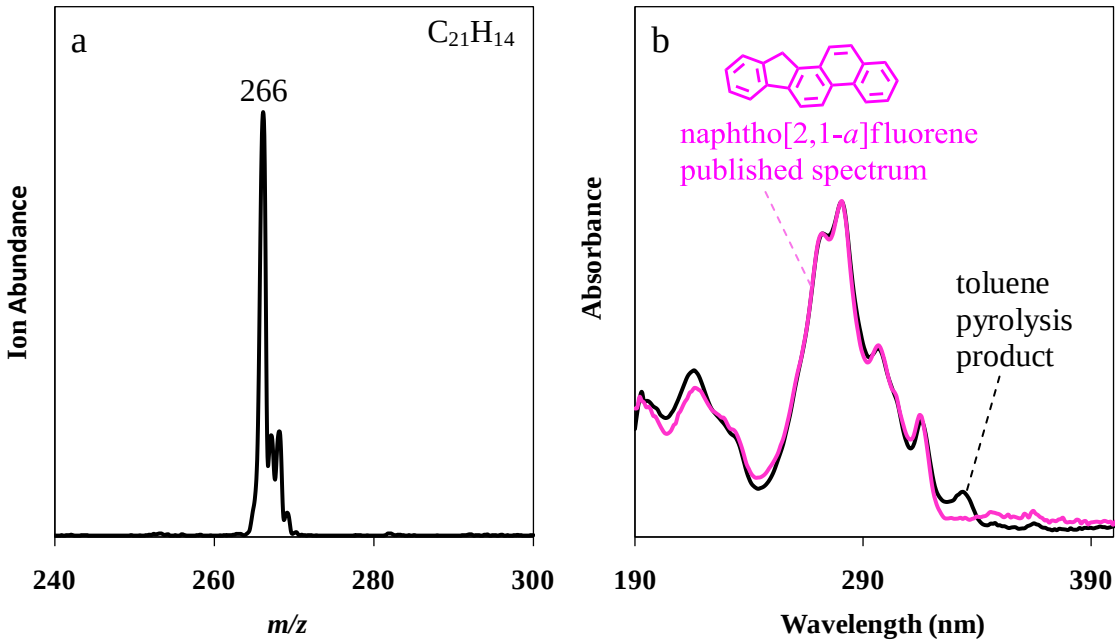

Figure 19. Mass spectrum (a) and UV spectrum (b) of a supercritical toluene pyrolysis product component. The published spectrum [33] of naphtho[2,1-*a*]fluorene is included in (b).

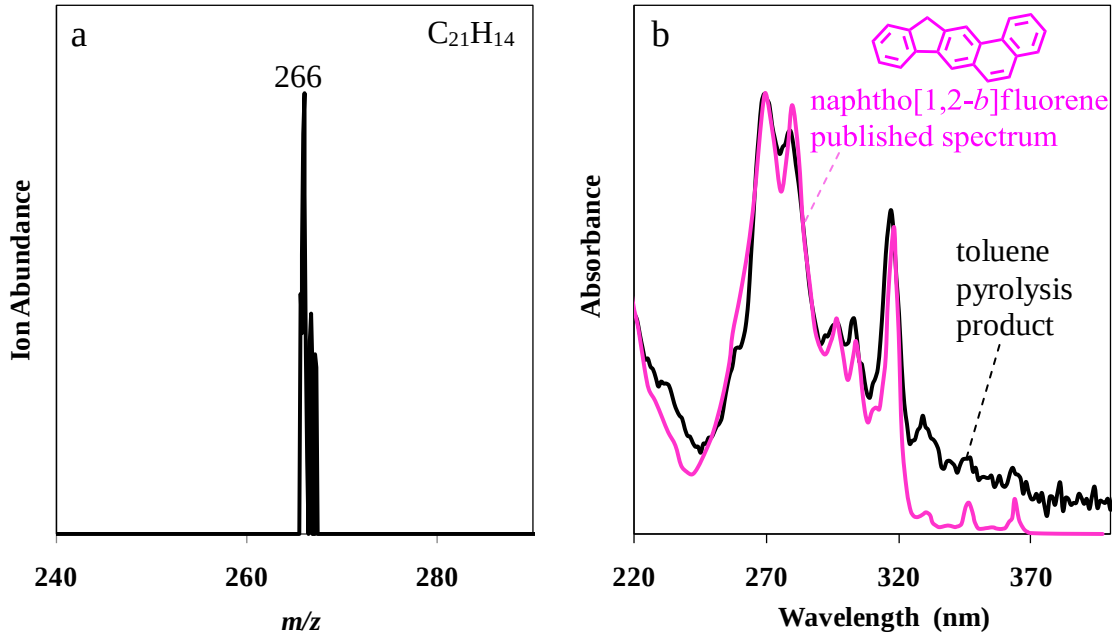

Figure 20. Mass spectrum (a) and UV spectrum (b) of a supercritical toluene pyrolysis product component. The published spectrum [34] of naphtho[1,2-*b*]fluorene is included in (b).

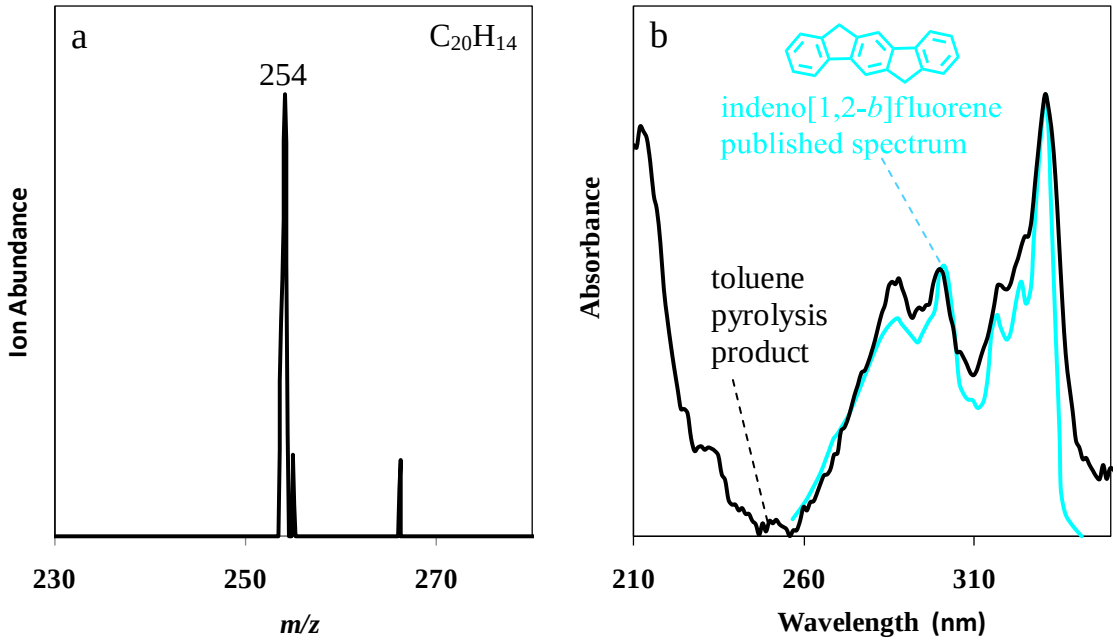

Figure 21. Mass spectrum (a) and UV spectrum (b) of a supercritical toluene pyrolysis product component. The published spectrum [35] of indeno[1,2-*b*]fluorene is included in (b).

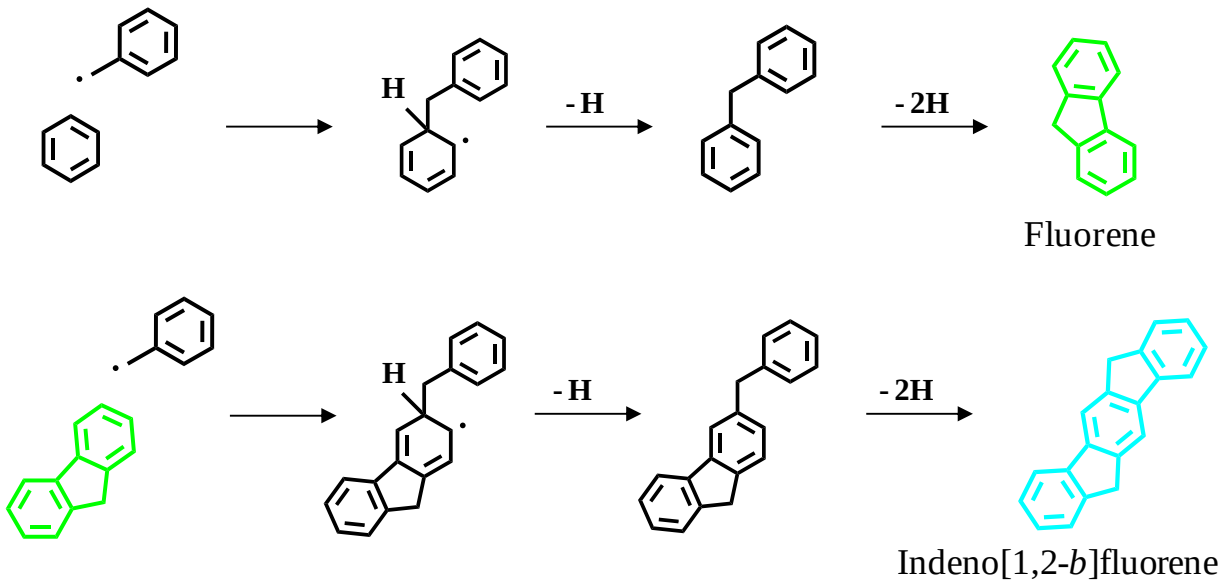

Figure 22. Reaction schemes to form fluorene and indeno[1,2-*b*]fluorene from the supercritical pyrolysis of toluene.

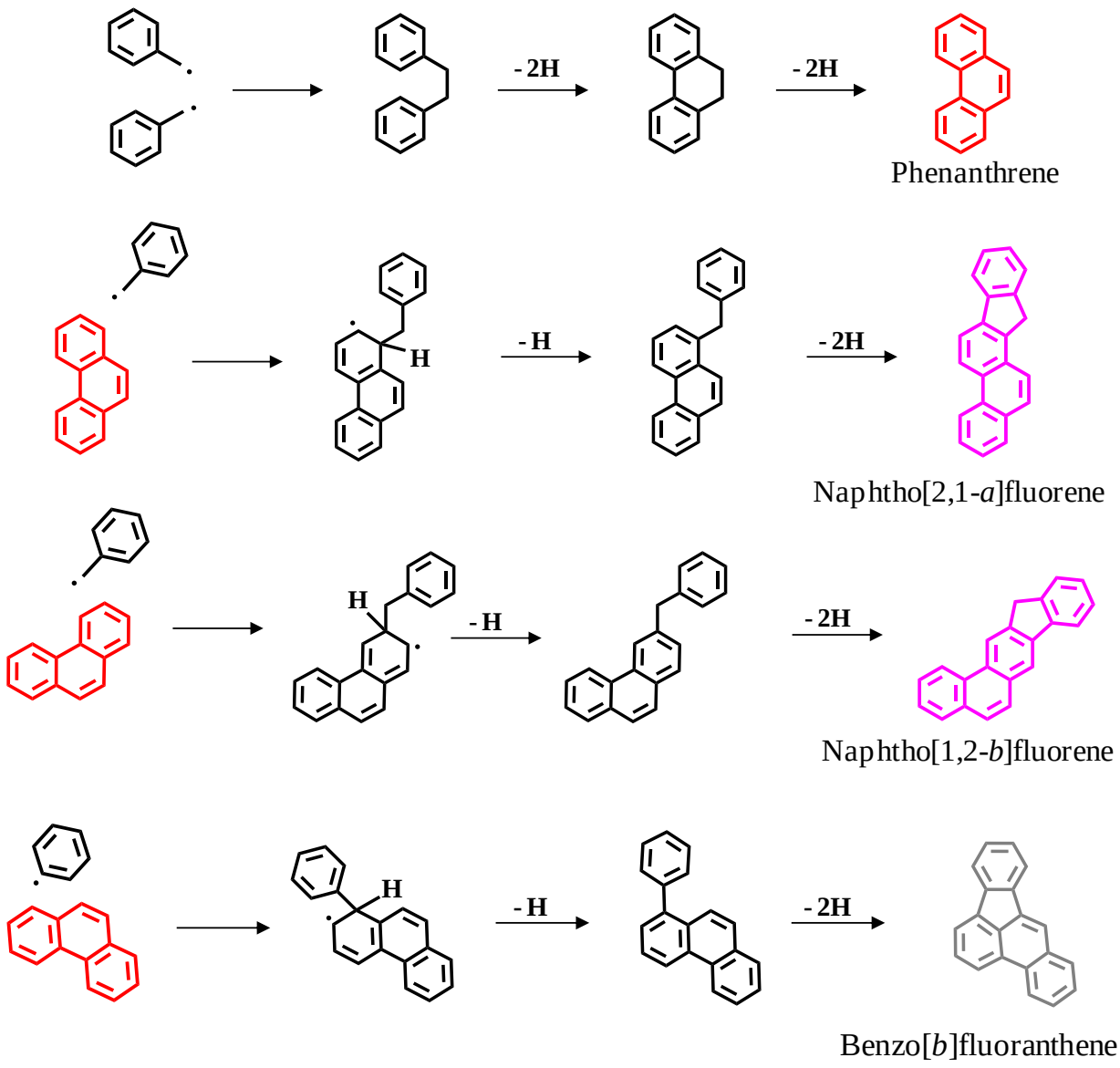

Figure 23. Reaction schemes to form phenanthrene, naphtho[2,1-*a*]fluorene, naphtho[1,2-*b*]fluorene, and benzo[*b*]fluoranthene from the supercritical pyrolysis of toluene.

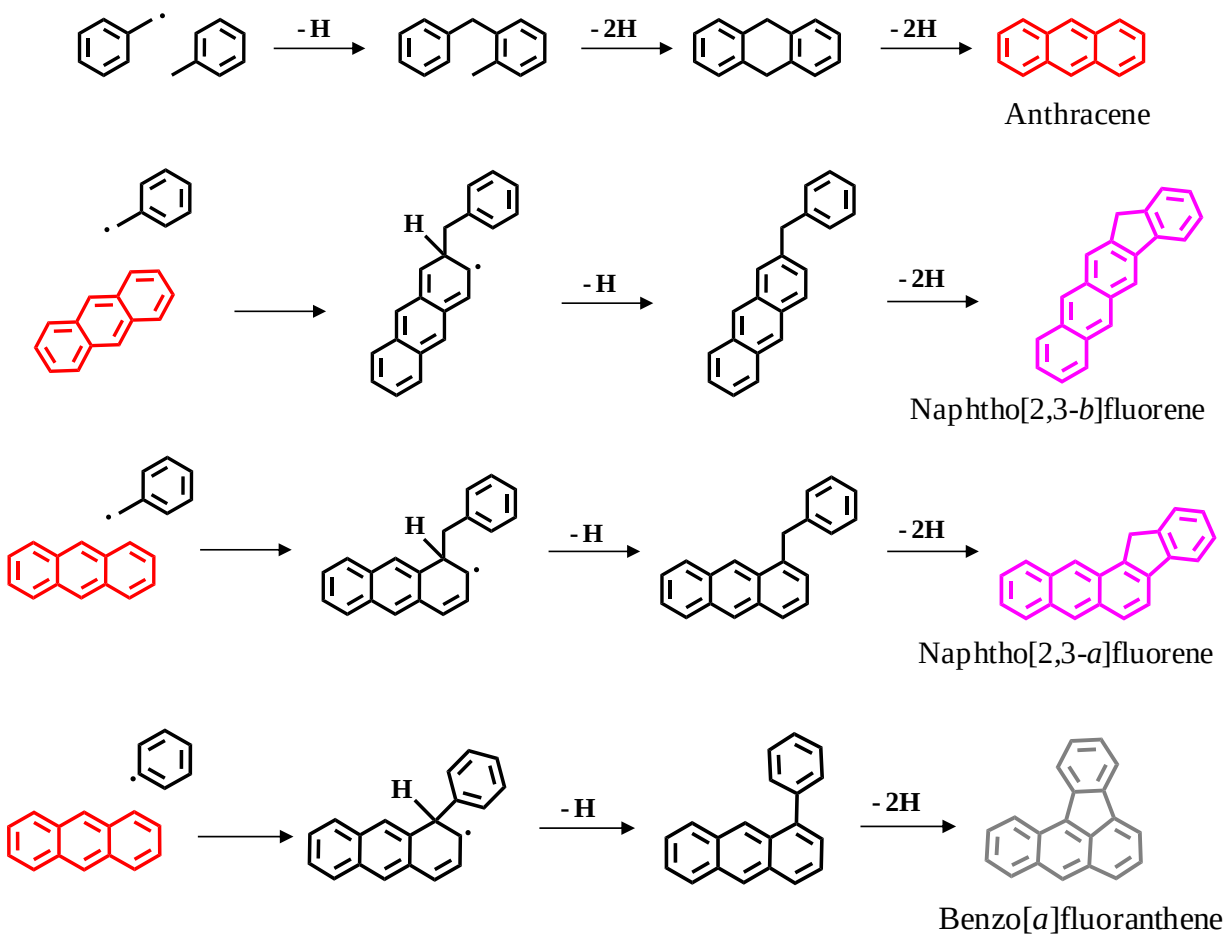

Figure 24. Reaction schemes to form anthracene, naphtho[2,3-*a*]fluorene, naphtho[2,3-*b*]fluorene and benzo[*a*]fluoranthene from the supercritical pyrolysis of toluene.

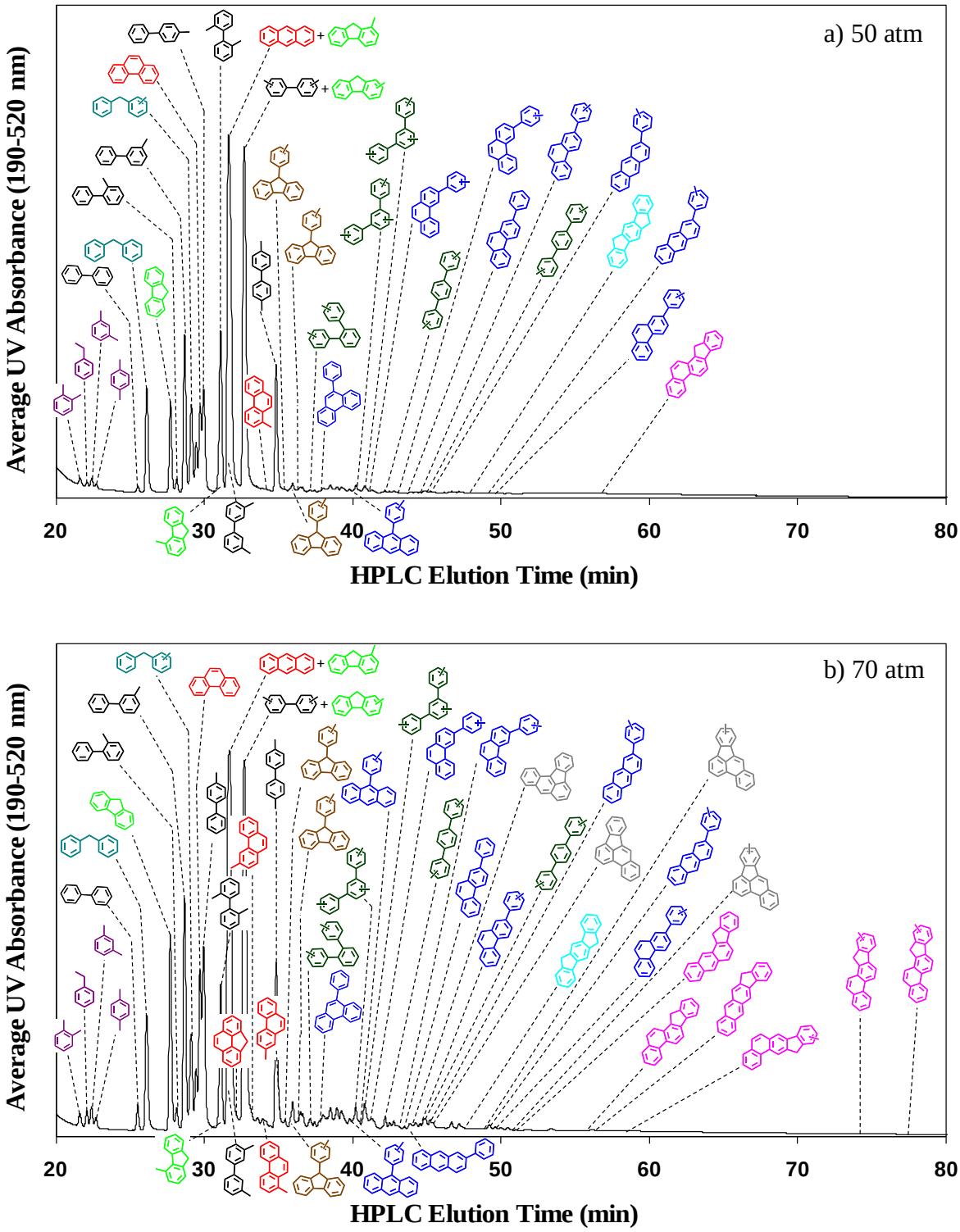

Figure 25. HPLC chromatograms of the products of supercritical toluene pyrolysis at 685°C, 140 sec, and pressures of (a) 50 atm and (b) 70 atm.

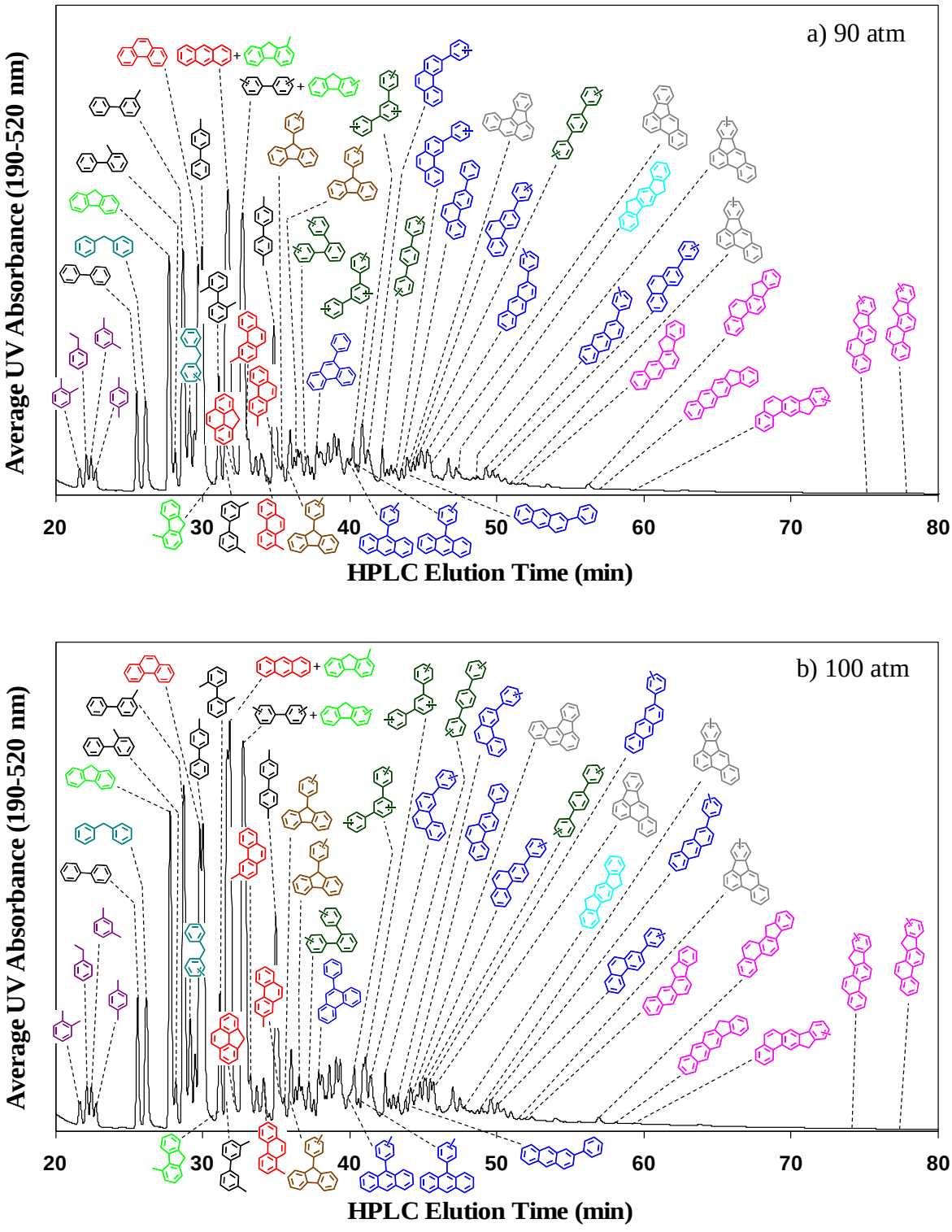

Figure 26. HPLC chromatograms of the products of supercritical toluene pyrolysis at 685°C, 140 sec, and pressures of (a) 90 atm and (b) 100 atm.

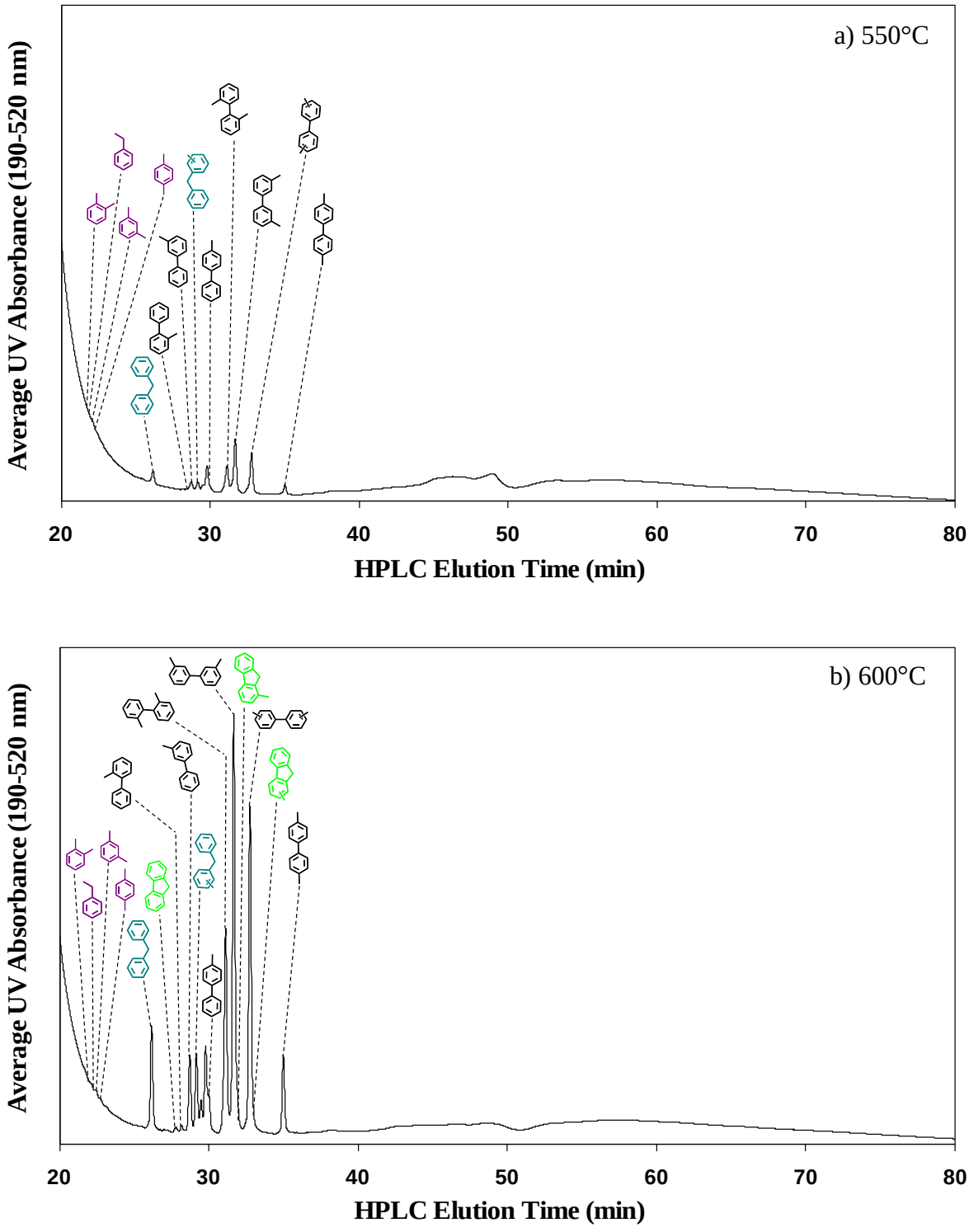

Figure 27. HPLC chromatograms of the products of supercritical toluene pyrolysis at 100 atm, 140 sec, and temperatures of (a) 550°C and (b) 600°C.

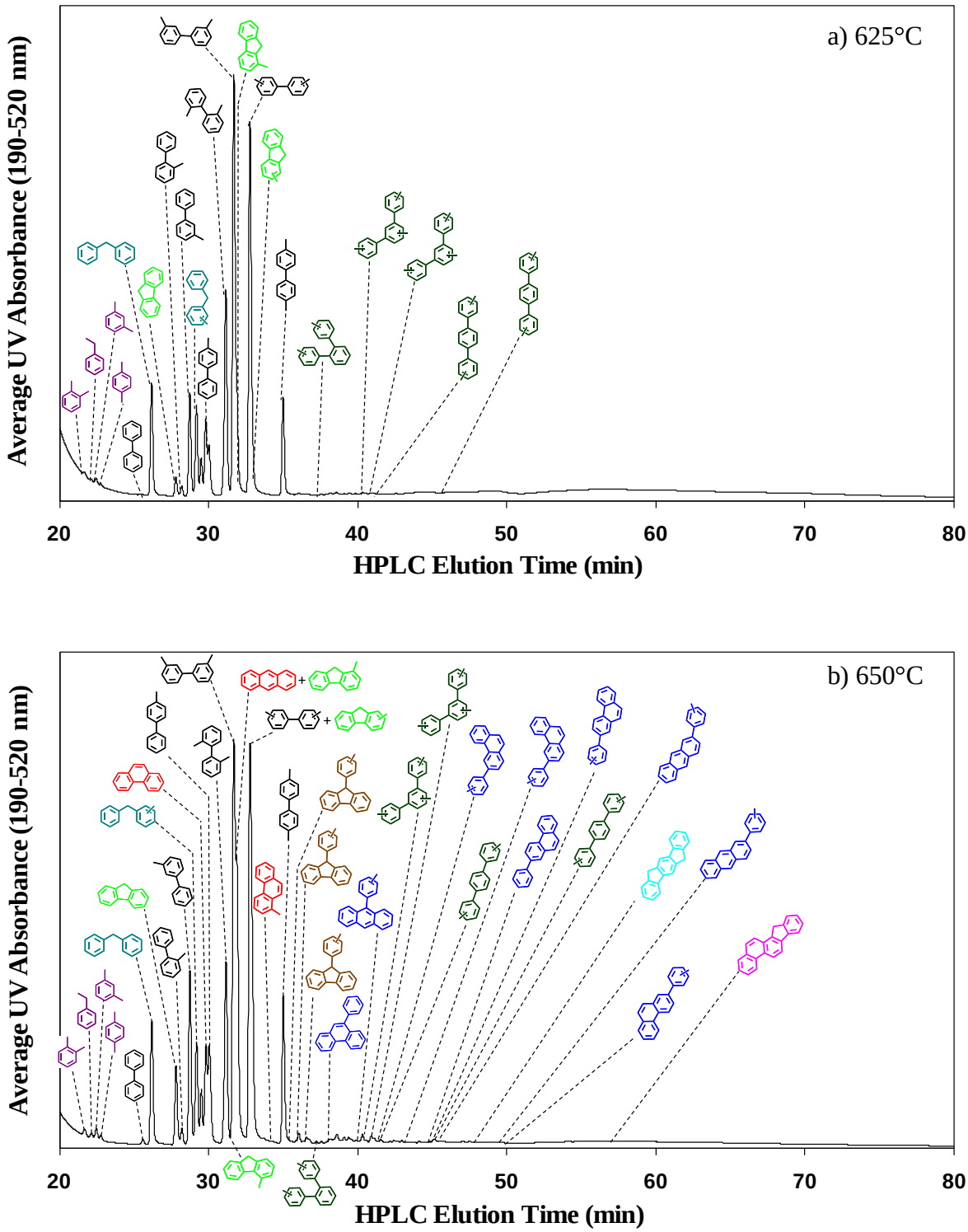

Figure 28. HPLC chromatograms of the products of supercritical toluene pyrolysis at 100 atm, 140 sec, and temperatures of (a) 625°C and (b) 650°C.

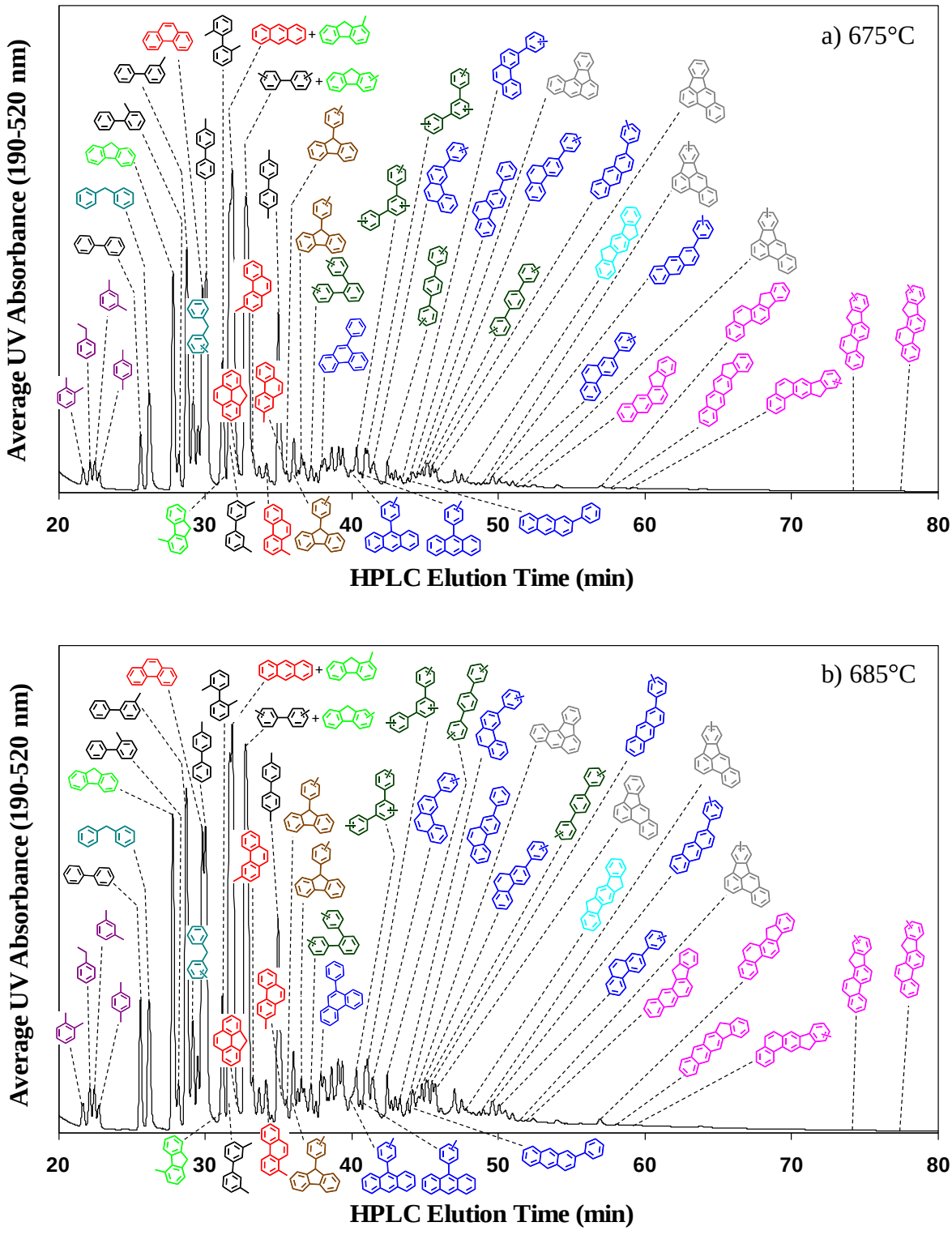

Figure 29. HPLC chromatograms of the products of supercritical toluene pyrolysis at 100 atm, 140 sec, and temperatures of (a) 675°C and (b) 685°C.

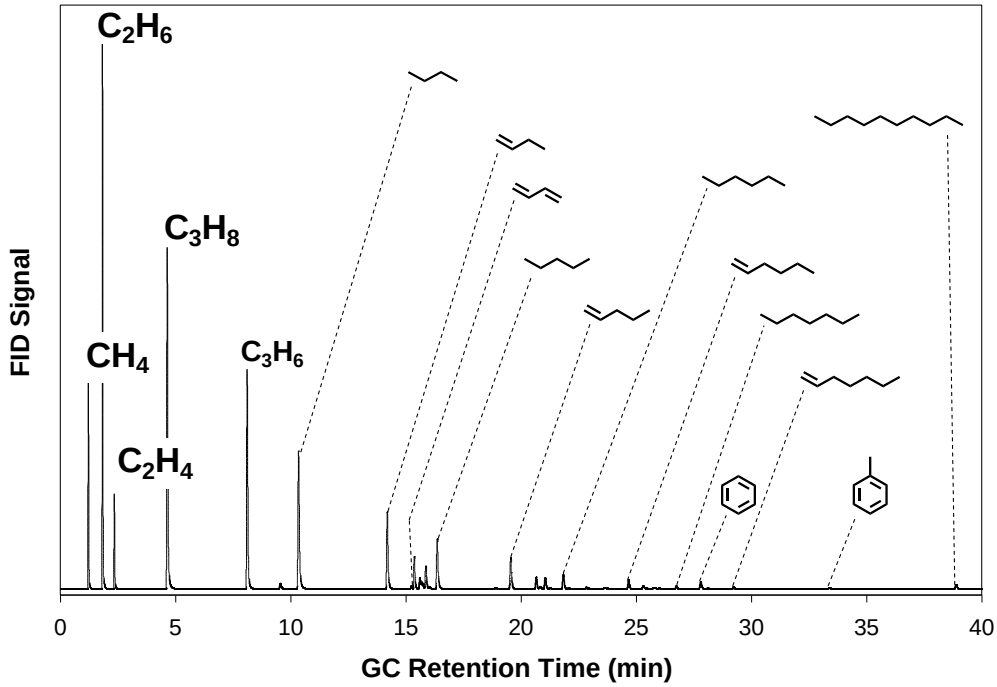

Figure 30. Gas chromatogram of the gas-phase products of supercritical *n*-decane pyrolysis at 570 °C, 100 atm, and 140 sec.

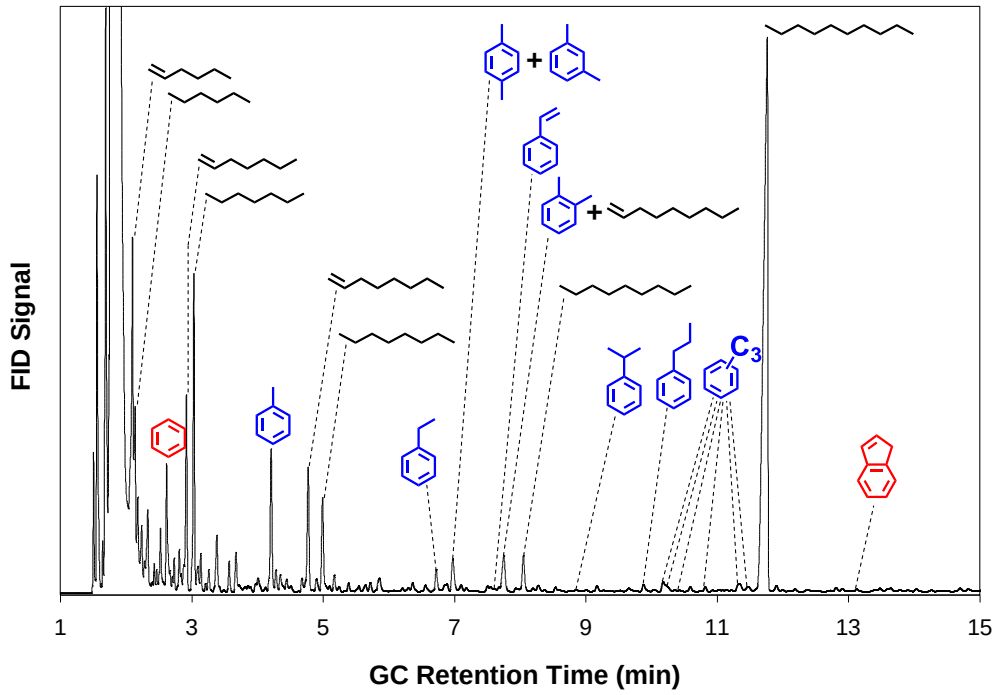

Figure 31. Gas chromatogram of the liquid-phase products of supercritical *n*-decane pyrolysis at 570 °C, 100 atm, and 140 sec. The large peak at 2 min is solvent.

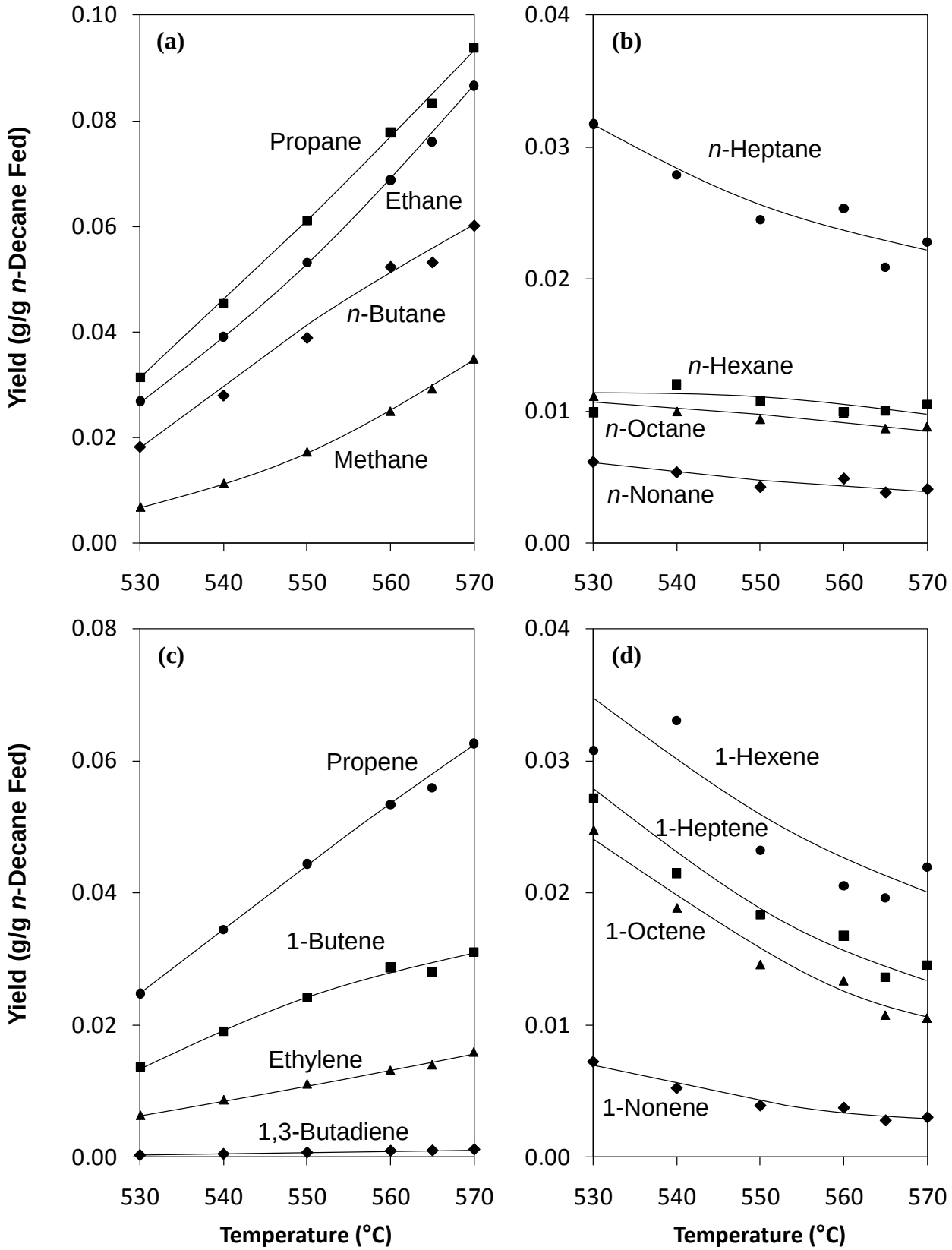

Figure 32. Yields, as functions of temperature, of the alkane and alkene products of supercritical *n*-decane pyrolysis at 100 atm and 140 sec: (a) C_1-C_4 alkanes; (b) C_6-C_9 alkanes; (c) C_2-C_4 1-alkenes and 1,3-butadiene; (d) C_6-C_9 1-alkenes.

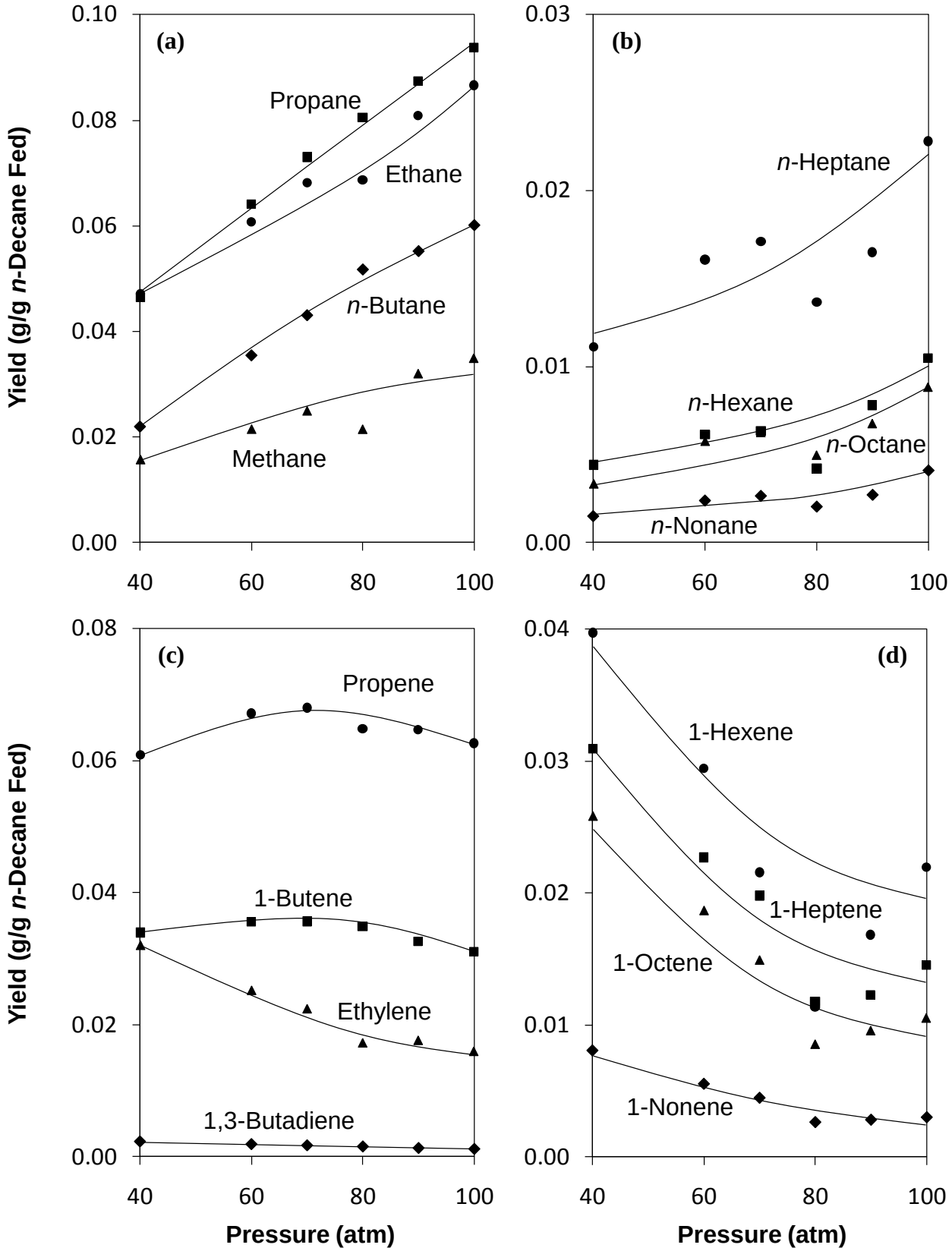

Figure 33. Yields, as functions of pressure, of the alkane and alkene products of supercritical *n*-decane pyrolysis at 570 °C and 140 sec: (a) C_1-C_4 alkanes; (b) C_6-C_9 alkanes; (c) C_2-C_4 1-alkenes and 1,3-butadiene; (d) C_6-C_9 1-alkenes.

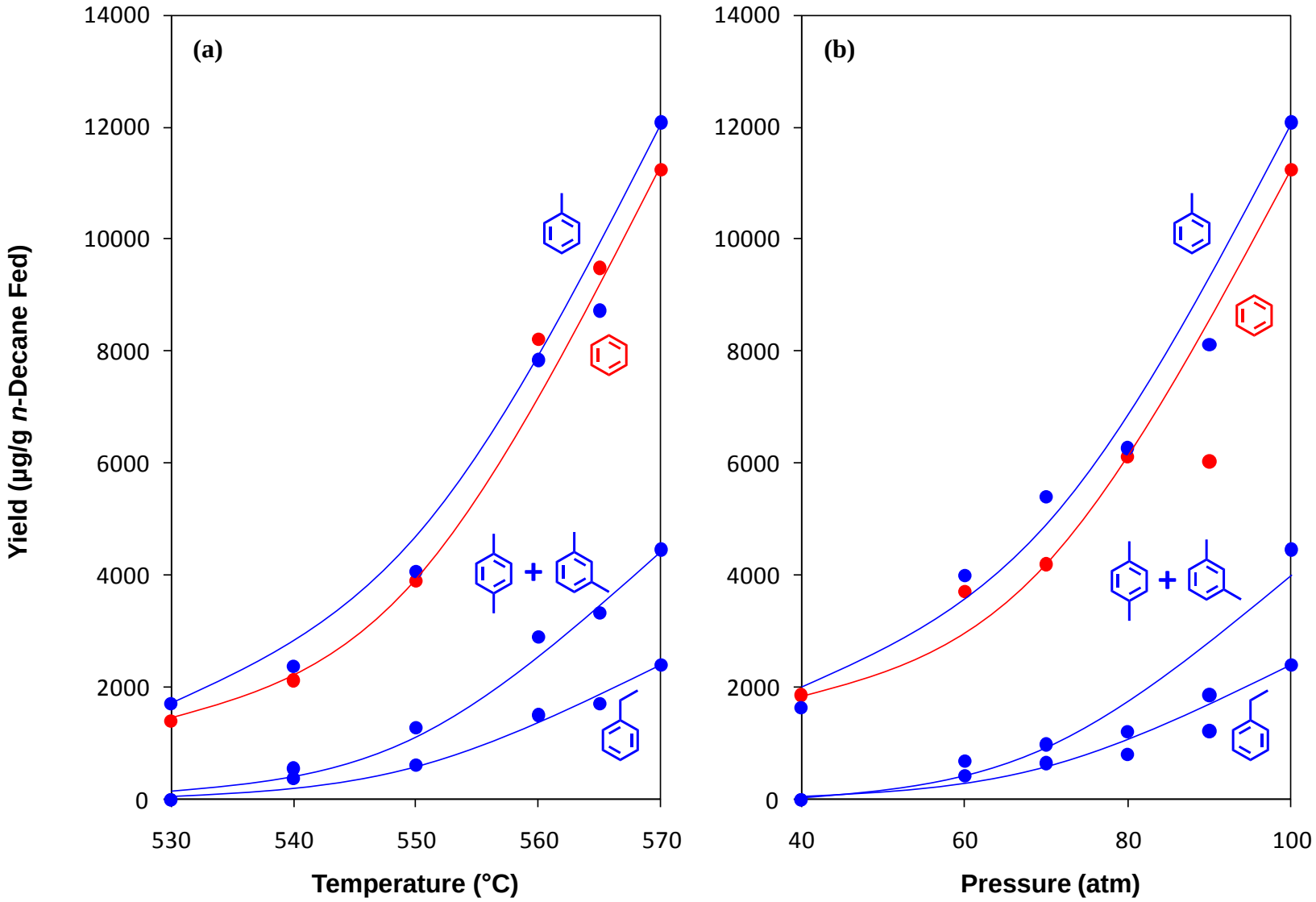

Figure 34. Yields of benzene, toluene, ethylbenzene, and *meta*- and *para*-xylene from the supercritical pyrolysis of *n*-decane: (a) as functions of temperature at 100 atm and 140 sec; (b) as functions of pressure at 570 °C and 140 sec. (*Ortho*-xylene is produced but has not been quantified since its peak is not well-enough resolved from that of 1-nonene on the gas chromatograph.).

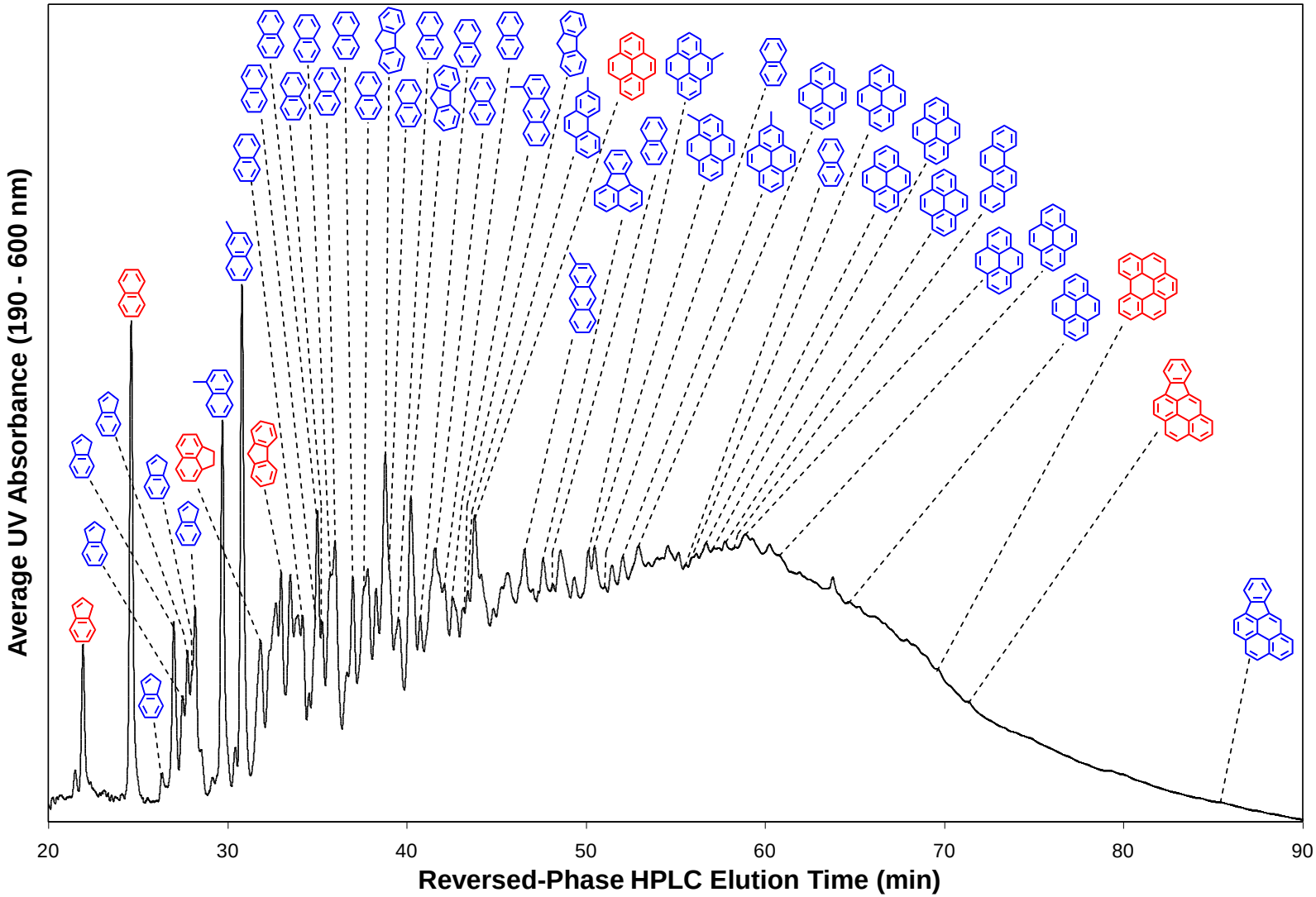

Figure 35. Reversed-phase HPLC chromatogram of the unfractionated liquid-phase products of supercritical *n*-decane pyrolysis at 570 °C, 100 atm, and 140 sec. Red structures are unsubstituted PAH whose exact structures are certain. Blue structures with single methyl groups in definite positions are methylated PAH whose exact structures are certain. The other blue structures are alkylated PAH whose aromatic portion of the structure is certain (and shown in blue), but there is uncertainty regarding the alkyl substituents.

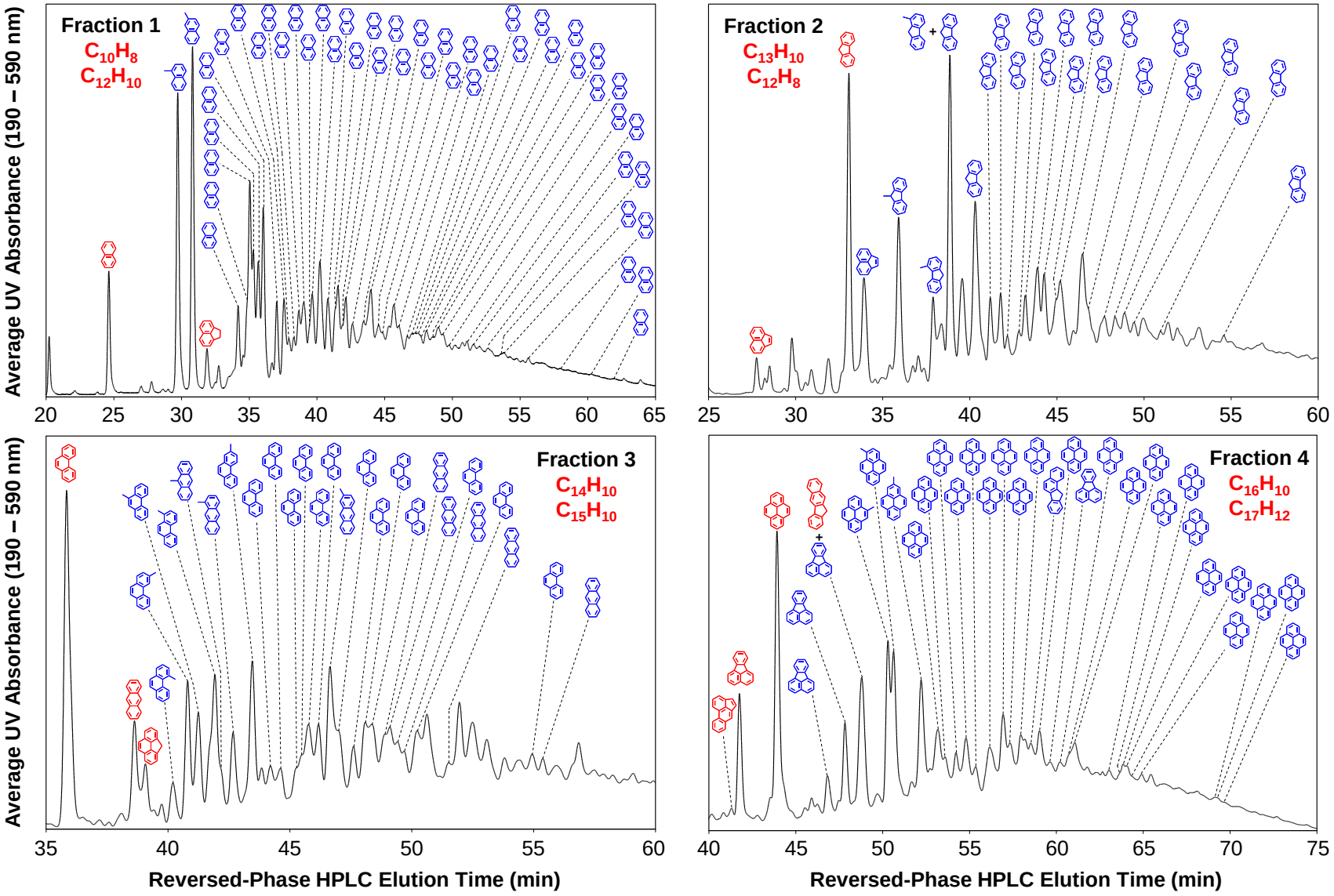

Figure 36. Reversed-phase HPLC chromatograms of fractions 1-4 of the liquid-phase products of supercritical *n*-decane pyrolysis at 570 °C, 100 atm, and 140 sec. Red structures are unsubstituted PAH whose exact structures are certain. Blue structures with single methyl groups in definite positions are methylated PAH whose exact structures are certain. The other blue structures are alkylated PAH whose aromatic portion of the structure is certain, but there is uncertainty regarding the alkyl substituents.

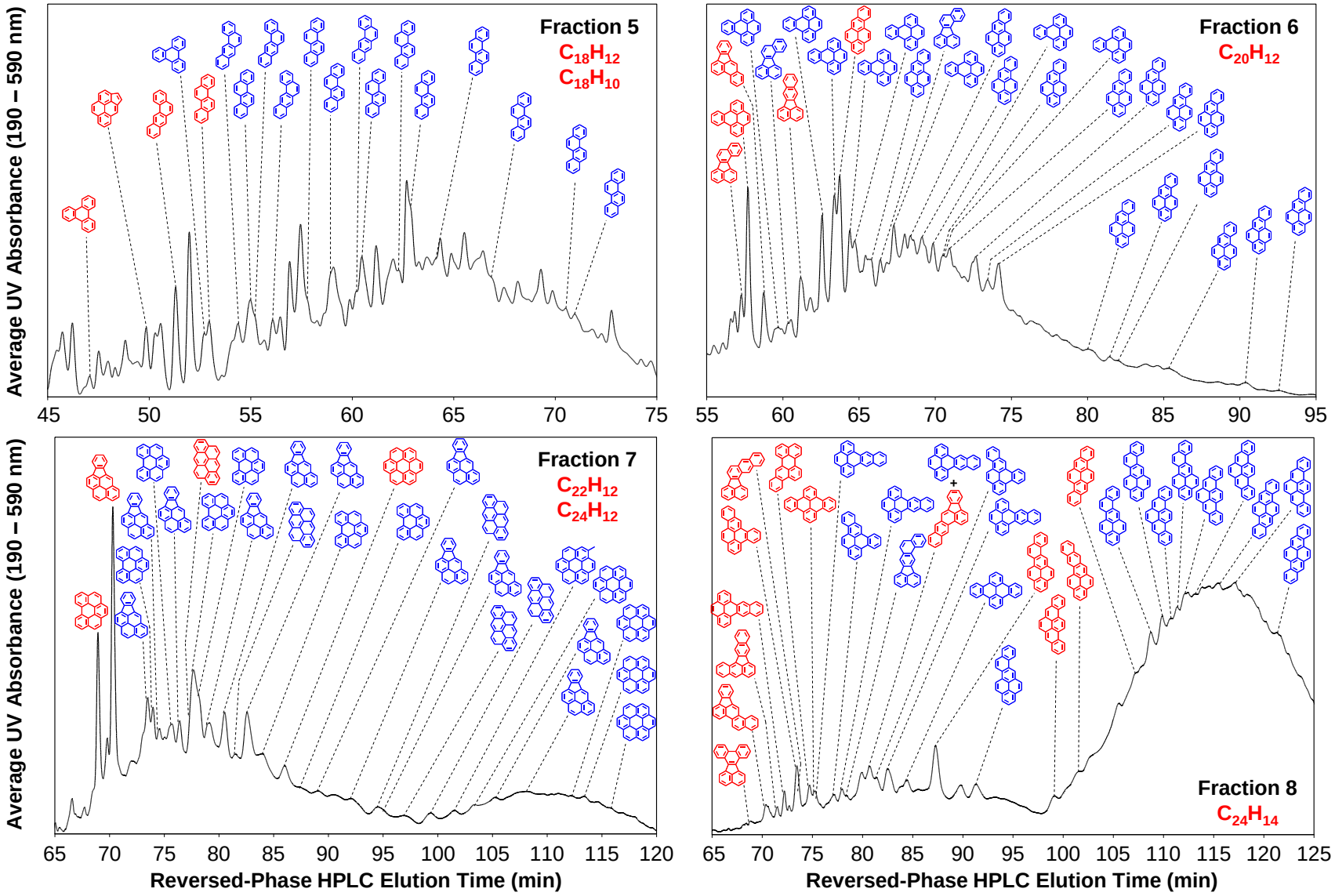

Figure 37. Reversed-phase HPLC chromatograms of fractions 5-8 of the liquid-phase products of supercritical *n*-decane pyrolysis at 570 °C, 100 atm, and 140 sec. Red structures are unsubstituted PAH whose exact structures are certain. Blue structures with single methyl groups in definite positions are methylated PAH whose exact structures are certain. The other blue structures are alkylated PAH whose aromatic portion of the structure is certain, but there is uncertainty regarding the alkyl substituents.

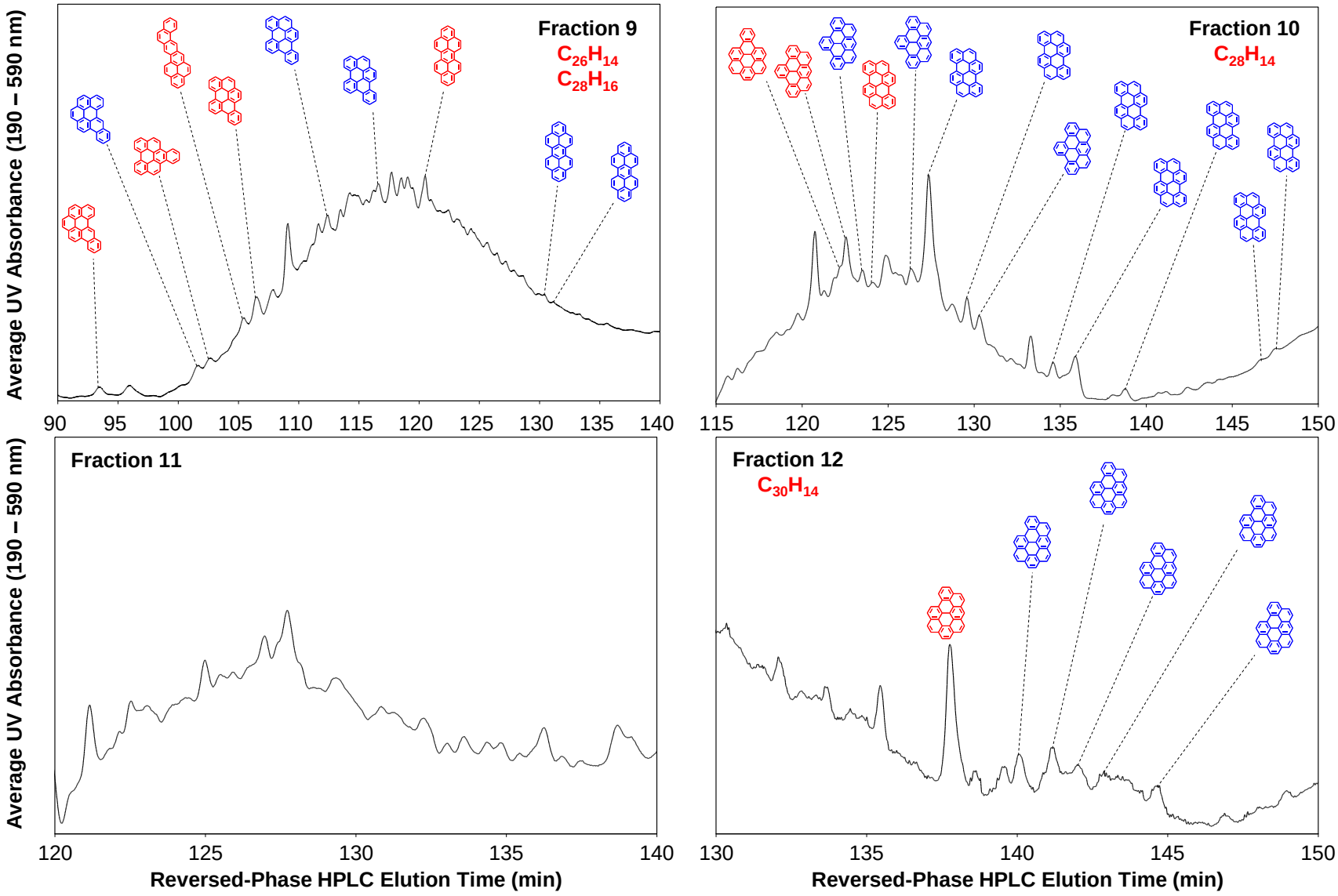

Figure 38. Reversed-phase HPLC chromatograms of fractions 9-12 of the liquid-phase products of supercritical *n*-decane pyrolysis at 570 °C, 100 atm, and 140 sec. Red structures are unsubstituted PAH whose exact structures are certain. Blue structures with single methyl groups in definite positions are methylated PAH whose exact structures are certain. The other blue structures are alkylated PAH whose aromatic portion of the structure is certain, but there is uncertainty regarding the alkyl substituents.

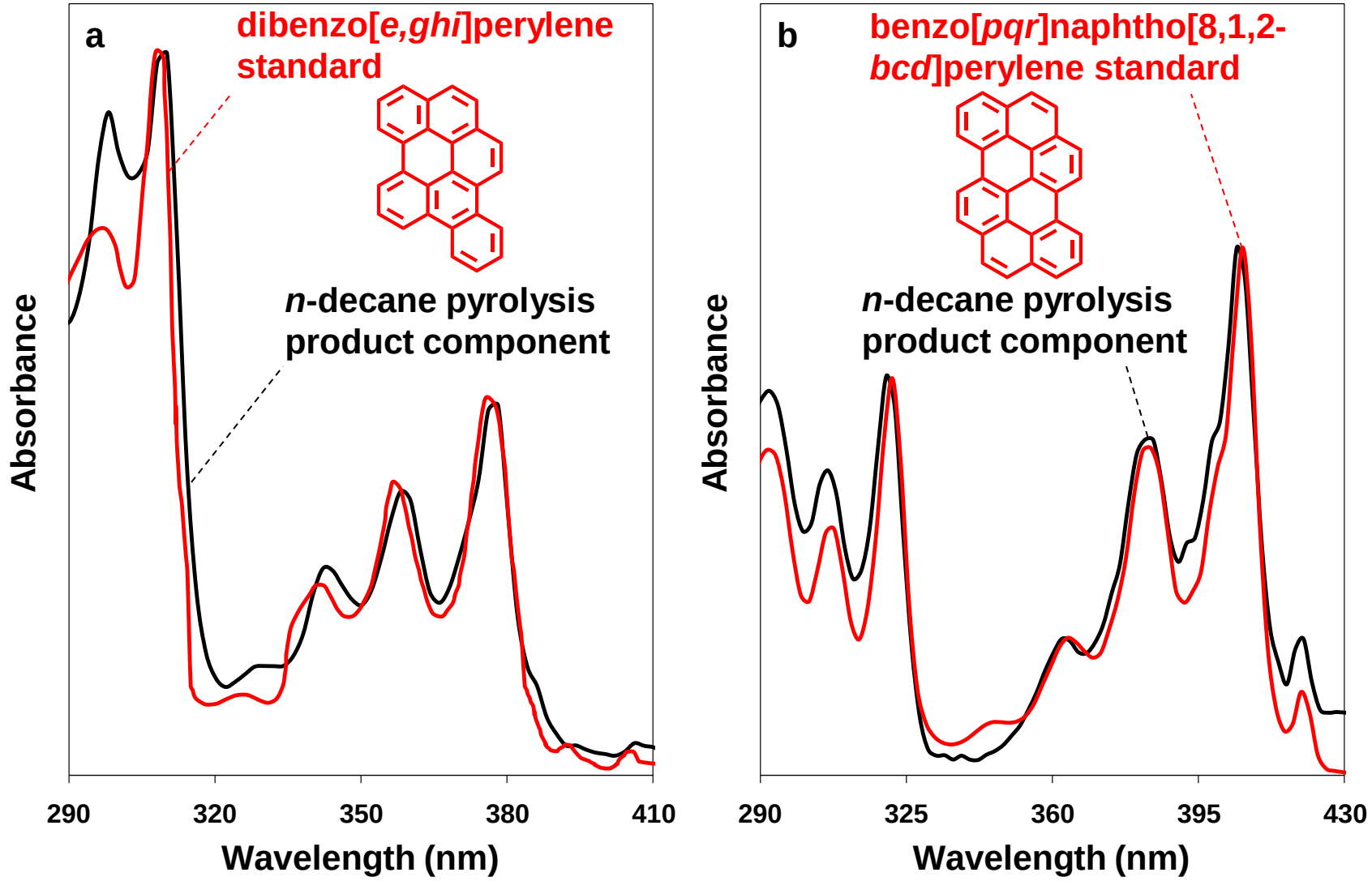

Figure 39. UV spectra of supercritical *n*-decane pyrolysis products identified as (a) dibenzo[*e,ghi*]perylene, in Fraction 9 of Figure 38, and (b) benzo[*pqr*]naphtho[8,1,2-*bcd*]perylene, in Fraction 10 of Figure 38—along with the UV spectra of the respective PAH reference standards. Reference standard of benzo[*pqr*]naphtho[8,1,2-*bcd*]perylene synthesized by Dr. John Fetzer. Published UV spectrum of dibenzo[*e,ghi*]perylene reference standard from Clar [37].

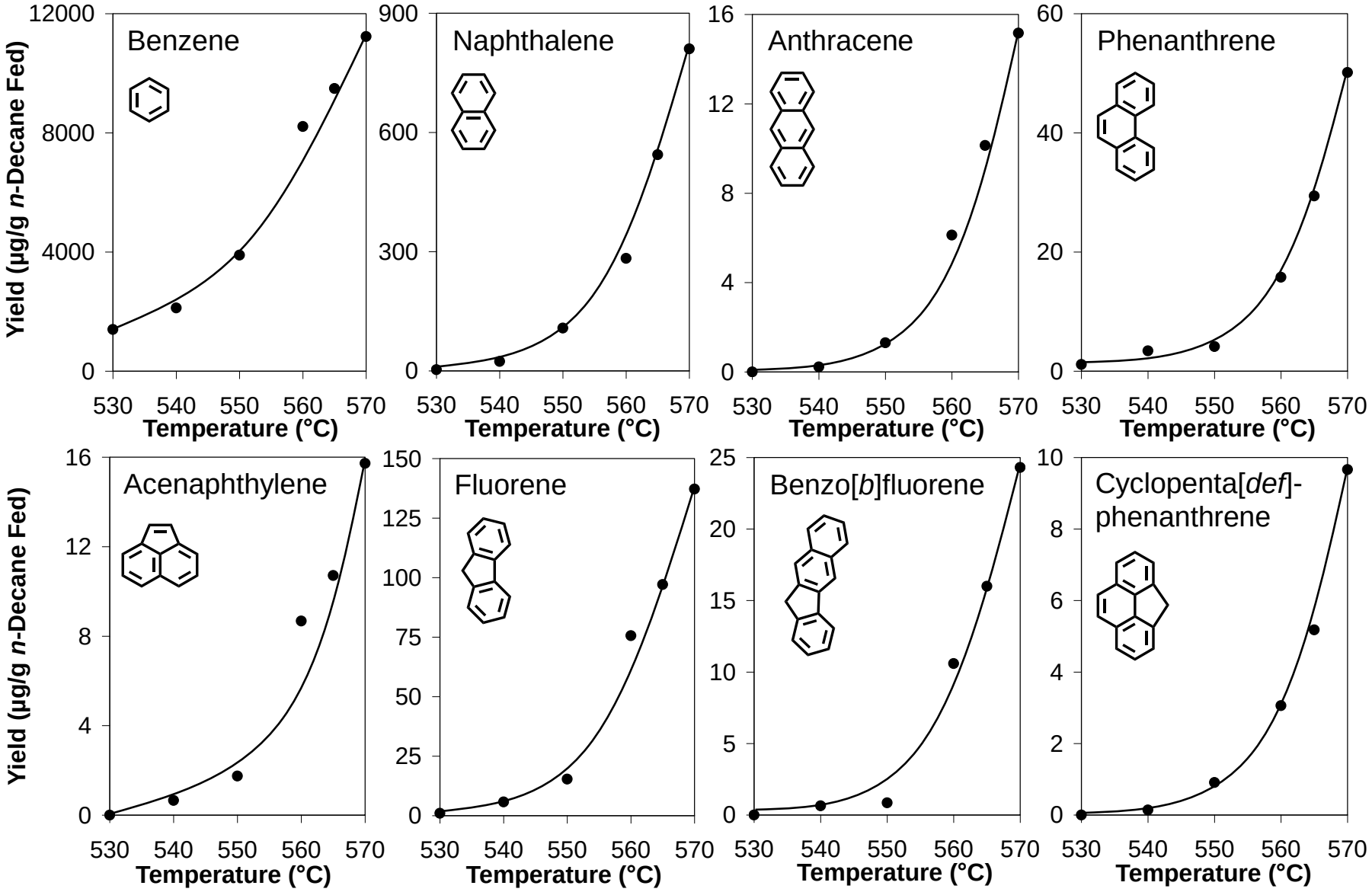

Figure 40. Yields, versus temperature, of one- to four-ring PAH products of supercritical *n*-decane pyrolysis at 100 atm and 140 sec.

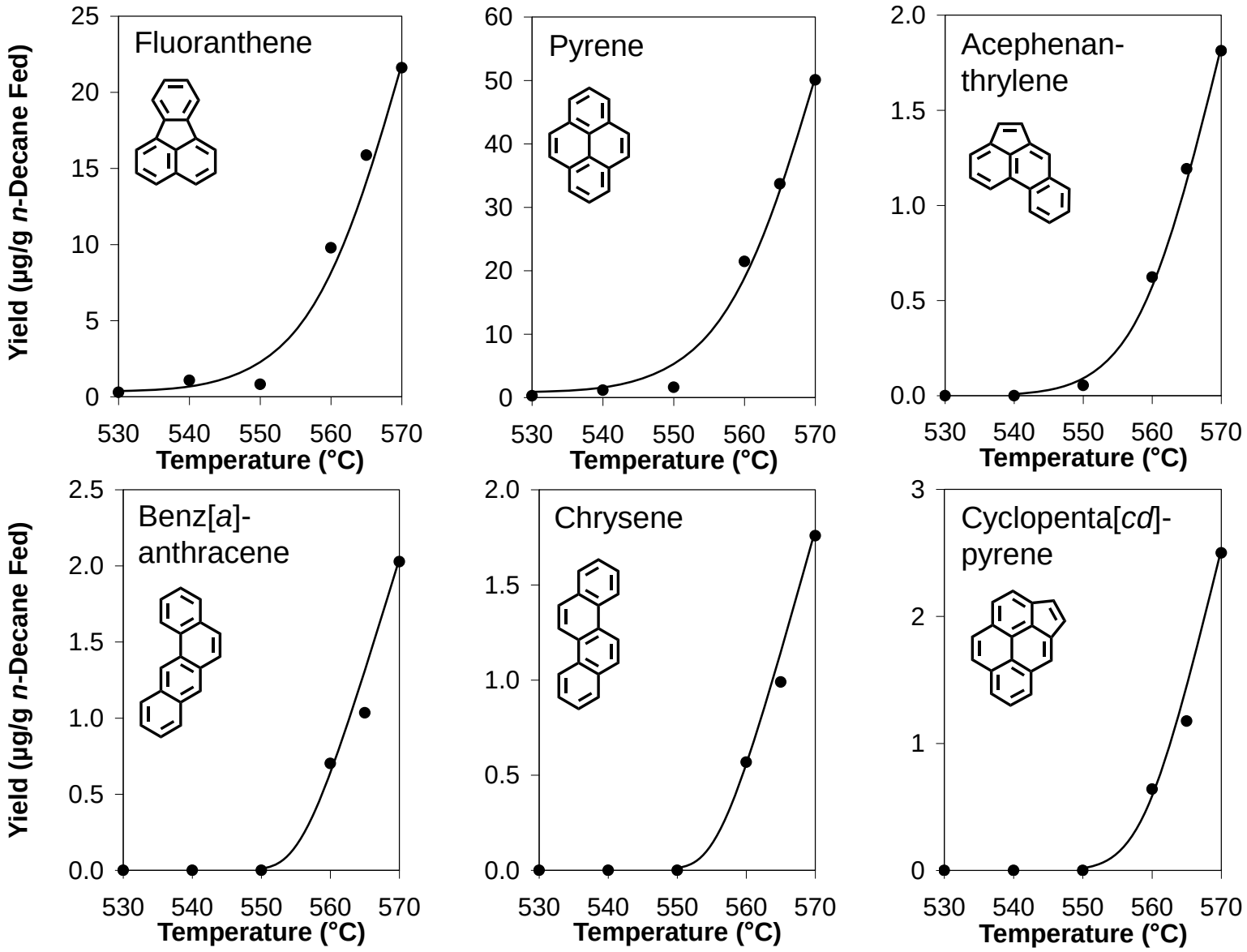

Figure 41. Yields, versus temperature, of four- and five-ring PAH products of supercritical *n*-decane pyrolysis at 100 atm and 140 sec.

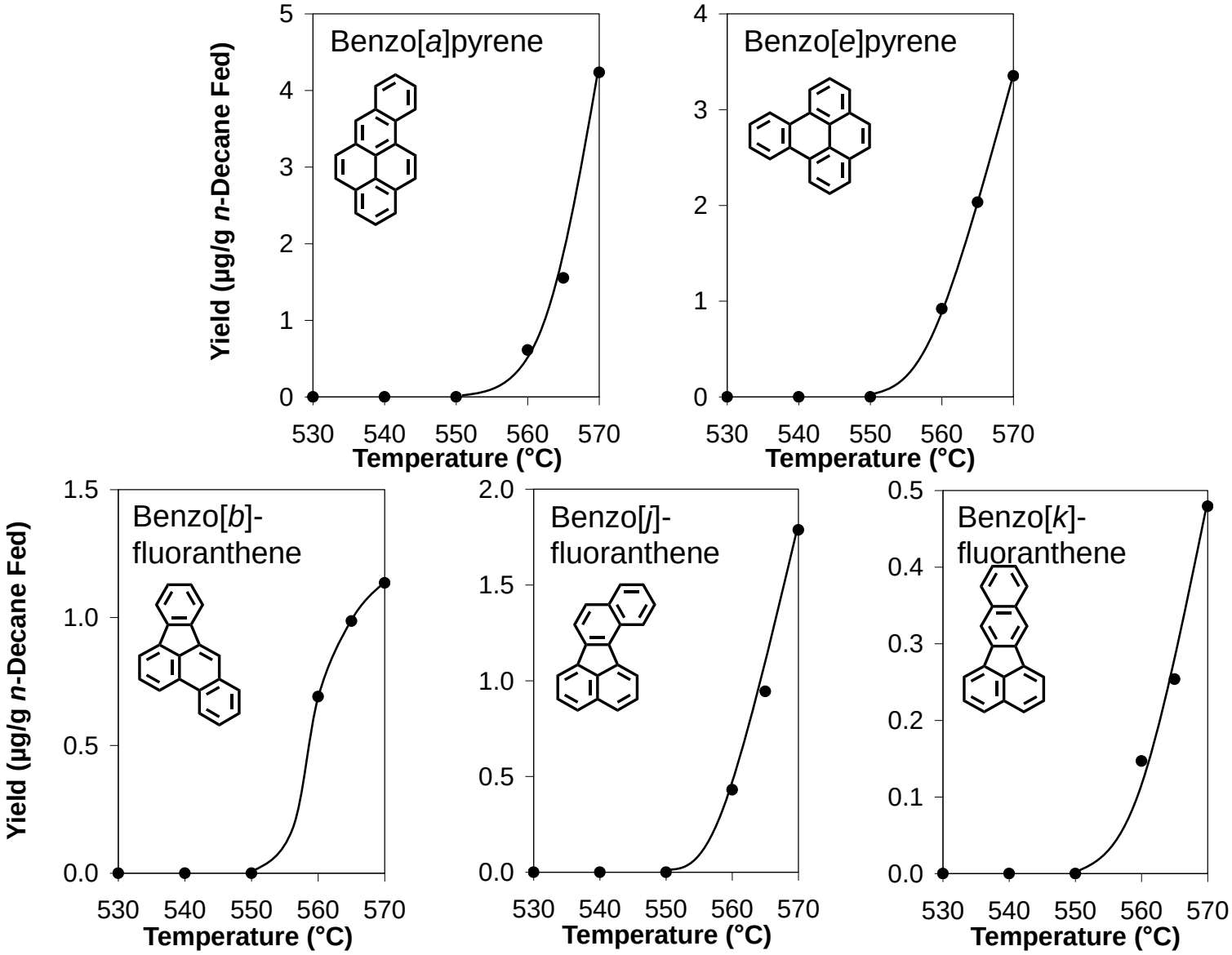

Figure 42. Yields, versus temperature, of five-ring $C_{20}H_{12}$ PAH products of supercritical *n*-decane pyrolysis at 100 atm and 140 sec.

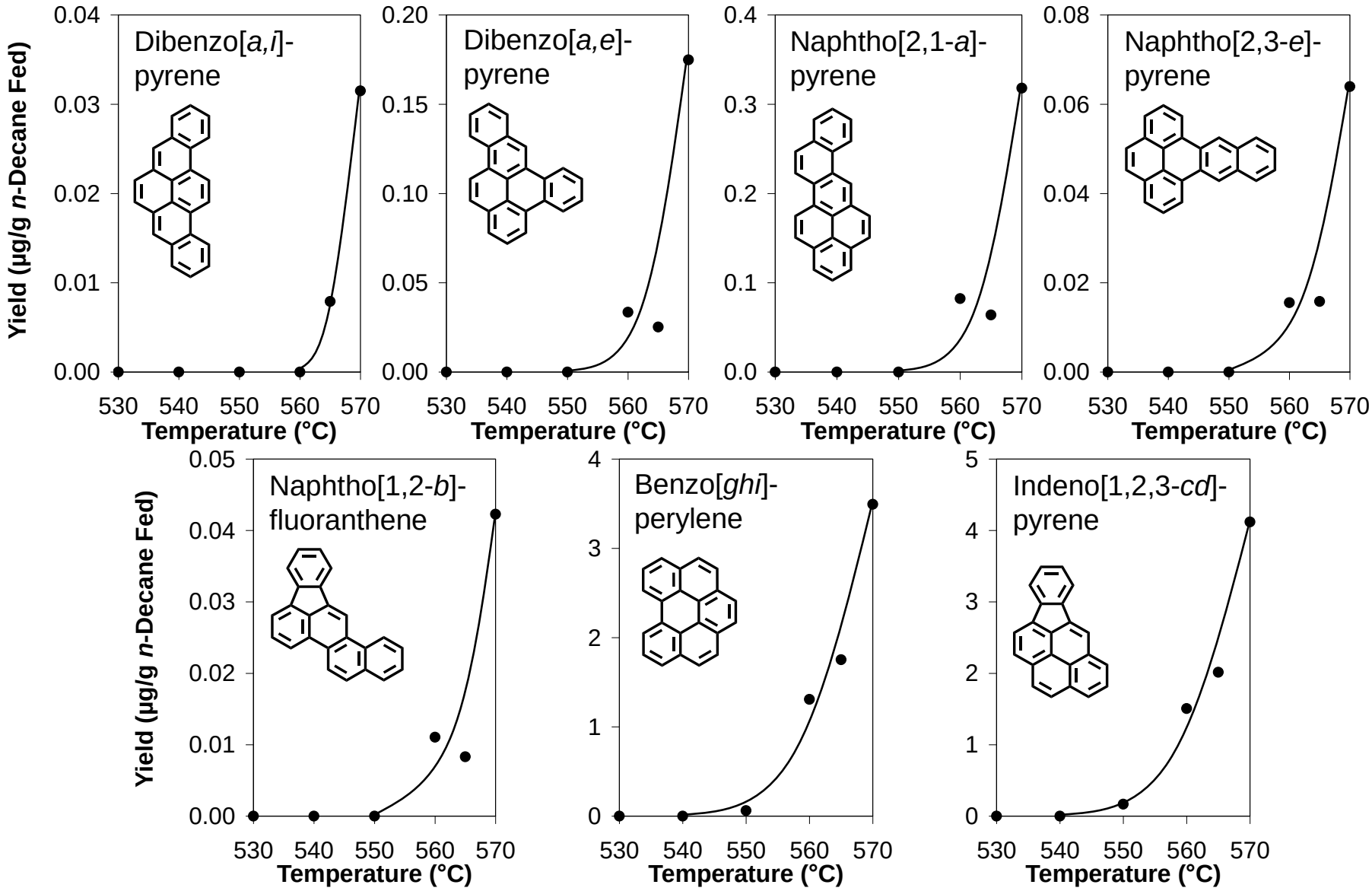

Figure 43. Yields, versus temperature, of six-ring $C_{24}H_{14}$ PAH products of supercritical *n*-decane pyrolysis at 100 atm and 140 sec.

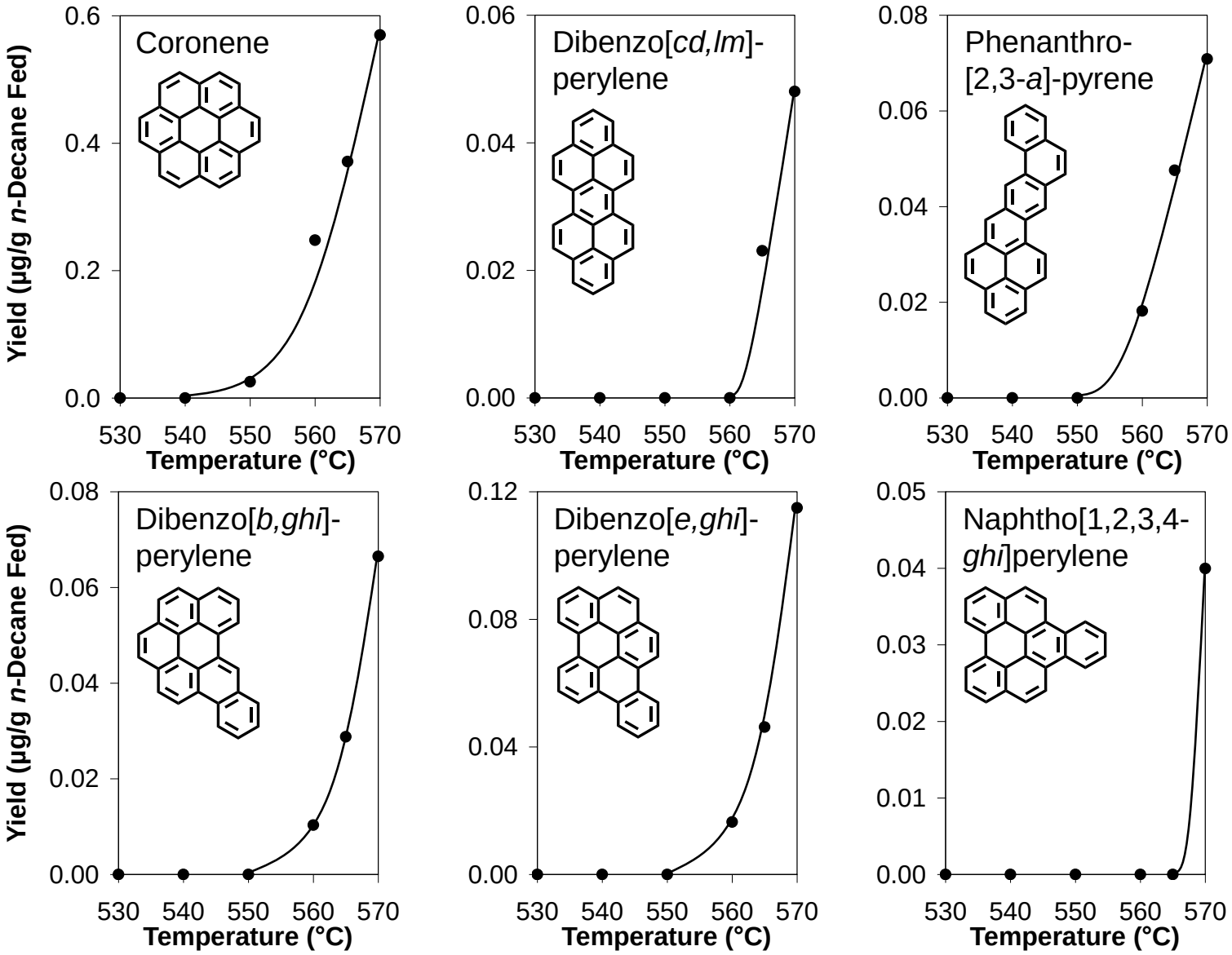

Figure 44. Yields, versus temperature, of seven-ring PAH products of supercritical *n*-decane pyrolysis at 100 atm and 140 sec.

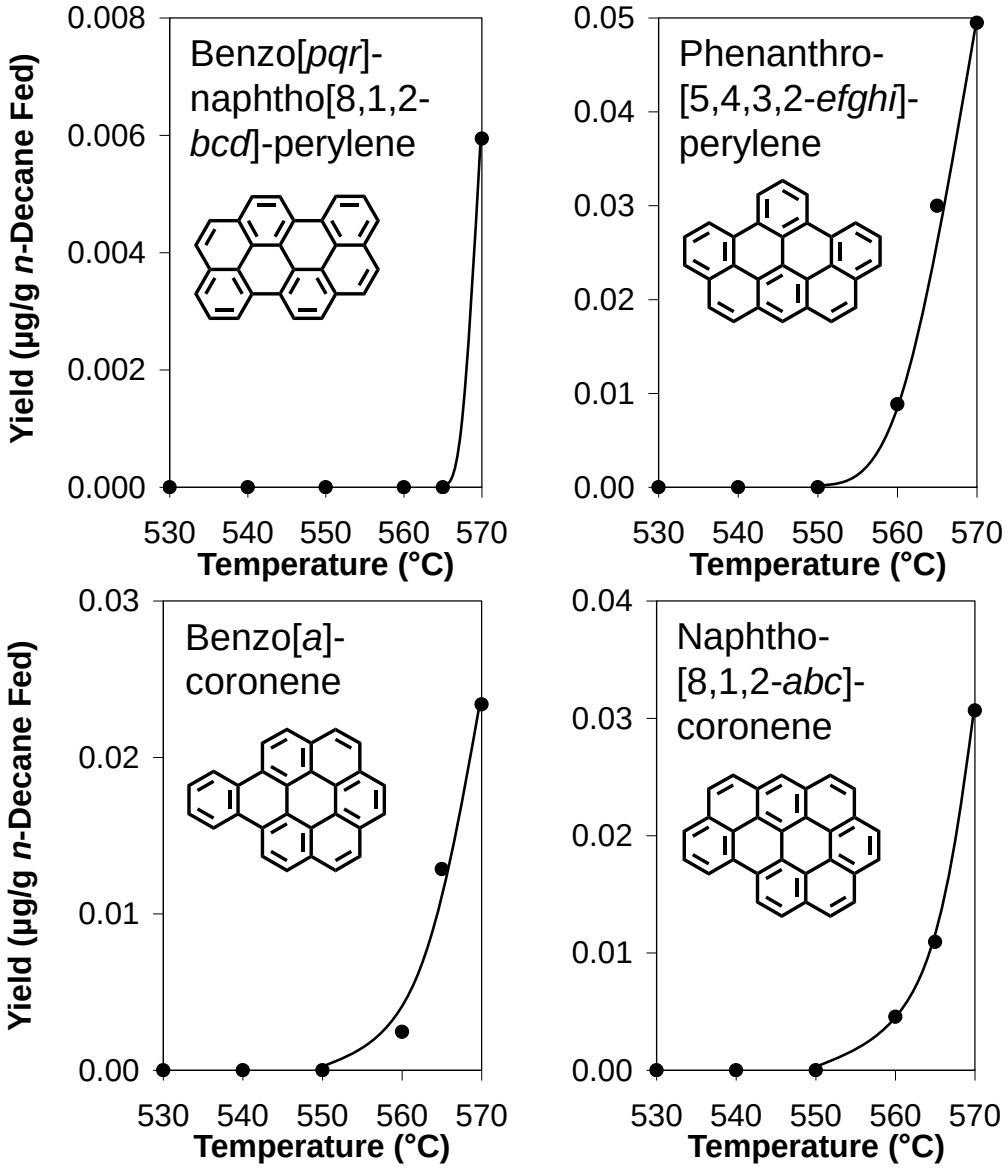

Figure 45. Yields, versus temperature, of eight- and nine-ring PAH products of supercritical *n*-decane pyrolysis at 100 atm and 140 sec.

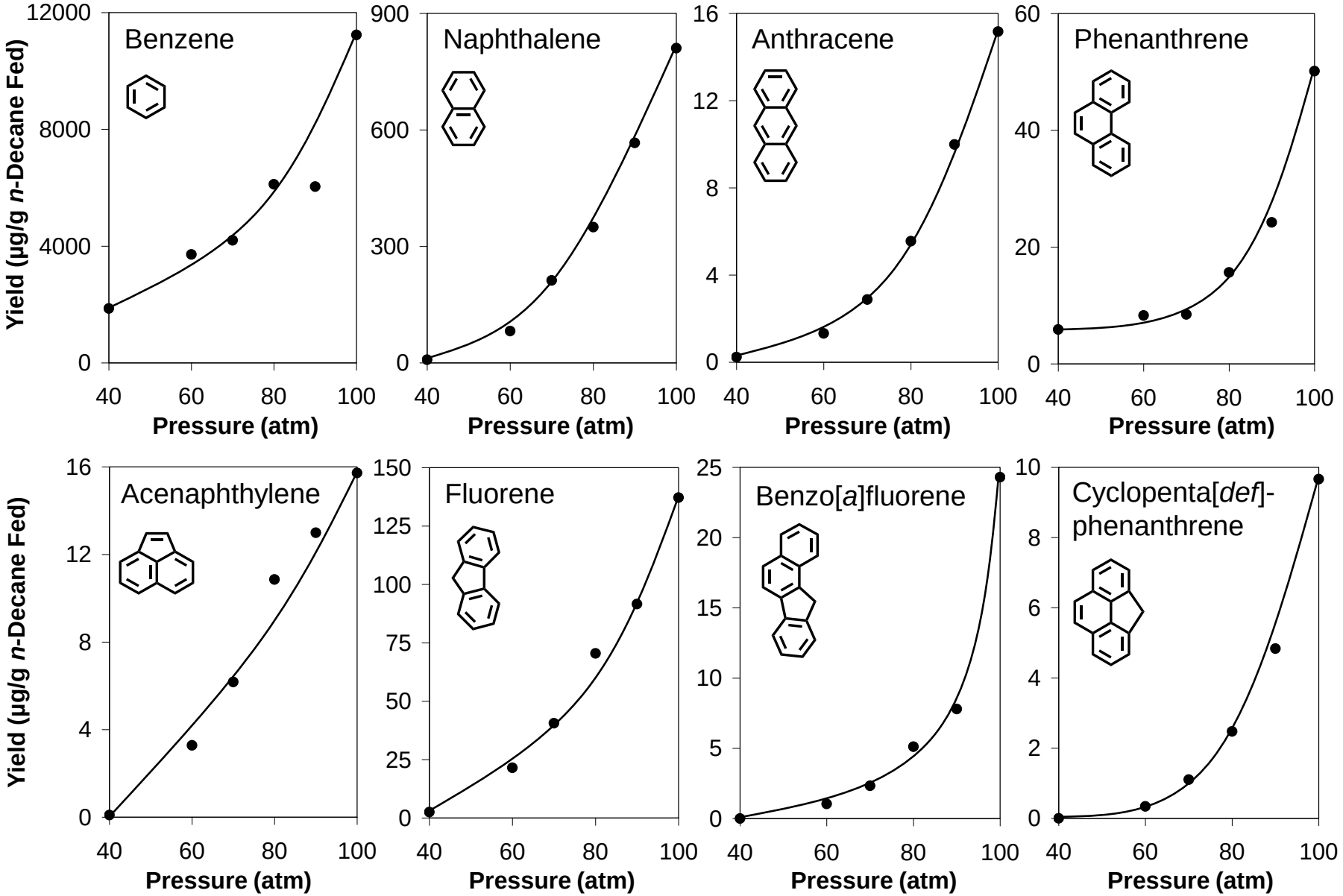

Figure 46. Yields, versus pressure, of one- to four-ring PAH products of supercritical *n*-decane pyrolysis at 570 °C and 140 sec.

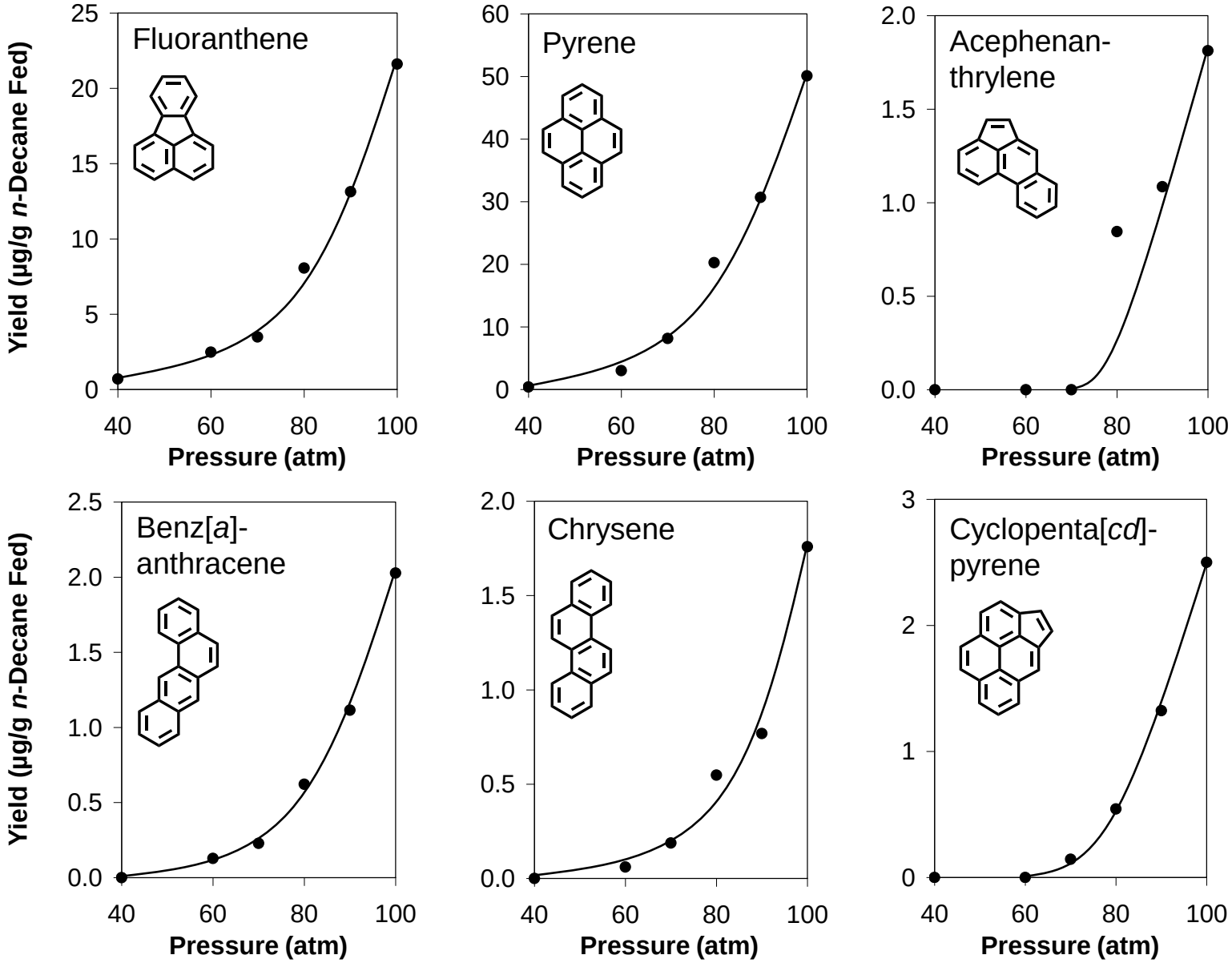

Figure 47. Yields, versus pressure, of four- and five-ring PAH products of supercritical *n*-decane pyrolysis at 570 °C and 140 sec.

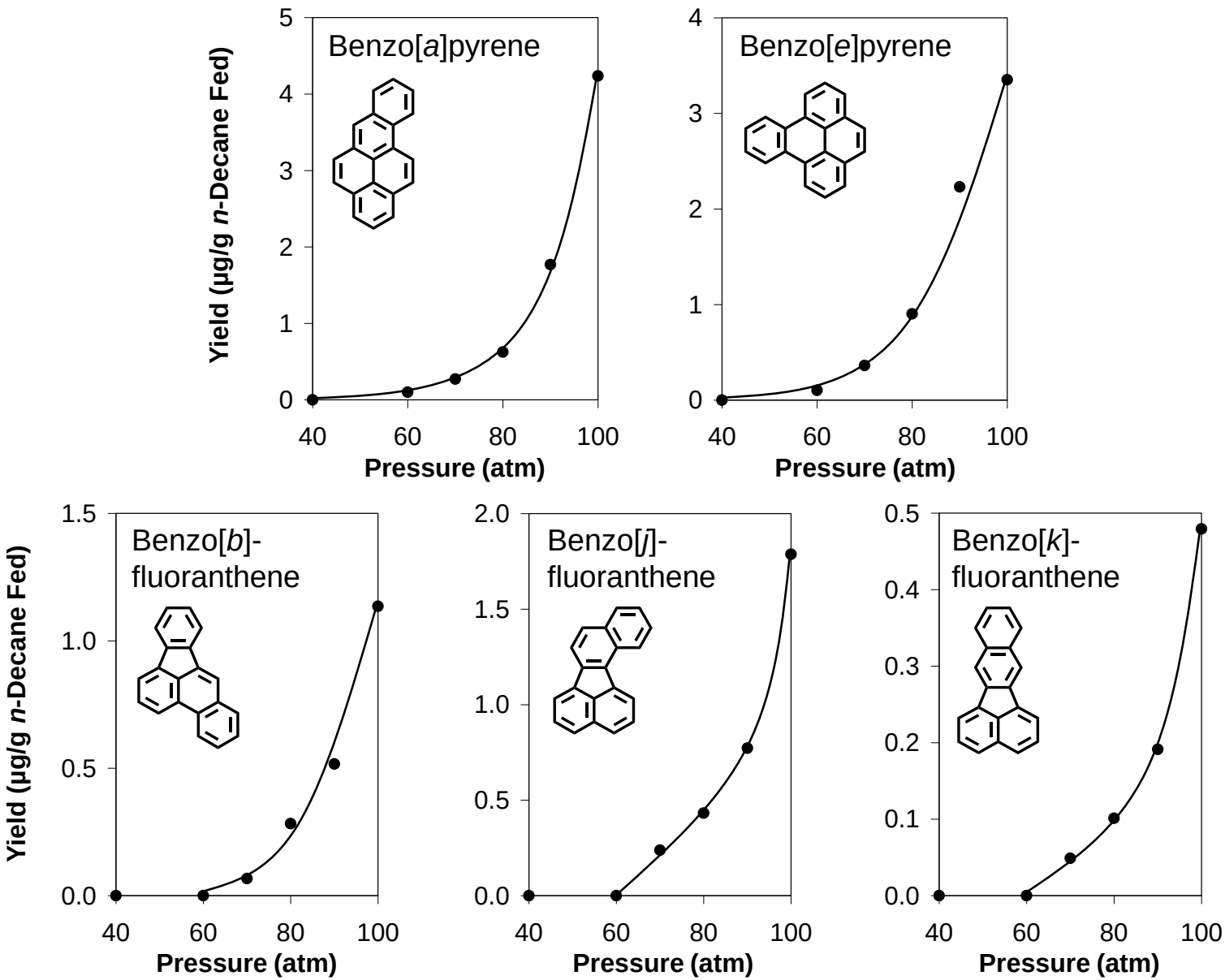

Figure 48. Yields, versus pressure, of five-ring $C_{20}H_{12}$ PAH products of supercritical *n*-decane pyrolysis at 570 °C and 140 sec.

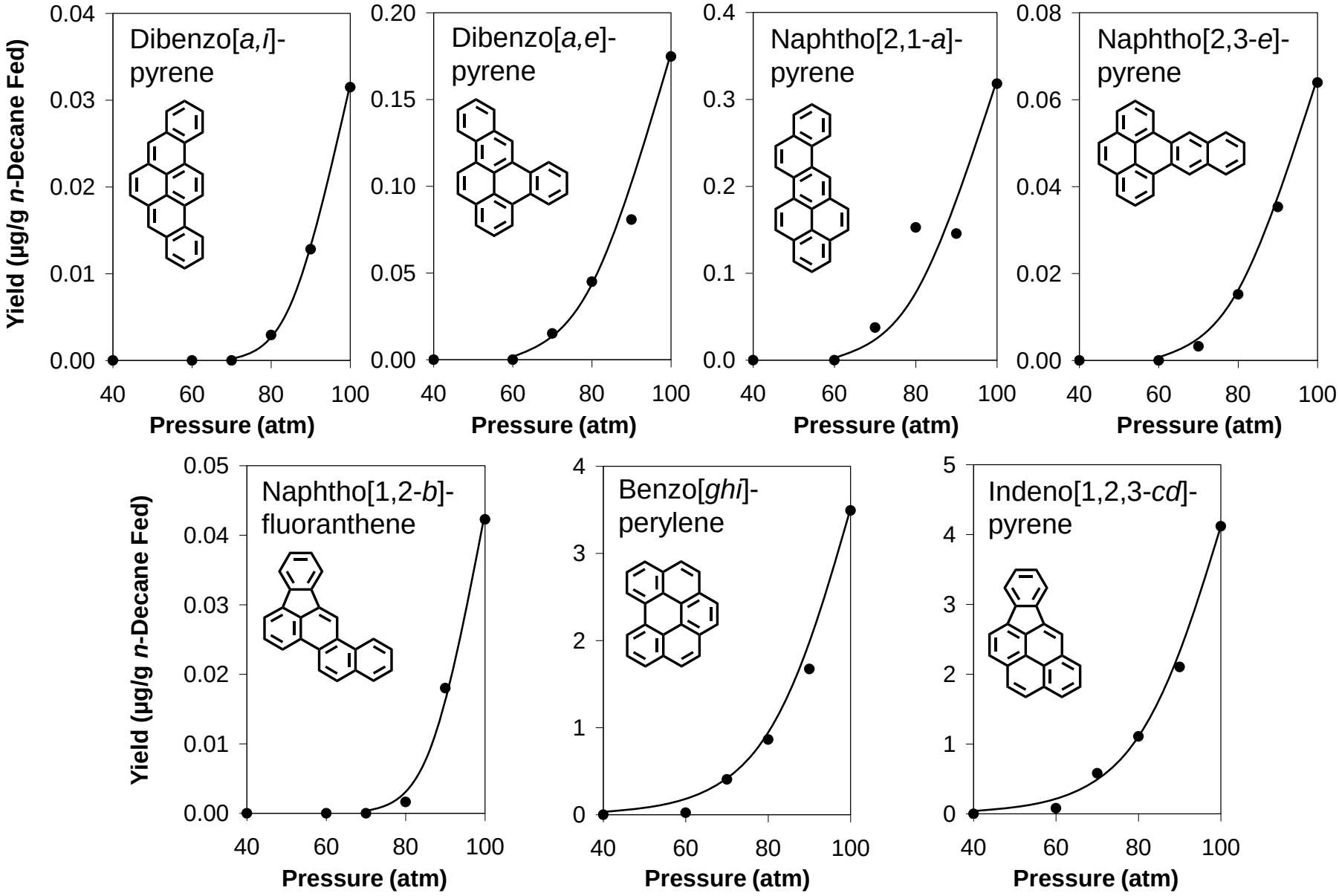

Figure 49. Yields, versus pressure, of six-ring PAH products of supercritical *n*-decane pyrolysis at 570 °C and 140 sec.

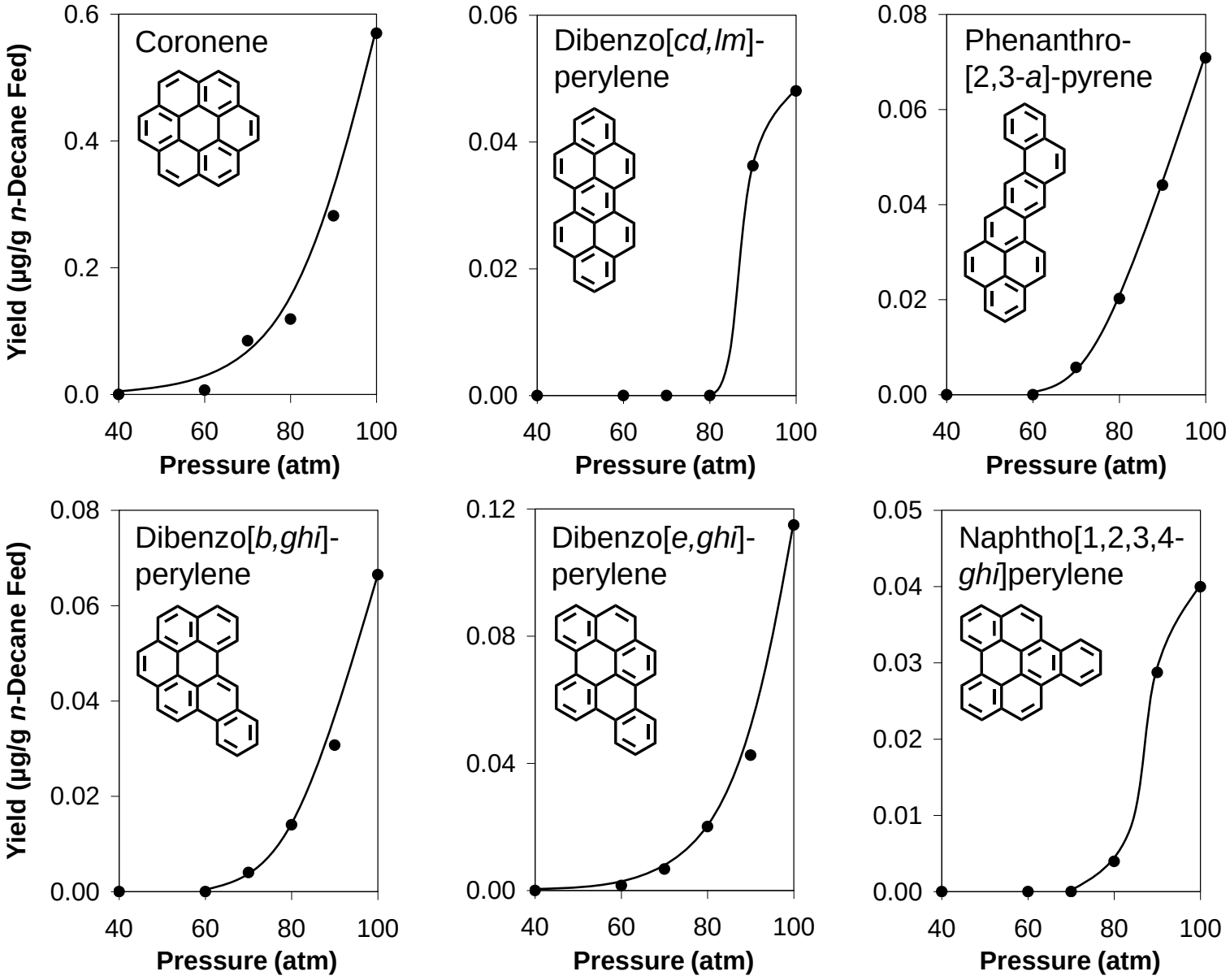

Figure 50. Yields, versus pressure, of seven-ring PAH products of supercritical *n*-decane pyrolysis at 570 °C and 140 sec.

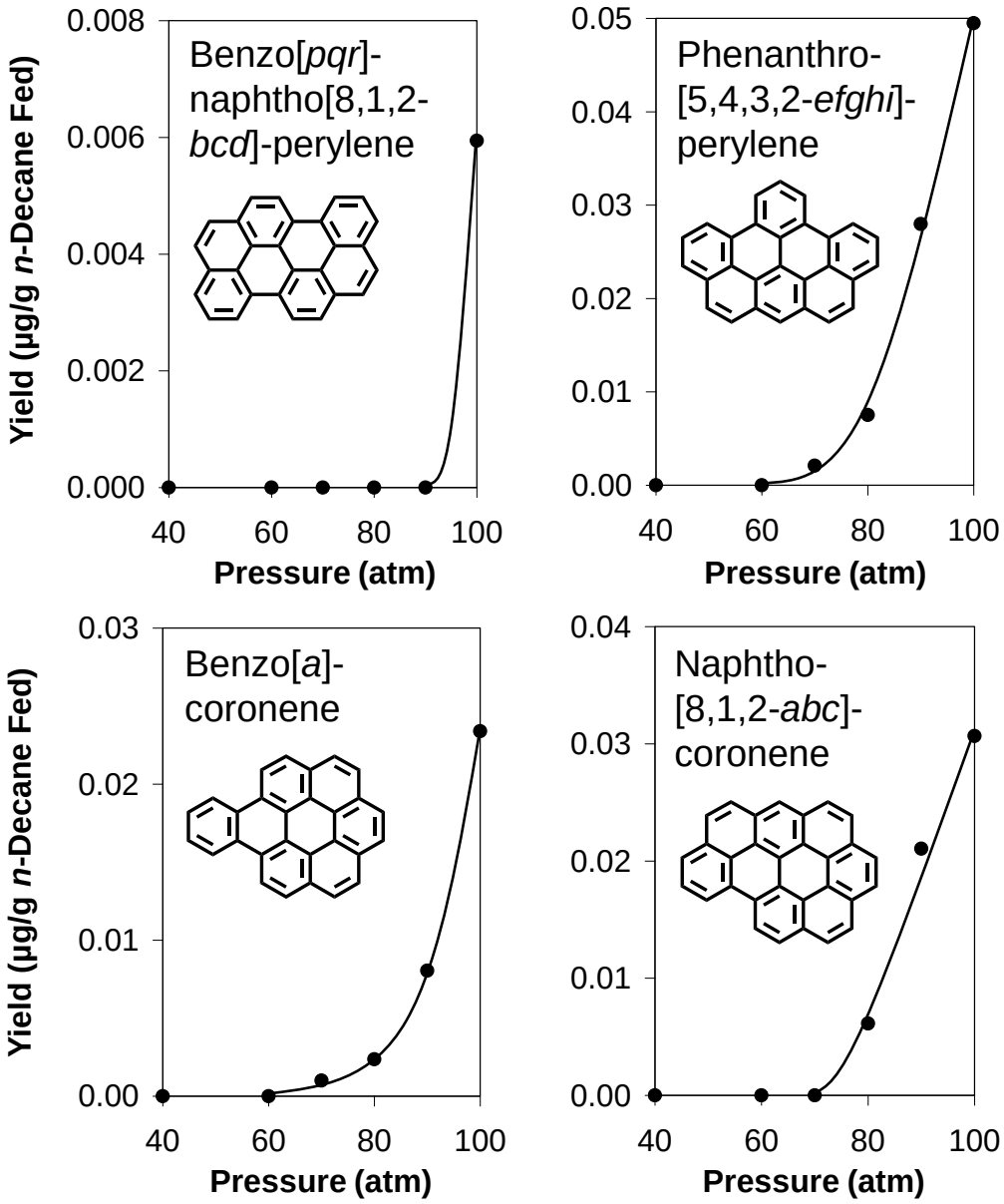

Figure 51. Yields, versus pressure, of eight- and nine-ring PAH products of supercritical *n*-decane pyrolysis at 570 °C and 140 sec.

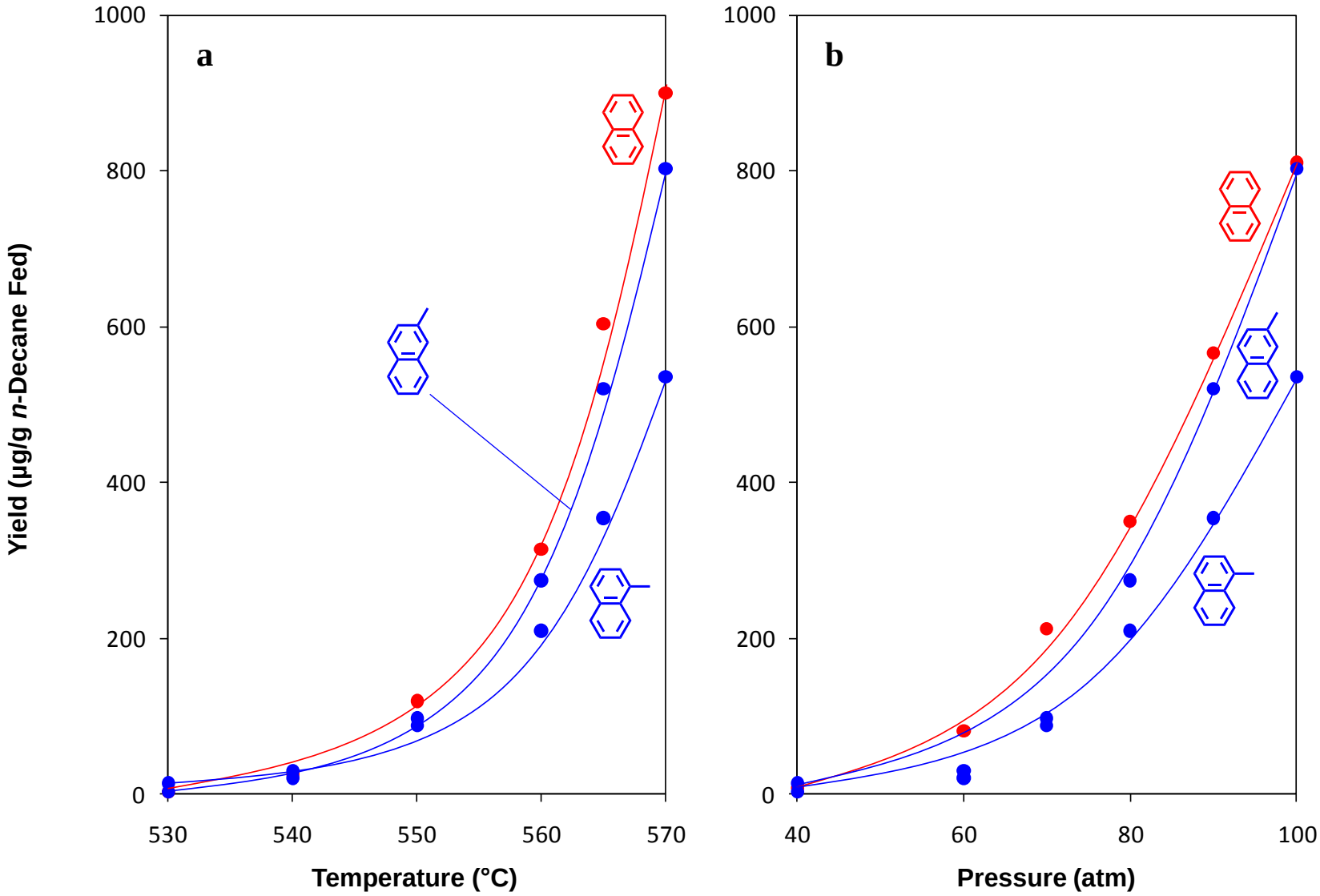

Figure 52. Yields of naphthalene, 1-methylnaphthalene, and 2-methylnaphthalene: (a) as functions of temperature at 100 atm and 140 sec; (b) as functions of pressure at 570 °C and 140 sec.

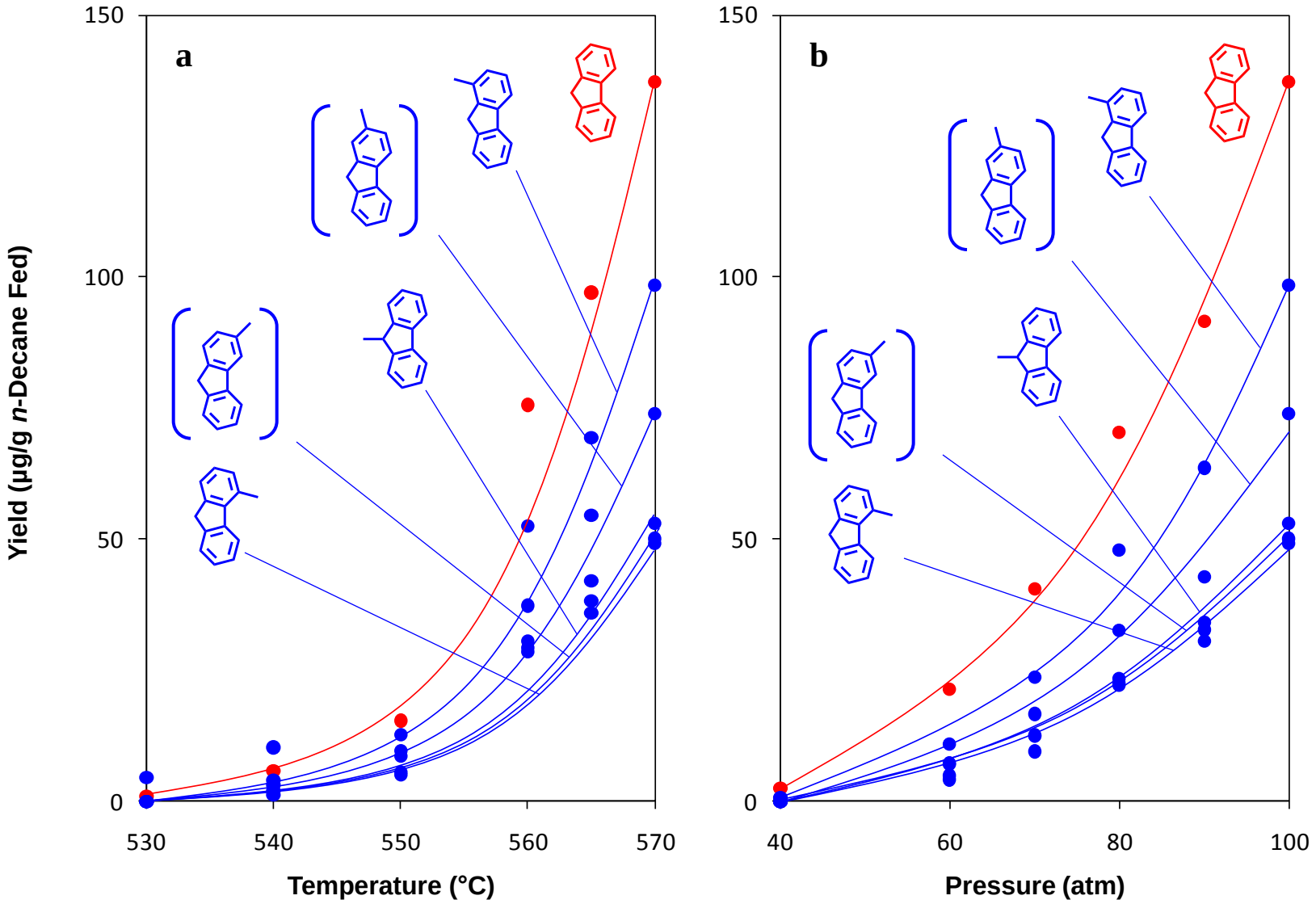

Figure 53. Yields of fluorene and the 1-, 2-, 3-, 4-, and 9-methylfluorenes: (a) as functions of temperature at 100 atm and 140 sec; (b) as functions of pressure at 570 °C and 140 sec. (The yield curves corresponding to the two bracketed methylfluorenes definitely are for 2-methylfluorene and 3-methylfluorene, but reference standards for these two isomers are lacking, so there is some uncertainty as to which is the "2" and which the "3." The "2" and "3" assignments shown are based on HPLC elution order and length-to-breadth ratios.)

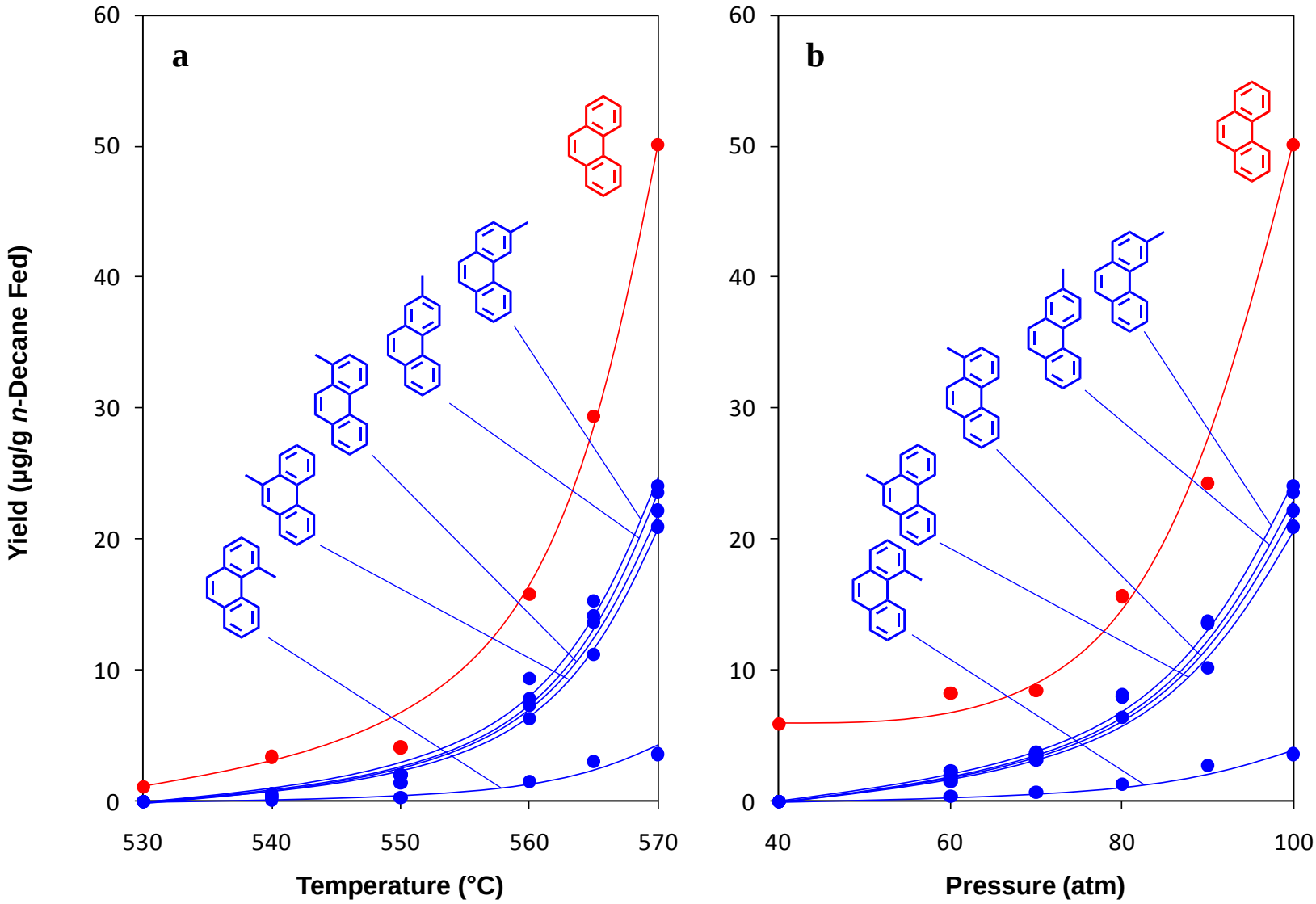

Figure 54. Yields of phenanthrene and the 1-, 2-, 3-, 4-, and 5-methylphenanthrenes: (a) as functions of temperature at 100 atm and 140 sec; (b) as functions of pressure at 570 °C and 140 sec.

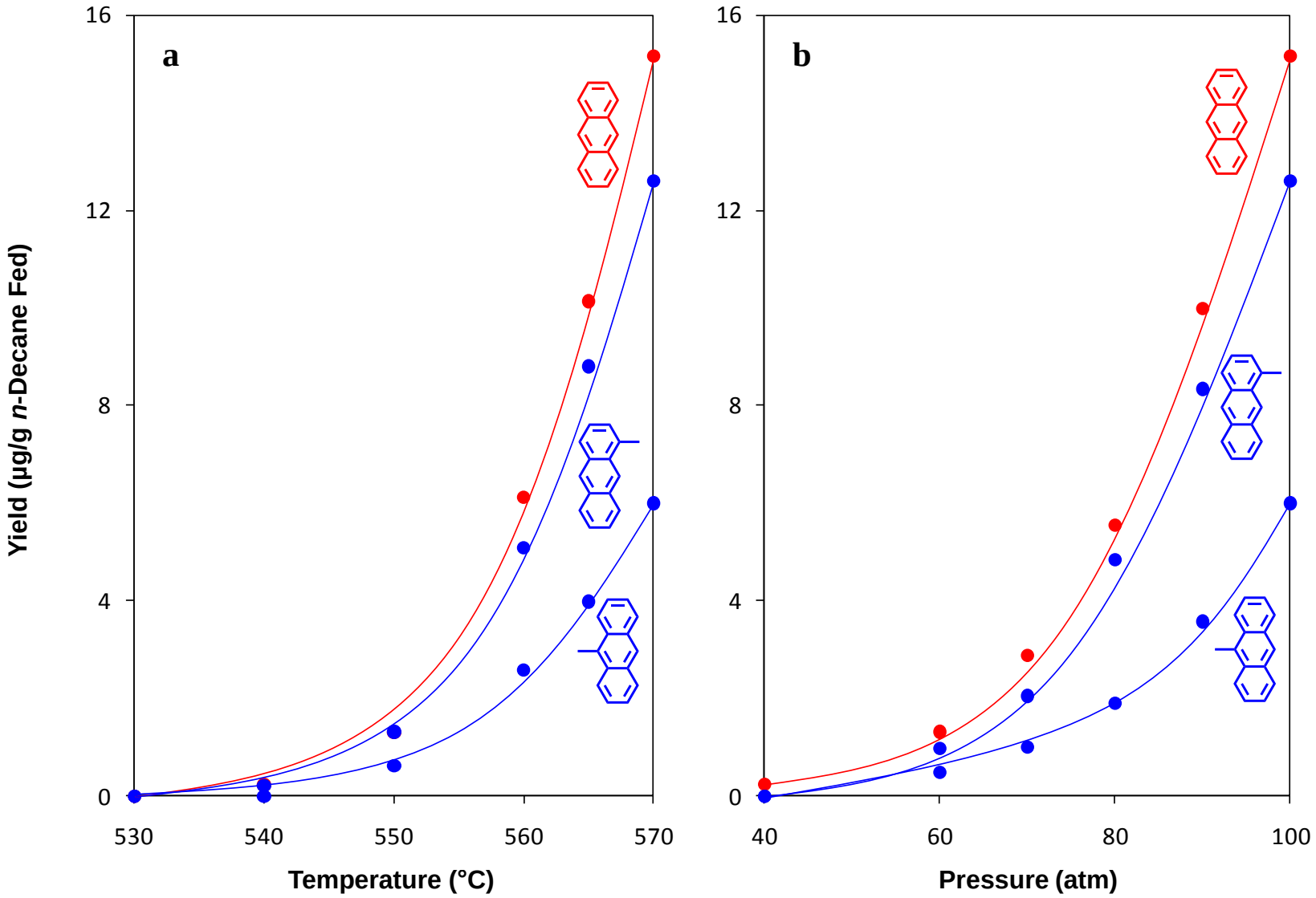

Figure 55. Yields of anthracene, 1-methylanthracene, and 9-methylanthracene: (a) as functions of temperature at 100 atm and 140 sec; (b) as functions of pressure at 570 °C and 140 sec. 2-methylanthracene is detected in the products but is not quantified due to interference from co-eluting alkylated phenanthrenes.

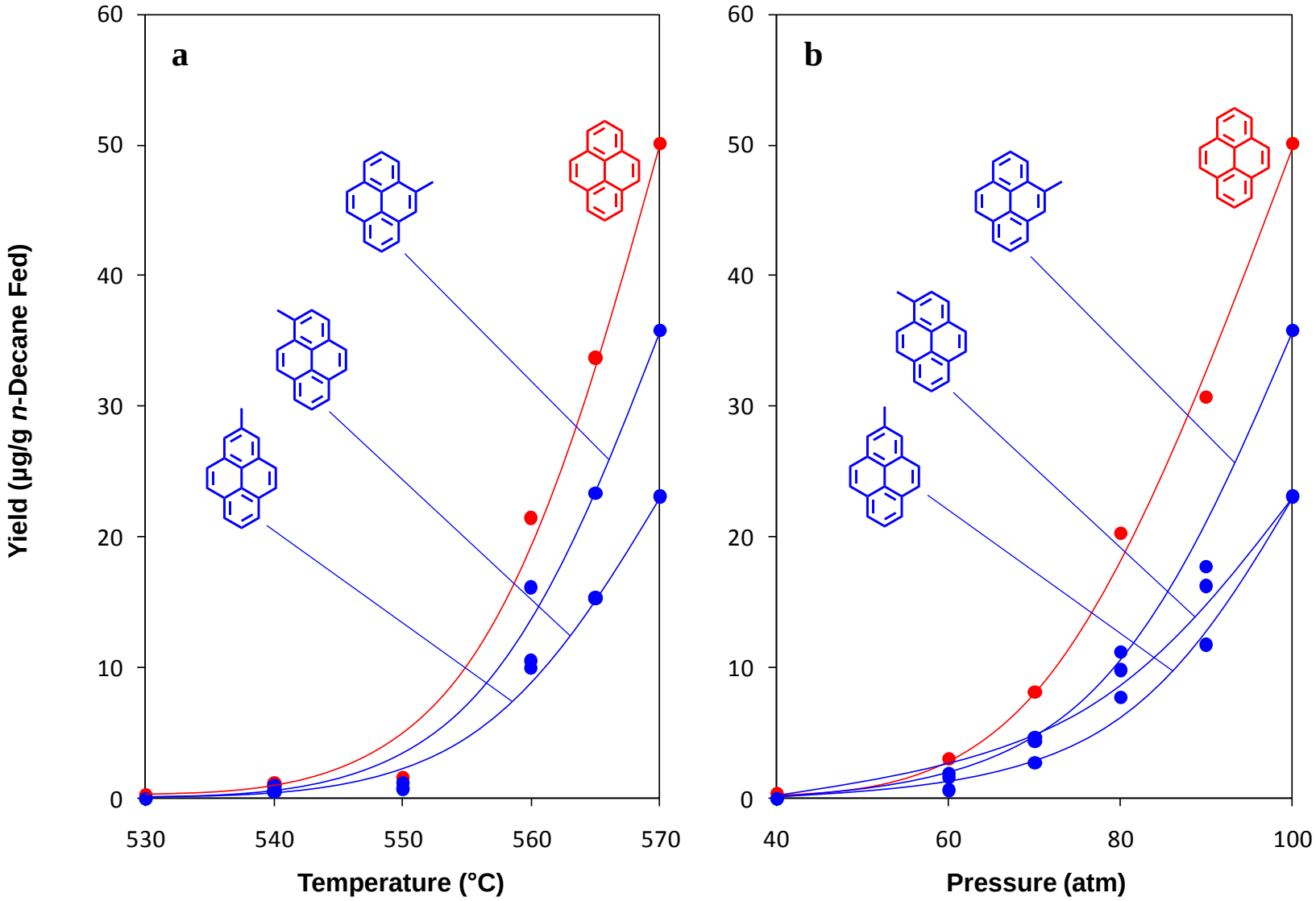

Figure 56. Yields of pyrene and the 1-, 2-, and 4-methylpyrenes: (a) as functions of temperature at 100 atm and 140 sec; (b) as functions of pressure at 570 °C and 140 sec.

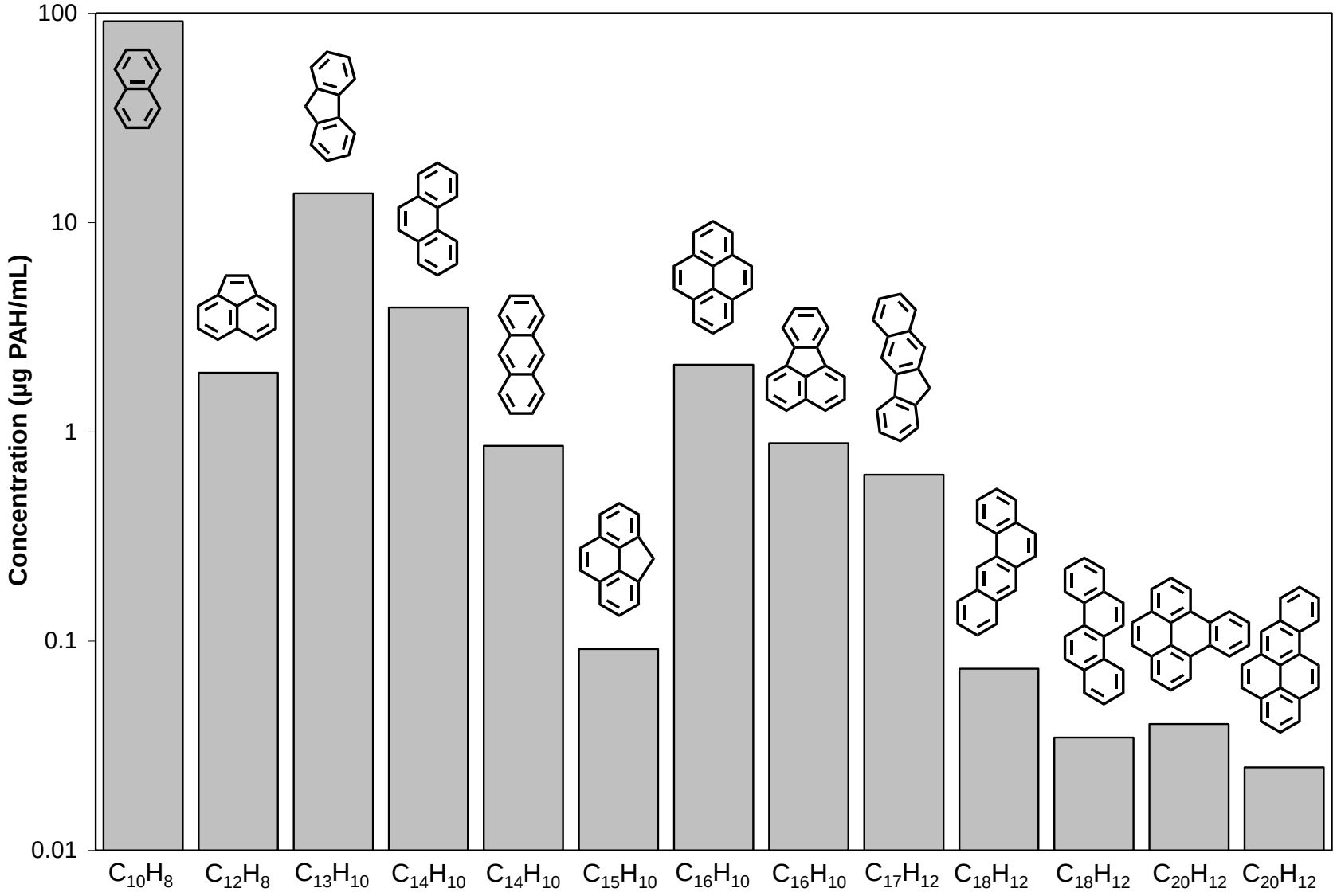

Figure 57. Concentrations of unsubstituted PAH in a sample of Fischer-Tropsch synthetic jet fuel, thermally stressed in a high-temperature flow reactor (with Silco steel tube) at the Air Force Research Laboratory (AFRL) at Wright-Patterson Air Force Base. Stressed fuel sample provided by Dr. Matthew DeWitt and Dr. Tim Edwards of AFRL.

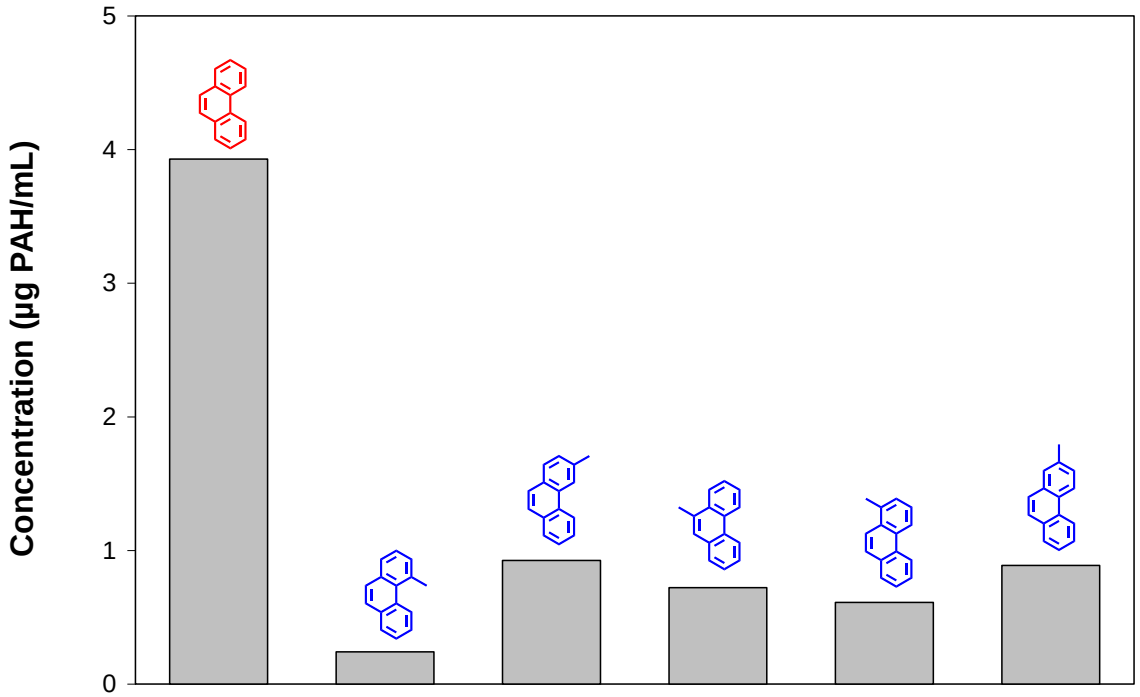

Figure 58. Concentrations of phenanthrene and the singly-methylated phenanthrenes in a sample of Fischer-Tropsch synthetic jet fuel, thermally stressed in a high-temperature flow reactor (with Silco steel tube) at AFRL, Wright-Patterson Air Force Base. Stressed fuel sample provided by Dr. Matthew DeWitt and Dr. Tim Edwards of AFRL.

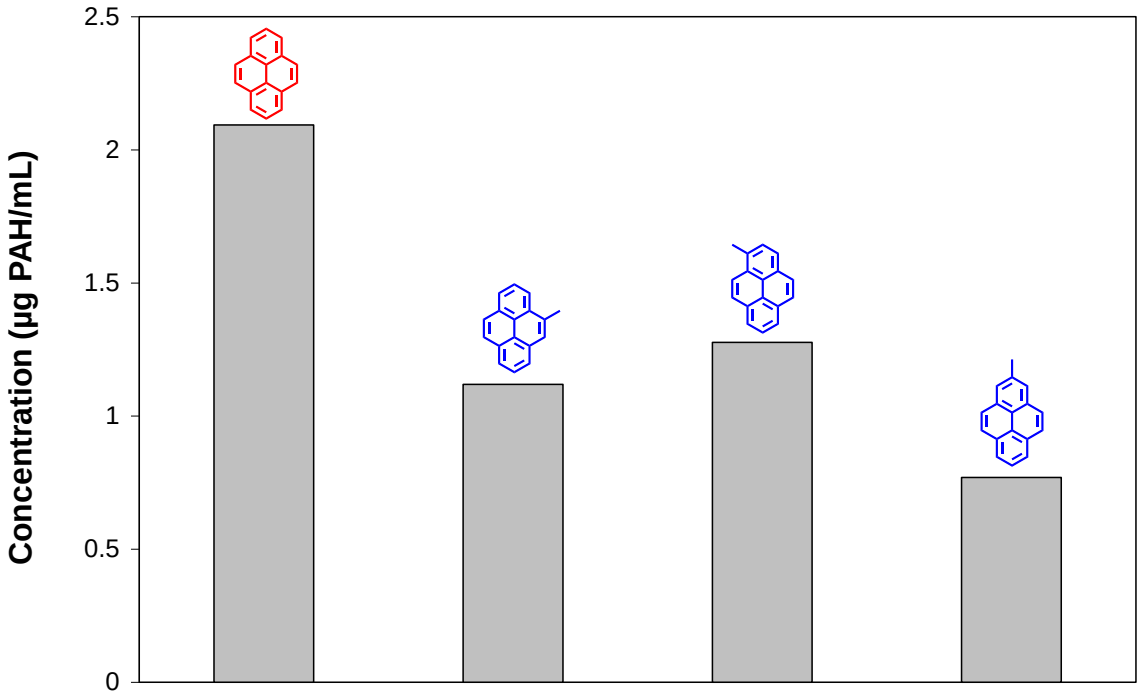

Figure 59. Concentrations of pyrene and the singly-methylated pyrenes in a sample of Fischer-Tropsch synthetic jet fuel, thermally stressed in a high-temperature flow reactor (with Silco steel tube) at AFRL, Wright-Patterson Air Force Base. Stressed fuel sample provided by Dr. Matthew DeWitt and Dr. Tim Edwards of AFRL.